Project funded by the European Commission under the 6th (EC) RTD Framework Programme (2002- 2006) within the framework of the specific research and technological development programme "Integrating and strengthening the European Research Area"

Project UpWind

Contract No.:
019945 (SES6)

"Integrated Wind Turbine Design"

RESEARCH REPORT
Optimized mechanical structures of direct-drive generators
(Deliverable No.: D 1B2.b.5)

AUTHOR:	Aris Zavvos; Alasdair McDonald; Markus Mueller
AFFILIATION:	University of Edinburgh
ADDRESS:	Institute for Energy Systems; The King's Buildings; Mayfield Rd.; Edinburgh EH9 3JL
TEL.:	+44 (131) 6 505602
EMAIL:	A.Zavvos@ed.ac.uk; alasdair.mcdonald@ngentec.com; Markus.Mueller@ed.ac.uk
FURTHER AUTHORS:	
REVIEWER:	Project members
APPROVER:	Jan Hemmelmann

Document Information

DOCUMENT TYPE	RESEARCH REPORT
DOCUMENT NAME:	Deliverable_1B2.b.5.pdf
REVISION:	1.0
REV.DATE:	03/08/2011
CLASSIFICATION:	R1: Restricted to project members
STATUS:	Approved

Optimized mechanical structures of direct-drive generators

Report for UPWIND 1B2.b.5

Aris Zavvos, Alasdair McDonald and Markus Mueller
University of Edinburgh

Introduction

Direct-drive generators for large wind turbines are large and heavy. Previous work reported to UPWIND has demonstrated that the mechanical design of these generators is very important in determining the overall weight. As wind turbine rating continue to grow beyond 5MW, the mechanical design of these generators becomes increasingly challenging.

This report follows on from "*Development of analytical tools for estimating inactive mass*" [1] and "*Structural optimisation of a radial-flux permanent magnet generator (for a direct-drive wind turbine) using a Genetic Algorithm*" [2] which produced analytical tools for estimating the structural mass required in large, low-speed electrical generators for large offshore direct-drive wind turbines. This work (also detailed in [3]) linked the mechanical design to the electromagnetic design, so that these generators could be designed and optimised. Some examples were given showing how optimising the electromagnetically active material in isolation can lead to non-optimal (in terms of weight) solutions as compared to this integrated approach. In "*Optimized mechanical structures of direct-drive generators*" both analytical and Finite Element methods are used to optimize generators and generator structures.

This report is split into three major sections. The first section is entitled "*Integrated electromagnetic-structural optimisation of iron cored PM generators for direct drive wind turbines*" and extends the work carried out in "*Structural optimisation of a radial-flux permanent magnet generator using a Genetic Algorithm*". The second section is entitled "*Shape Optimisation of generator structures with arms*" and uses a Finite Element Analysis tool to optimise rotor and stator structures for large direct radial-flux generators. The final section is entitled "*Shape Optimisation of generator structures with discs*" and uses the same Finite Element Analysis tool to optimise rotor and stator structures – this time with disc type shapes – for large direct radial-flux generators.

The resulting methodologies can be used by generator design teams to reduce machine weight and the results are useful at different stages in the design process. Although the models have been applied mainly to radial-flux permanent magnet synchronous generators, the tools and methodologies can (and have been) applied to other machine types.

Section 1. Integrated electromagnetic-structural optimisation of iron cored PM generators for direct drive wind turbines

1.1 Model

A mathematical model of the generator was created in MATLAB for this purpose that would minimise the cost and the materials used for the structure with the use of genetic algorithms. This optimisation was carried out for three different generator structures, one with armed rotor and stator, one with disc rotor and stator and one with disc rotor and armed stator. The three different combinations of rotor and stator structures that were tested are illustrated in Figure 1. The structural and the electromagnetic model of these different machines are explained in this section.

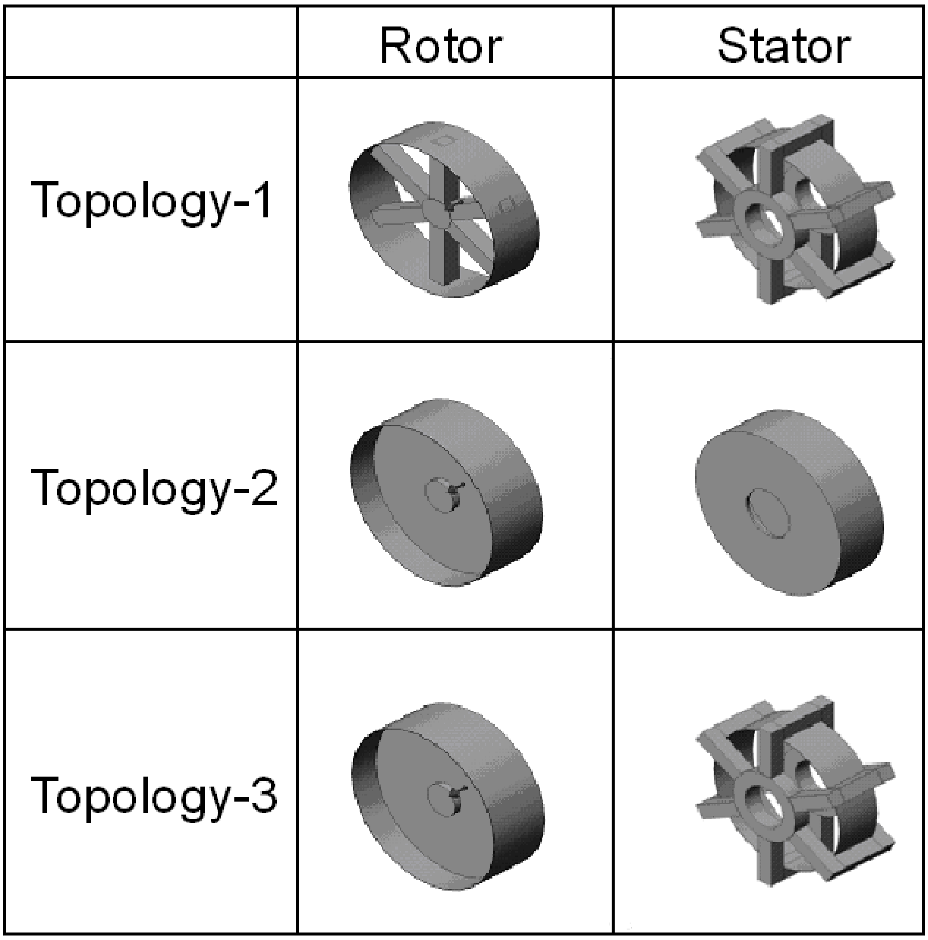

Figure 1 – The three different generator topologies: Topology-1: Generator with armed rotor and armed stator. Topology-2: Generator with disc rotor and disc stator. Topology-3: Generator with disc rotor and armed stator **[3]**Error! Reference source not found.

1.1.1 Structural model

The nature of the structural forces acting on a Permanent Magnet Direct Drive generator (PMDD) is the same to those on a conventional wind turbine generator. It is the physical size of these machines though that gives rise to the loads that these forces apply on the structure of the PMDD generator. These main forces were described analytically by McDonald in [3] and are namely listed here.

- The shear stress (σ) - This is the 'useful' airgap force that gives rise to torque. Because the shear stress is perpendicular to the airgap it does not serve to close the airgap.
- The normal component of Maxwell stress (q) - The radial attraction force trying to close the gap.

- Gravitational force - Due to the tilt angle of the wind turbine rotor axis to the horizontal (typically about 5º), gravity acts on the generator in the axial direction when the generator is being transported, assembled or lifted. Gravitational pull gives rise to two different components (major & minor) that can narrow or widen the airgap. The nature of these deflections depends on the construction of the rotor and the stator of the machine.
- The thermal expansion due to heat - In a direct drive generator, thermal expansion could cause a change in the airgap clearance, which affects the Maxwell stress. In a radial flux machine though it mainly affects the outer stator and does not tend to close the airgap.
- The forces and moments from the rotor blades - Although these forces may be a major factor leading to shortening of the airgap, they will not be considered in this study as they are closer to the wind turbine design optimisation and not the generator design.
- The acceleration due to the rotation of the rotor - Angular acceleration leads to a centripetal force that is a radially outward and into the airgap and a moment that acts on the rotor's arms or disc. These forces cause a torsional deflection on the arms or the discs of the machine.

For the structural modelling of the PMDD generator, only the loads that could be a threat to the airgap clearance were included. The three main deflections that were calculated analytically were the radial deflection that is caused due to the normal component of the Maxwell stress *q*, the axial deflection due to gravity and the tortional deflection due to the centripetal force. 0depicts the three different deflections on the structure of a rotor with arms.

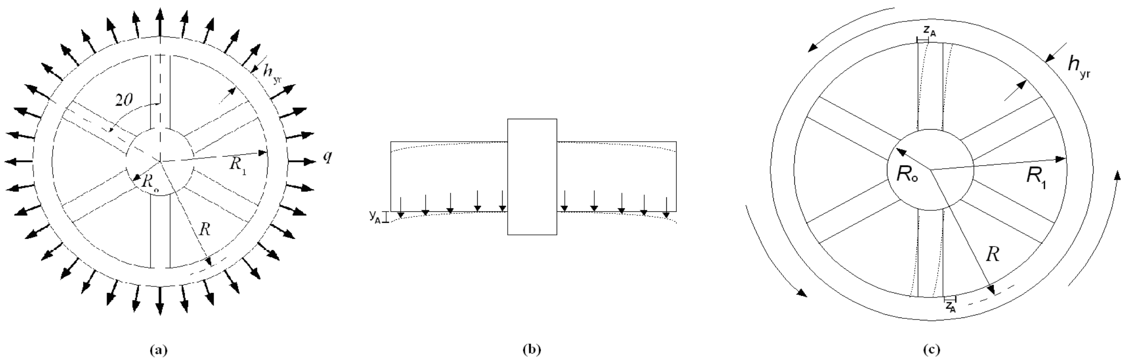

Figure 2: Cross section of structure. (a) Deflection due to Maxwell stress (b) Deflection due to weight component of the arms/disc of the structure (c) The torsional deflection z_A on a rotor with six arms

The normal component of Maxwell stress *q* is proportional to the square of the flux density in the airgap as shown in (1).

$$q = B^2 / 2\mu_o \tag{1}$$

where *B* is the flux density in the airgap and μ_o is the permeability of free space. Figure 2a depicts *q* on a rotor with arms.

Equation (2) shows the radial deflection (*u*) due to the normal component of Maxwell stress.

$$u = qR^2 / Et \tag{2}$$

where *q* is the uniform radial pressure applied to a thin walled cylindrical vessel, *R* is the radius of cylinder of the structure that is examined, *t* is the thickness of cylinder (rotor or stator with arms or disc) and *E* the Young's modulus.

The axial deflection y_A due to gravity is the sum of the major ($y_{a,i}$) and the minor ($y_{a,ii}$) gravity component.

$$y_A = y_{a,i} + y_{a,ii} \tag{3}$$

Depending on the construction of the rotor and the stator of the machine, $y_{a,i}$ and $y_{a,ii}$ are calculated accordingly. The analytical models of $y_{a,i}$ and $y_{a,ii}$ for the different types of generator structures are described in detail in [3]. Figure 2b shows the axial deflection y_A of a rotor due to gravity.

The torsional deflection z can only be calculated for structures with arms as given in (4)

$$z = \frac{\left(\frac{2\pi R l}{2n}\right)\sigma l^3}{3EI_{\text{arm.tor}}} \tag{4}$$

where is R the radius of the structure, l is the axial length, n is the number of arms on it, σ is the shear stress and $I_{\text{arm,tor}}$ the moment of the area of the stator arm. Figure 2c depicts the torsional deflection of a rotor with arms.

The analytical models that describe the radial, axial and torsional deflection for each type of structure (rotor or stator with arms or with discs) are given in detail by McDonald in [3]. The deflections that the analytical models returned for each different structure were used as criteria to optimise the mass and cost, whilst ensuring a robust design. The allowable values of the above criteria were 10% of the airgap clearance for the radial deflection, 2% of the axial length for the gravitational deflection and a relative twist of 0.01° of torsional deflection.

1.1.2 Electromagnetic model

The electromagnetically active material of a PMDD generator consists of the permanent magnets mounted on the surface of the rotor, the copper windings on the stator of the machine and the steel placed on the stator's teeth and back. It is assumed that the stator's iron is infinitely permeable so that only the airgap region need be modelled. Within the airgap it is assumed that all flux crosses the airgap normal to the stator surface. Leakage flux paths are ignored. The amount of copper per unit of airgap surface area is assumed to be constant.

The mass of the permanent magnet on the rotor of the machine was calculated as shown in (5)

$$mass_{\text{PM}} = 2\pi R l \left({b_{\text{m}}}/{\tau_{\rho}} \right) h_{\text{m}} \rho_{\text{PM}} \tag{5}$$

where R is the rotor radius, l_s is the axial length of the rotor, b_m the magnet's breadth, τ_ρ the pole pitch of the machine, h_m the height of the magnet and ρ_{PM} the permanent magnet's density.

The mathematical model that was used for the calculation of the height of the permanent magnet on the rotor was the same as McDonald and Mueller describe in [2],

$$h_{\text{m}} = \frac{l_{\text{g}}}{B_{\text{r}} \frac{4}{\pi} \sin\left(\frac{b_{\text{m}}}{\tau_{\rho}} \frac{\pi}{2}\right)} \frac{1}{\left(\left({1}/{B_{\text{g}}} \right) - \left({1}/{B_{\text{r}} \frac{4}{\pi} \sin\left(\frac{b_{\text{m}}}{\tau_{\rho}} \frac{\pi}{2}\right)} \right) \right)} \tag{6}$$

where l_g the airgap clearance between the rotor and the stator, B_r the remanent flux density of the magnets and B_g the flux density in the airgap.

The mathematical model that describes the mass of the copper windings that are wound around the slots of the stator was given by Zavvos in [7]. Since a constant amount of copper per unit airgap surface area was assumed, the total amount of copper in the slots and the steel in the teeth of the stator structure could be calculated accordingly (plus copper in endwinding based on number of poles and pole pitch).

$$mass_{\text{copper}} = s h_{\text{s}} b_{\text{s}} (l + 2\tau_{\rho}) \rho_{\text{copper}} K_{\text{fill}} \tag{7}$$

Where s the number of the stator's slots, h_s the height of the stator's slot, b_s the width of the stator's slot, l_s the stator's axial length, ρ_{copper} the copper's density and K_{fill} the slot's fill factor.

The number of slots on the stator was calculated as shown in (8)

$$s = \frac{2\pi R_s}{b_s + b_t} \tag{8}$$

where R_s is the stator's radius and b_t is the breadth of the stator's tooth. For simplification it was assumed that $b_s = b_t$.

Steel can be found on the stator's teeth and on the yoke of the stator. The mass of the steel placed on the stator can be found for the given slot and tooth dimensions and for specific stator yoke height (h_{ys}) according to (9) [7]

$$mass_{steel} = sh_s b_s l \rho_{steel} + \pi l \left[\left(R_s + \frac{h_{ys}}{2} \right)^2 - \left(R_s - \frac{h_{ys}}{2} \right)^2 \right] \tag{9}$$

Figure 3 shows the cross section of the two poles where the active material of the rotor and the stator is placed and the direction of the magnetic flux.

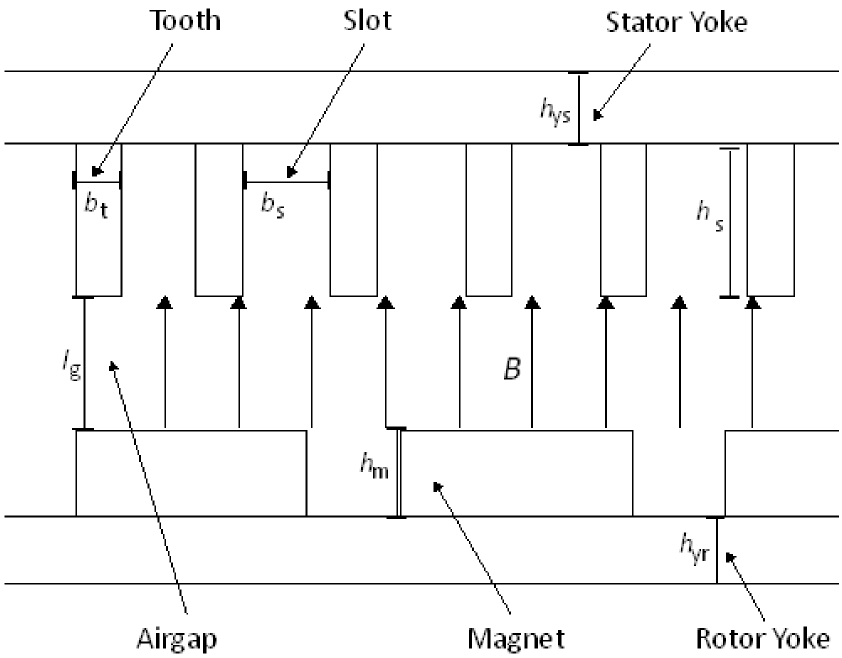

Figure 3 - Linear cross section of RF PMDD generator

The structural and electromagnetic parameters for the active material h_m, b_m, h_s, b_s, b_t, K_{fill}, B_r and B_g were based on the electromagnetic design presented by Bang in [6]. The weight of the permanent magnets was included in the weight of the rotor and the weight of the copper windings and the steel on the stator was included in the stator's weight.

For radial flux machines with slotted stators, the flux per pole is reduced due to the slotted armature. This effect can be accounted for by introducing the Carter coefficient K_c into the calculation of the field produced by the magnets.

$$K_c = \frac{\tau_t}{\tau_t - \gamma l_g'} \tag{10}$$

where $l_g' = l_g + h_m/\mu_r$ (11), τ_t is the armature slot pitch calculated as

$$\tau_t = \frac{2\pi R_s}{s} \tag{12}$$

and

$$\gamma = \frac{4}{\pi} \left\{ \frac{b_s}{2l_g'} \tan^{-1}\left(\frac{b_s}{2l_g'} \right) - \ln \sqrt{1 + \left(\frac{b_s}{2l_g'} \right)^2} \right\} \tag{13}$$

Therefore, the effective airgap l_{ge} for an internal rotor machine is given by

$$l_{ge} = l_g + (K_c - 1) l_g' \tag{14}$$

However, for small slot openings such as the tested cases here ($b_s/D \cong 3.7\%$), the effect of the stator slotting on the calculation of flux per pole can be neglected. Thus it was not included into the calculations.

1.1.3 The optimisation process

The MATLAB Genetic Algorithm Toolbox was used as an optimisation tool for this research [4],[5]. A Genetic Algorithm is an optimisation process inspired by biological evolution. The toolbox creates a number of random "generations" of an object that is under examination through the use of simulated evolution. Each generation is evaluated according to an objective function and the "best" generation of those created is returned at the end of every optimisation run. This generation will not be the lightest or the cheapest structure that can be created but just the one that scored the highest during that particular run of the toolbox. Thus, a large number of runs had to be done for each structure in order to come up with the best (lightest/cheapest) possible solution.

The objective function that was created for the means of this research seeks to minimise the total mass or the total cost of the structure while meeting the deflection criteria that were mentioned in section 1.1.1. These deflections should not exceed their limits in order for the structural design to be robust enough to maintain the necessary airgap clearance, but the dimensions of the machine (radius and axial length) should at the same time be great enough to provide the necessary torque needed for the nominal power output of the generator (5MW in this case). Structures of excessive weight or structures that could not match the deflection and torque limitations were penalised, thus leading to the best possible structure that can produce the necessary torque for the machine.

The structural variables that were used to create and describe the different generations of structures are listed below and are illustrated in Figure 4 .

- the radius of the structure, R
- the axial length of the structure, l
- the number of arms, n (only for structures with arms)
- arm dimension, b & d (only for structures with arms)
- arm thickness, t_{wr} & t_{ws} (only for structures with arms)
- disc thickness, t_d (only for structures with discs)
- the thickness of the structure's back iron, h_{yr} & h_{ys} for rotor & stator
- the length of the airgap, l_g
- the density flux, B_g

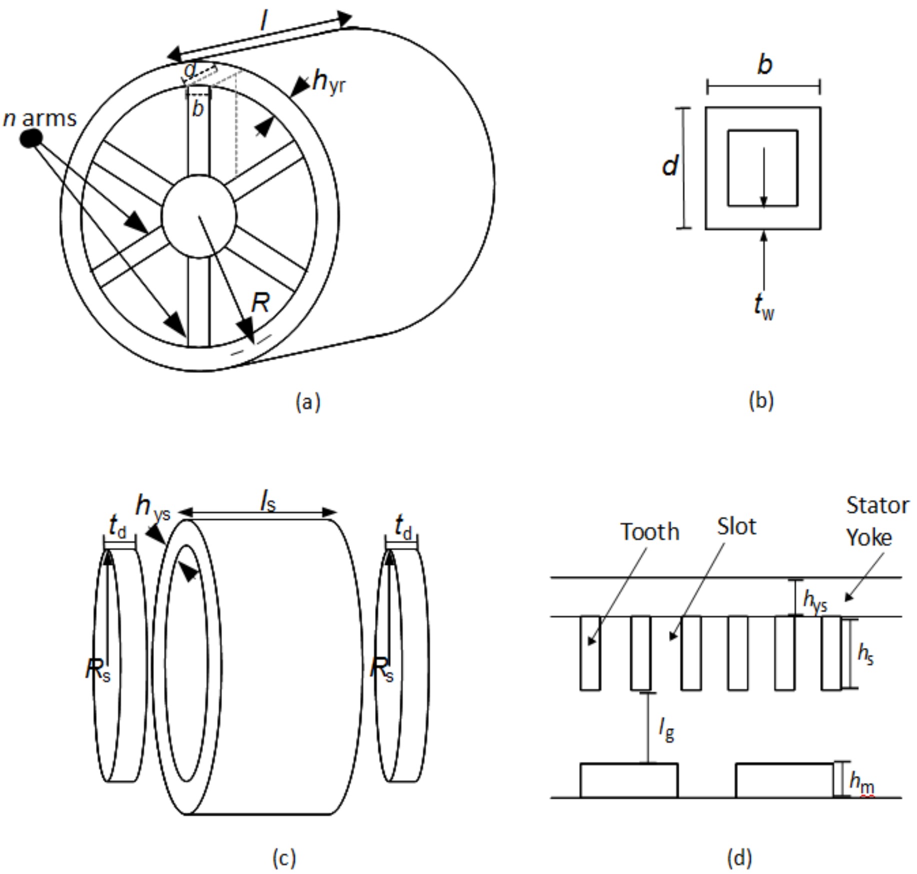

Figure 4 : Depiction of the variable dimensions that were used for the optimisation of the generator structures. (a) The variables that describe a structure with arms (b) The variables that describe a hollow arms (c) The variables that describe a structure with discs (d) The variables that describe the electromagnetic model.

1.2 Structural Optimisation

The three different generator topologies that were modelled and optimised are depicted in Figure 1. Topology-1 consists of an armed rotor and an armed stator. Both structures have hollow arms supporting them. Topology-2 consists of a rotor with disc and a stator with discs. Topology-3 consists of a rotor with disc and a stator with hollow arms. The structural optimisation of the different PMDD designs was achieved by using the analytical deflection models described in section 1.1.2 as constraints and the optimisation process described in section 1.1.3.

1.2.1 Topology-1: PMDD generator with arms

An existing analytical tool developed by McDonald and Mueller in [2] was extended to model and optimise a complete generator structure with arms.

In the first stages of the optimisation process, a constant airgap ($l_g/D=10\%$) and flux density ($B_g=1.1T$) were considered. The shear stress (σ) and the dimensions of the active parts on the rotor and the stator were then calculated for that flux, based on the UpWind design in [2].

The mathematical models of the rotor and the stator that describe both active and structural material of the generator were then combined to produce a full model of a PMDD generator with arms (referred to as *Structural Model*).

A more sophisticated model was then created by allowing the airgap length (l_g) to vary (referred to as *Airgap Model*). The mass of the permanent magnet on the rotor would vary in proportion in this case according to (5).

For the final stage of the optimisation process, the flux density in the airgap (B_g) was free to vary as well (referred to as *Flux Model*). In the last case where the flux density was free to vary, the shear stress (σ) was scaled in proportion with the airgap flux density and so the airgap varied accordingly. The new shear stress was calculated in this case by multiplying the flux density of the generator's airgap by the ratio of the shear stress that was used for all previous cases to the original flux density that was used in the UpWind design as shown in (15).

$$\sigma = B_g \frac{\sigma_{UpWind}}{B_{g_{UpWind}}} \tag{15}$$

This variation in the shear stress according to the flux density also affects the radial and torsional deflection, which are key criteria for the optimisation process.

The aspect ratio ($K_{\mathrm{rad}} = l/D$) of the most lightweight structure is presented in each case in order to see how the structural parameters of the generator change for the different structural optimisations.

1.2.2 Results

The optimal aspect ratios and masses of the lightest structures, along with the optimal values for the airgap length and the airgap flux density, are listed in Table 1.

Type of analytical model	*Structural Model*	*Airgap Model*	*Flux Model*
K_{rad}	1.002	1.121	0.71
B_g (T)	1.1	1.1	0.808
l_g/D (%)	0.1	0.21	0.21
Mass Rotor (kg)	49000	39000	35000
Mass Stator (kg)	88000	86000	83000
Total Mass (kg)	137000	125000	118000

Table 1: Dimensions and masses of most lightweight structures of a 5MW generator with arms

As Table 1 indicates, higher aspect ratios with longer airgap length and smaller flux density led to lighter structures for the first topology (Topology-1).

Although a small airgap length is consider as optimal for PMDD generators (approximately one thousandth of the airgap diameter), after allowing the airgap length to vary independently the best results would occur for an airgap length much greater than before, twice the so-called optimal airgap.

Allowing the flux density to vary, resulted in a lower flux density and led to even lighter structures. A greater flux density would give rise to the shear stress in proportion, so in order for the structure to be stiffer the structural mass that would support it would have to increase as well, making it much heavier.

1.2.3 Topology-2: PMDD generator with discs

A mathematical model of a generator with discs was created using the mathematical models described in section 1.1.2. The same optimisation process was carried out once again.

Since there is no formula to describe the torsional deflection of structures with discs, the objective function of this model was missing one constraint. The torsional deflection criterion was evaluated on a second stage for this structure, using a Finite Element Analysis (FEA) tool.

1.2.4 Results

The optimal aspect ratios and masses of the lighter structures, along with the optimal values for the airgap length and the airgap flux density, are listed in Table 2.

Type of analytical model	*Structural Model*	*Airgap Model*	*Flux Model*
K_{rad}	1.131	1.28	1.12
B_g (T)	1.1	1.1	1.05
l_g/D (%)	0.1	0.14	0.14
Mass Rotor (kg)	20000	22000	21000
Mass Stator (kg)	70000	67000	66000
Total Mass (kg)	90000	89000	87000

Table 2: Dimensions and masses of most lightweight structures of a 5MW generator with discs

Table 2 indicates that higher aspect ratios led to lighter structures for the second topology as well (Topology-2). Small airgap lengths and large flux densities led to the lighter strictures in this case though.

After allowing the airgap length to vary independently, the best results would appear for the minimum allowed value. This is contradictory to the results of the structural optimisation of Topology-1, where the most lightweight structure occurred for larger airgaps.

Higher airgap densities gave the lightest structures for Topology-2 unlike the results of the same optimisation for Topology-1, where the smaller the flux density, the lighter the structure. This is probably due to the absence of the torsional stress, which could not be modelled, from the constraints of the objective function.

In order to see if the dimensions of the most lightweight structures agree with the maximum deflection criteria, the torsional deflection was investigated. With the help of a FEA tool (0) the torsional deflection of the rotor and the stator with discs was calculated for the given torque. The torsional deflection that the FEA tool returned was almost three times greater than the allowable one (0.01° of relative twist). Therefore the disc thickness of both the rotor and the stator had to be increased in order to achieve a torsional deflection that was within limitations. This increase in the thickness of the discs added extra structural weight on both structures of this generator. The final structural weights of the rotor and the stator for Topology-2 are listed in Table 3.

Type of analytical model	*Structural Model*	*Airgap Model*	*Flux Model*
Mass Rotor (kg)	28000	29000	28000

Mass Stator (kg)	77000	74000	72000
Total Mass (kg)	105000	103000	100000

Table 3: New masses of most lightweight structures of a 5MW generator with discs

1.2.5 Topology-3: PMDD generator with disc rotor and armed stator

The mathematical models that describe a disc rotor and an armed stator were combined to give a third topology of a PMDD generator structure (Topology-3).

The same optimisation process was carried out once again. The necessary increase in the thickness of the rotor disk due to the torsional deflection criterion was included from the beginning for this topology by increasing the minimum disk thickness in the optimisation tool.

1.2.6 Results

The optimal aspect ratios and masses of the lighter structures, along with the optimal values for the airgap length and the airgap flux density, are listed in Table 4.

Type of analytical model	*Structural Model*	*Airgap Model*	*Flux Model*
K_{rad}	1.40	1.29	1.87
B_g (T)	1.1	1.1	1.21
l_g/D (%)	0.1	0.11	0.07
Mass Rotor (kg)	28000	29000	29000
Mass Stator (kg)	82000	81000	81000
Total Mass (kg)	110000	110000	110000

Table 4: Dimensions and masses of most lightweight structures of a 5MW generator with disc rotor and armed stator

Table 4 indicates that, once again, higher aspect ratios led to lighter structures for Topology-3 for all three analytical models. Small airgap lengths and large flux densities led to the lighter structures in this case though.

After allowing the airgap length to vary independently, the best results would appear for the minimum allowed value. The airgap length was even smaller compared to the same optimisation for Topology-2, very close to the value that is considered to be optimal for iron-cored direct drive generators ($l_g = D/1000$).

The aspect ratio of the machine decreased in this case, leading to an increase of its structural mass. The total mass of the machine does not increase though because the small airgap length of the machine led to decrease of its active mass, keeping the total weight on the same level as before.

Finally, when the flux density in the airgap was allowed to vary, the results had the same trend as those of Topology-2. The most lightweight structures occurred for a very large aspect ratio, small airgap length and high flux density. This was the largest aspect ratio that occurred in all optimisations (K_{rad} = 1.87) and the largest flux density as well (B_g = 1.21 T).

In this final optimisation for Topology-3, the most lightweight structure occurred for a larger aspect ratio. Although this increase in the aspect ratio decreased the structural mass of the machine, the very large flux density increased the active mass, leading once again to the same result for the total mass of the generator.

1.3 Cost Optimisation

Apart from the structural optimisation of both the active and inactive parts of the generator, a cost optimisation was also done using the same mathematical models. This was achieved by introducing costs for the materials used in the construction of the generator into the objective function. The costs that were introduced were

- The cost of steel (€5/kg)
- The cost of copper (€15/kg)
- The cost of PM material (€35/kg)

Although structural steel is cheaper than laminations, they were treated the same for simplification. A more detailed cost optimisation for a generator would also include the manufacturing costs which are not included in this cost analysis. Expensive structures and structures that could not match the deflection and torque limitations were penalised, thus leading to the cheapest possible structure that can produce the necessary torque for the machine.

1.3.1 Topology-1: PMDD generator with arms

Using the previously defined models and the above mentioned costs, a simple cost optimisation was achieved. The optimal aspect ratios, the total costs and masses of the cheapest structures, along with the optimal values for the airgap length and the airgap flux density, are listed in Table 5.

Type of analytical model	*Structural Model*	*Airgap Model*	*Flux Model*
K_{rad}	1.302	1.254	0.913
B_g (T)	1.1	1.1	0.89
l_g/D (%)	0.1	0.15	0.22
Mass Rotor (kg)	48000	45000	33000
Mass Stator (kg)	88000	85000	62000
Total Mass (kg)	136000	130000	95000
Total Cost (€)	881000	864000	687000

Table 5: Dimensions, masses and total costs of cheaper structures of a 5MW generator with arms

When introducing costs for the materials of the structure and repeating the optimisation process, larger aspect ratios and smaller airgap lengths were preferred for Topology-1. The airgap length was once again greater than the fixed optimal one, but not as great as for the structural optimisation. This is because the active materials of the generator, the magnet on the rotor and the copper on the stator, are much more expensive than the steel used for the structure. Therefore, the optimisation program reduces the extra cost of these materials by increasing the radius of the structure and keeping a smaller airgap length at the same time.

1.3.2 Topology-2: PMDD generator with discs

The same cost optimisation was undertaken for Topology-2. Table 6 shows the optimal aspect ratios, the total costs and masses of the cheapest structures, along with the optimal values for the airgap length and the airgap flux density.

Type of analytical model	*Structural Model*	*Airgap Model*	*Flux Model*
K_{rad}	1.06	0.775	0.686
B_g (T)	1.1	1.1	0.934
l_g/D(%)	0.1	0.09	0.06
Mass Rotor (kg)	30000	31000	31000
Mass Stator (kg)	48000	48000	50000
Total Mass (kg)	78000	79000	81000
Total Cost (€)	600000	570000	553000

Table 6: Dimensions, masses and total costs of cheaper structures of a 5MW generator with discs

After introducing costs for the materials of the generator with discs structure and repeating the optimisation process, high aspect ratios were preferred once more, but not as great as the ones that occurred for the same topology during its structural optimisation. The airgap length and flux density converged to the ideal values.

Although the total mass of the generator increased when using the cost optimisation for the *Airgap Model* and the *Flux Model*, the total cost decreased. This can be attributed to the great price difference between active and inactive materials. Since steel is much cheaper compared to permanent magnets and copper, the optimisation program reduced the total cost by adding extra inactive material (decrease of aspect ratio) and reducing the active material on the structure (minimum airgap length and smaller flux density).

1.3.3 Topology-3: PMDD generator with disc rotor and armed stator

The same cost optimisation was undertaken for Topology-3. Table 7 shows the optimal aspect ratios, the total costs and masses of the cheapest structures, along with the optimal values for the airgap length and the airgap flux density.

Type of analytical model	*Structural Model*	*Airgap Model*	*Flux Model*
K_{rad}	1.35	1.00	0.97
B_g (T)	1.1	1.1	0.964
l_g/D (%)	0.1	0.08	0.05
Mass Rotor (kg)	29000	29000	29000
Mass Stator (kg)	80000	80000	86000
Total Mass (kg)	109000	109000	115000
Total Cost (€)	749000	719000	702000

Table 7: Dimensions, masses and total costs of cheaper structures of a 5MW generator with disc rotor and armed stator

Once again, high aspect ratios were preferred in the three different optimisation models for Topology-3, but not as great as those obtained during the structural optimisation of the same topology. When the airgap length was free to vary, it tended towards the minimum value. The flux density in the airgap was decreased by a small amount when it was introduced as a variable in the optimisation process.

The same trend that was noticed for Topology-2 between the total mass of the generator and its total cost was repeated for this topology as well. The optimisation process tried to reduce the total cost for this type of generator by adding extra structural material and taking away as much active material as possible. This was achieved by reducing the aspect ratio and the flux density of the machine, while keeping the airgap to the minimum possible value.

1.4 Comparison

Figure 5 shows the weights and the costs of the best structures that occurred during the structural or the cost optimisation of the three different topologies for the three different optimisation models that were used (fixed airgap length and flux density - variable airgap length and fixed flux density - variable airgap length and flux density).

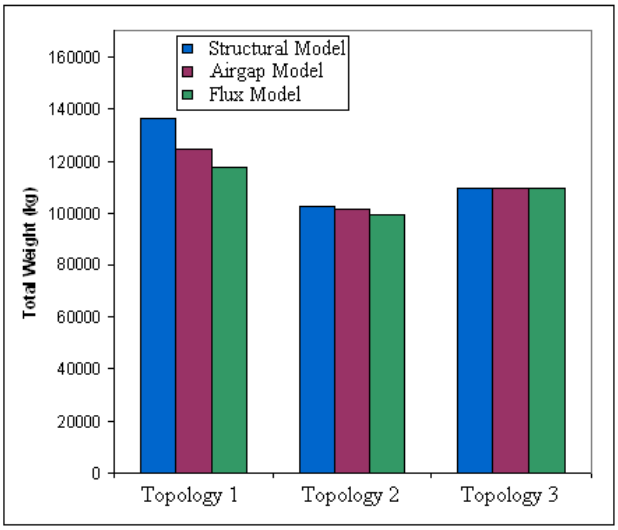

(a)

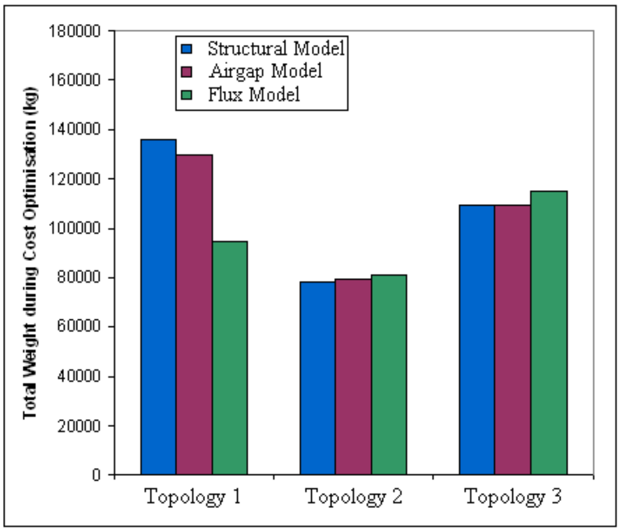

(b)

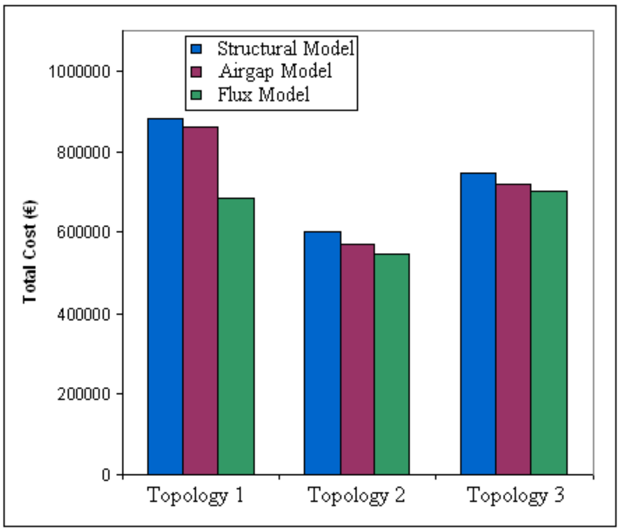

(c)

Figure 5 : Comparison of total weight and total cost of the three different topologies (a) Total weight for structural optimisation (b) Total weight for cost optimisation (c) Total cost for cost optimisation

Figure 5 (a) shows the weight of the best structures that occurred during the structural optimisation. The weight of Topology-1 and 2 decreases as the airgap and the flux density are introduced as variables. Topology-2 had the smallest weight in this case.

Figure 5 (b) shows the weight of the best structures that occurred during the cost optimisation. The weight of Topology-1 decreases as the airgap and the flux density are introduced as variables, while it increases for Topology-2 and 3. This difference between Topology-1 and the other two can be attributed to the fact that higher aspect ratios were preferred in that case. Topology-2 had the smallest weight in this case as well.

Figure 5 (c) shows the cost of the best structures that occurred during the cost optimisation. The cost of all three topologies decreases as the airgap and the flux density are introduced as variables. Topology-2 had the smallest cost in this case as well.

1.5 Conclusions

The optimisation of the cost and the materials used for the structure of a direct drive generator was the main aim of this research. Structural and electromagnetic characteristics of a PMDD generator were integrated together in order to get the best results. Three different generator topologies with arms and discs were tested and optimised with the help of the genetic algorithm toolbox. The main conclusions and discussions that can be extracted after comparing the results of the different generator types are outlined in this section.

During the structural and cost optimisation of the three topologies, higher aspect ratios were preferred in all the cases that were tested (fixed airgap length and flux density - variable airgap length and fixed flux density - variable airgap length and flux density). This is because as the axial length increases, the structure becomes more rigid against the radial and the torsional deflection, thus requiring less structural material to maintain its shape. Although there was a drop in the aspect ratio of the structures during their cost optimisation, the aspect ratio remained high in all cases.

Regarding the different topologies, the generator with discs (Topology-2) was lighter and cheaper compared to the other two. This could be attributed either to the fact that generators with discs are generally lighter compared to structures with arms.

It is a common rule for the development of a direct drive generator, to allow an airgap between the rotor and the stator of an approximate length $l_g = D / 1000$ (≈4mm for a 4m diameter). The optimisation process verified this structural rule for generator structures whose topology included at least one disc structure (Topology-2 or Topology-3). This was not the case though for armed generators. For the case of Topology-1, a greater airgap length (l_g) is preferred (≈9 or 10mm). This is due to the fact that the structures with disc are stiffer, hence more resistant to the radial deflection. Therefore they do not have the need of a larger airgap like the structures with arms do. Although this might be the case, another explanation could be that the optimisation models do not describe accurately all parameters and deflections. In order to come to a conclusion regarding this matter, further work is needed.

As far as the flux density is concerned, a relatively weak airgap flux density (B_g) would lead to lighter and cheaper structures in the case of a direct drive generator with an armed rotor, whereas a high one is preferred for a generator with disc rotor. A large flux density tends to give a larger deflection in the radial direction. Since the rotor with disc is stiffer than its armed counterpart, it can withstand greater radial deflections and so the flux density does not need to be reduced in its case.

The results presented reinforce the need to optimise both the electromagnetic and structural design together.

Section 2 Shape Optimisation of generator structures with arms

2.1 Introduction

For this research the arm of a structure of a rotor with arms was designed including part of the rotor's back and the shaft of the rotor. Symmetry regions were added on both sides of the structural model so that the Finite Element Analysis (FEA) tool would "think" that this model is part of a whole structure with arms, as it has been modelled and depicted in Figure 6 .

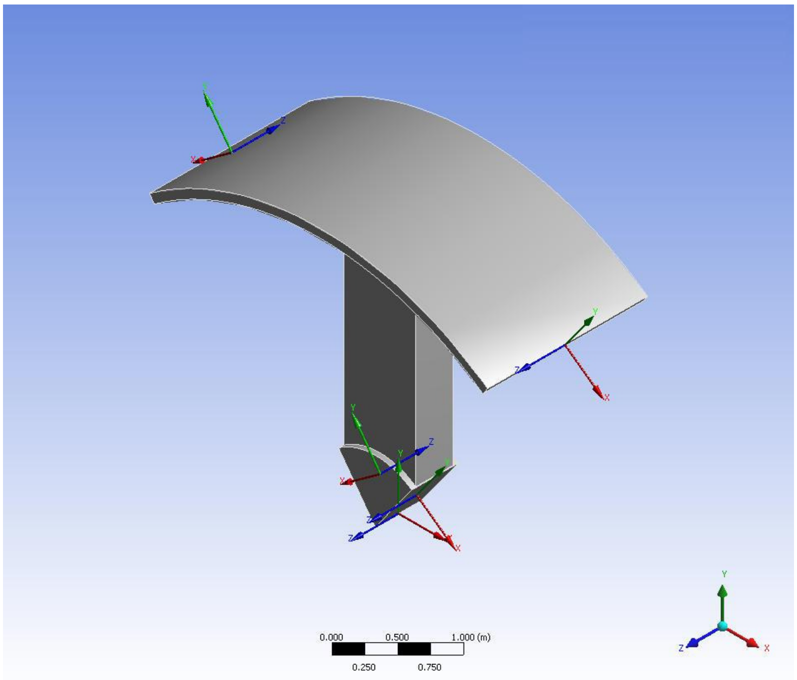

Figure 6 - Original shape and symmetry regions

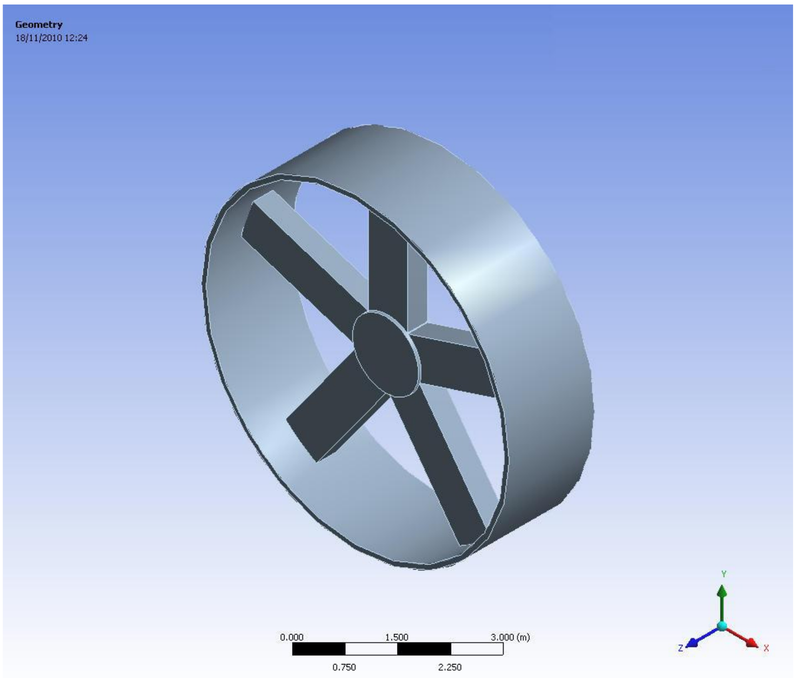

Figure 7 – Complete structure of rotor with 5 arms

Figure 8 shows the dimensions of the modelled arm of the structure. The dimensions in the original case were:

- R = 3m (the radius of the rotor)
- l = 1.717m (axial length)
- $K_{rad} = 0.3$
- d = 0.4m (arm's depth)
- $h_{yr} = 0.09$m (rotor back thickness)

The radius of the rotor shaft was R_o=0.5m while the breadth b of the arm was calculated according to Eqn 16.

$$b = \frac{2\pi R_o}{n} \tag{16}$$

where R_o the radius of the shaft and n the number of arms of the structure. For the illustrated scenario the number of arms was set to five (n=5).

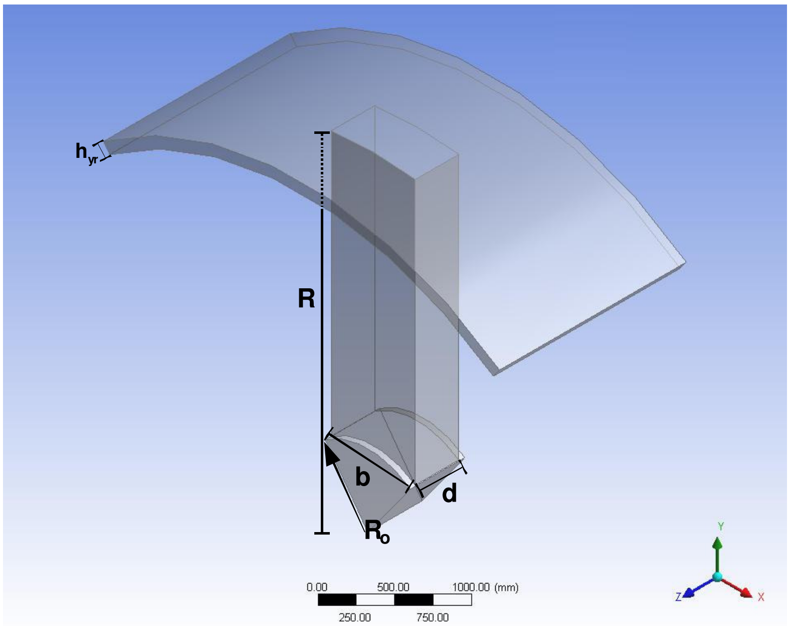

Figure 8 – Structural Dimensions

This structural design was chosen to model a 5MW generator with arms. The dimensions of the machine were great enough to provide the necessary torque needed for the nominal power output of such a generator. At the same time, the rotor back and the arm's dimensions were chosen to be great enough to maintain the necessary airgap clearance against the structural forces that act on the generator's structure (Maxwell stress – gravitational stress – circumferential stress).

The geometry mentioned above was then introduced to the shape optimisation tool. The loads that applied on this geometry were chosen to be the same that would apply on the rotor of a 5MW direct drive generator:

- The radial pressure on the surface of the rotor due to the normal component of the Maxwell stress (q = 280 kPa).

- A moment that gives rise to a stress in the tangential direction (circumferential stress), which represents the force that the magnetic field of the stator applies to the rotor and vice versa as the stator acts like a "brake" to the circular movement of the rotor (M_o = 4.42 MNm).

The target reduction for the given body that should be stiff enough to withstand the above mentioned loads was set to 30%. The output of the shape finder can be seen in Figure 9 .

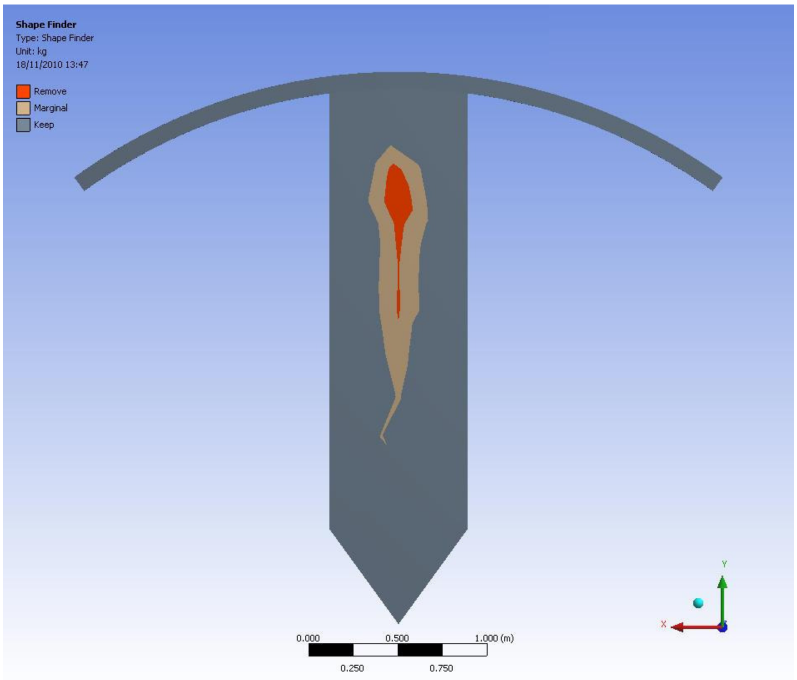

Figure 9 - Structure after shape optimisation

It seems that the major part that could be removed from the structure illustrated above is an elliptical part in the upper section of the arm. In order to understand how this shape changes according to all the possible variables, a number of experiments took place in order to specify how and in what degree each parameter affects the outcome of the shape optimisation tool.

The possible parameters that were tested were:

- The radial stress (normal component of Maxwell stress)
- The circumferential moment
- The radius of the structure (R)
- The number of arms (n) or the arms' breadth (b)
- The arm's depth (d)
- The percentage of target reduction (%)

In each case, only one of the parameters varies when all the others are kept to their original values which are K_{rad}=0.3, R=3m, d=0.4m, h_{yr}=0.09m, radial stress q=280kPa, moment M_o=4.42MNm and target reduction=30%. The axial length of the structure varies when the radius varies in order to retain the same K_{rad}. The breadth of the arm varies according to the number of arms that the final structure of the rotor is supposed to have.

The first step to take in order to understand why the shape optimisation tool comes up with specific results would be to experiment on the two major forces that apply on the given model (Radial & Circumferential stress).

2.2 Testing the Different Parameters

2.2.1 Increasing Radial Stress

For the first stage of this research, the tested structure was subjected to optimisation taking under consideration only the radial deflection that is applied on it – a moment was not included in this case. This happened in order to understand how the Maxwell stress affects the given structure. The Maxwell stress increased from 80kPa up to 680kPa. Figure 10 illustrates some of the resulting outputs of the shape optimisation tool for this case.

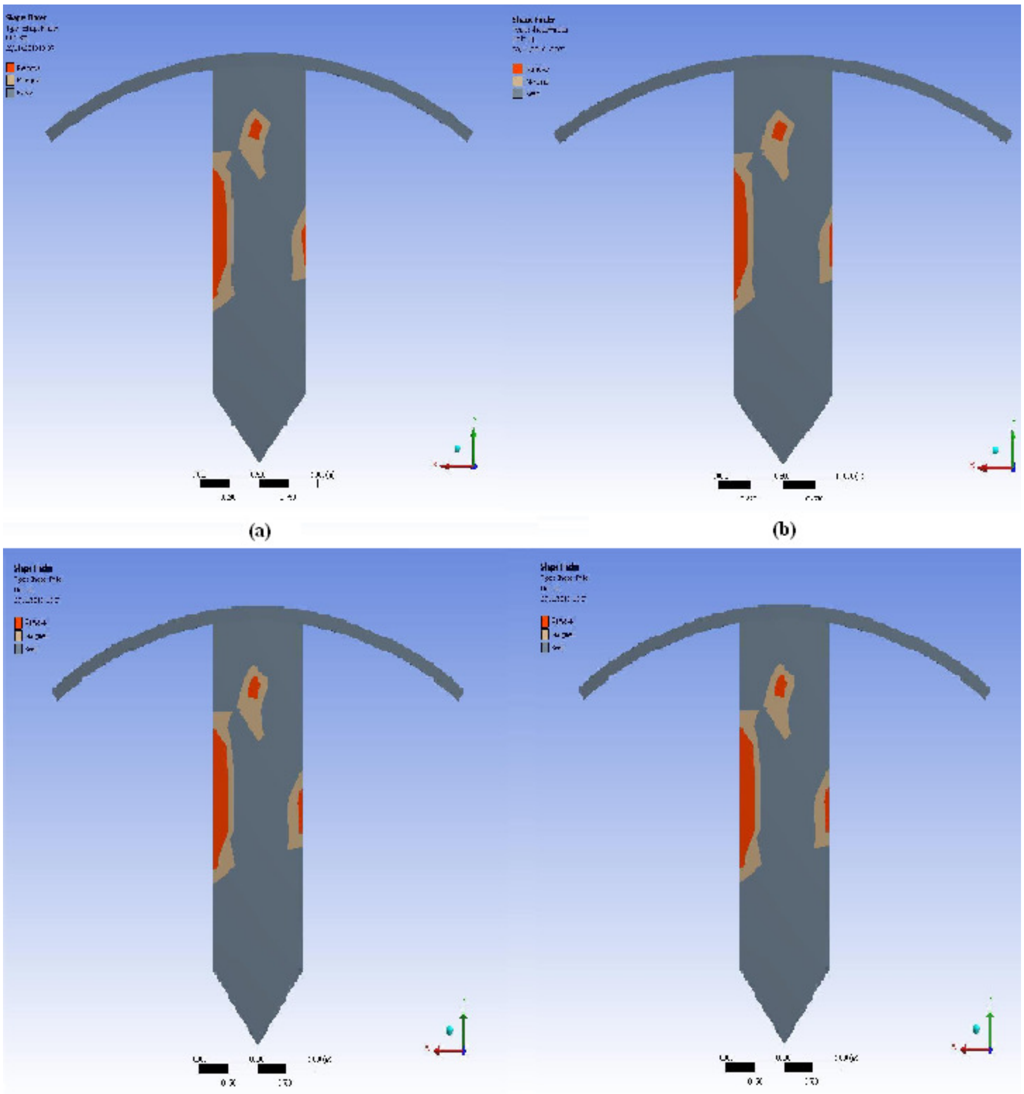

Figure 10 - (a) 80kPa, (b) 280kPa, (c) 480kPa, (d) 680kPa

As Figure 10 suggests, the part near the sides of the arm could be removed if just the radial stress was to be taken under consideration. Furthermore, it seems like the unnecessary part of the structure remains the same in all tested cases.

In a second stage the moment that gives rise to the circumferential stress was introduced as well. Figure 11 illustrates the same results for the given structure including the circumferential stress.

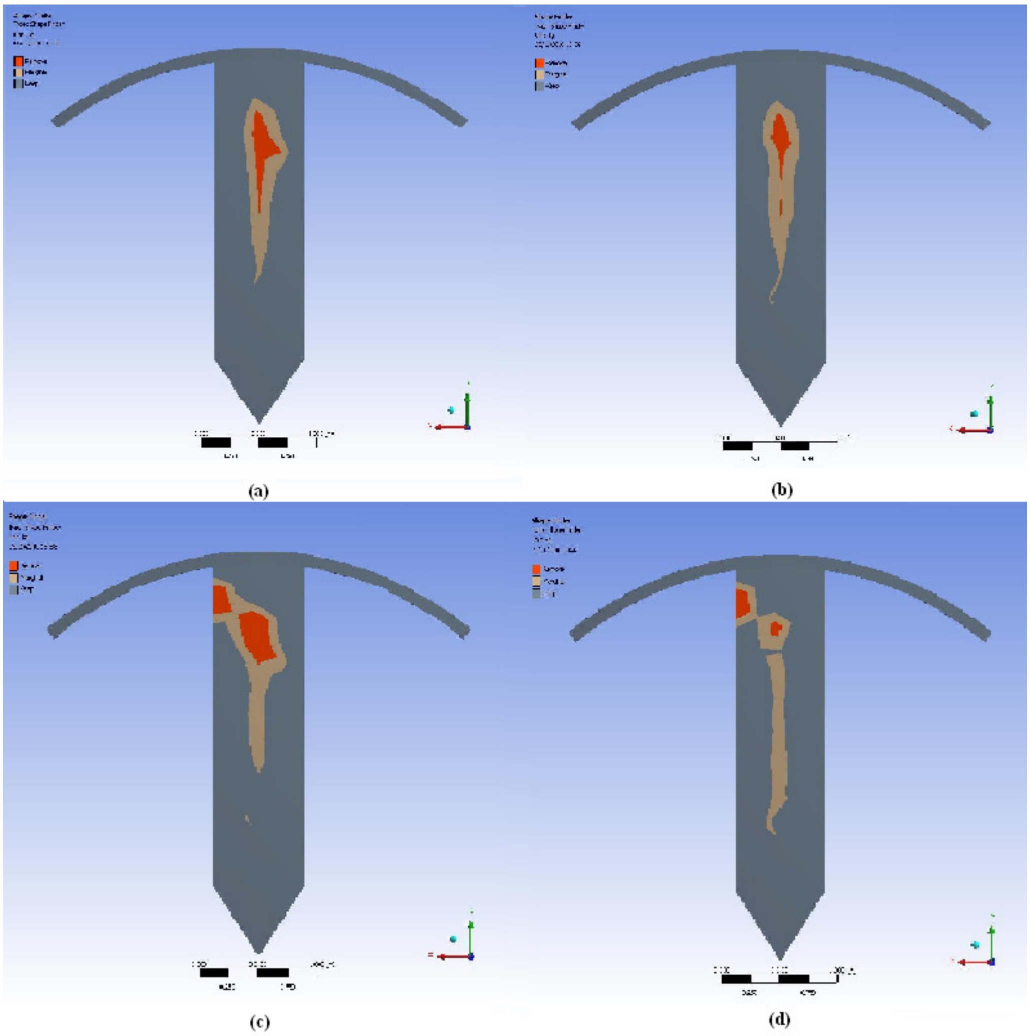

Figure 11 - (a) 80kPa, (b) 280kPa, (c) 480kPa, (d) 680kPa

Figure 11 shows that when the moment is taken into consideration as well, the part that could be removed changes dramatically in shape and location. For a small radial stress the unnecessary part is located in the upper-middle part of the arm and as the radial stress increases it becomes smaller and "moves" towards the upper-left part of the shape.

This can be attributed to the fact that in order to withstand the increasing radial stress, the arms of the structure should be solid in their centre.

2.2.2 Increasing Moment

Using the same procedure as before, a rising moment was introduced in the program on its own without any radial stress acting on the structure. The moment increased from 2.42MNm up to 8.42MNm. Figure 12 illustrates some of the resulting outputs of the shape optimisation tool for this case.

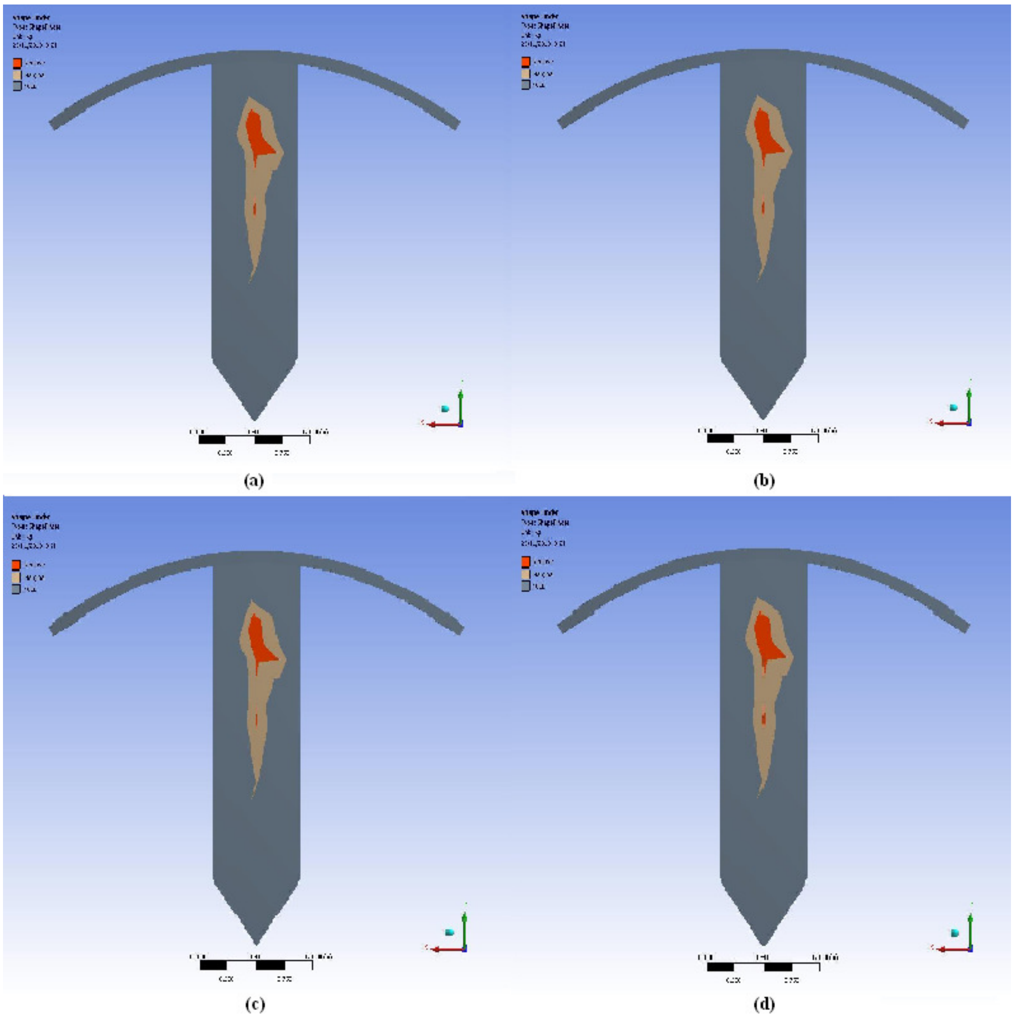

Figure 12 - (a) 2.42MNm, (b) 4.42MNm, (c) 6.42MNm, (d) 8.42MNm

As Figure 12 suggests, the part near the upper-middle part of the arm could be removed if just the circumferential stress applied on the tested structure. The unnecessary part of the structure remains the same as the moment increases.

In a second stage the radial stress was introduced as well. Figure 13 illustrates the same results for the given structure including the stress on the radial direction.

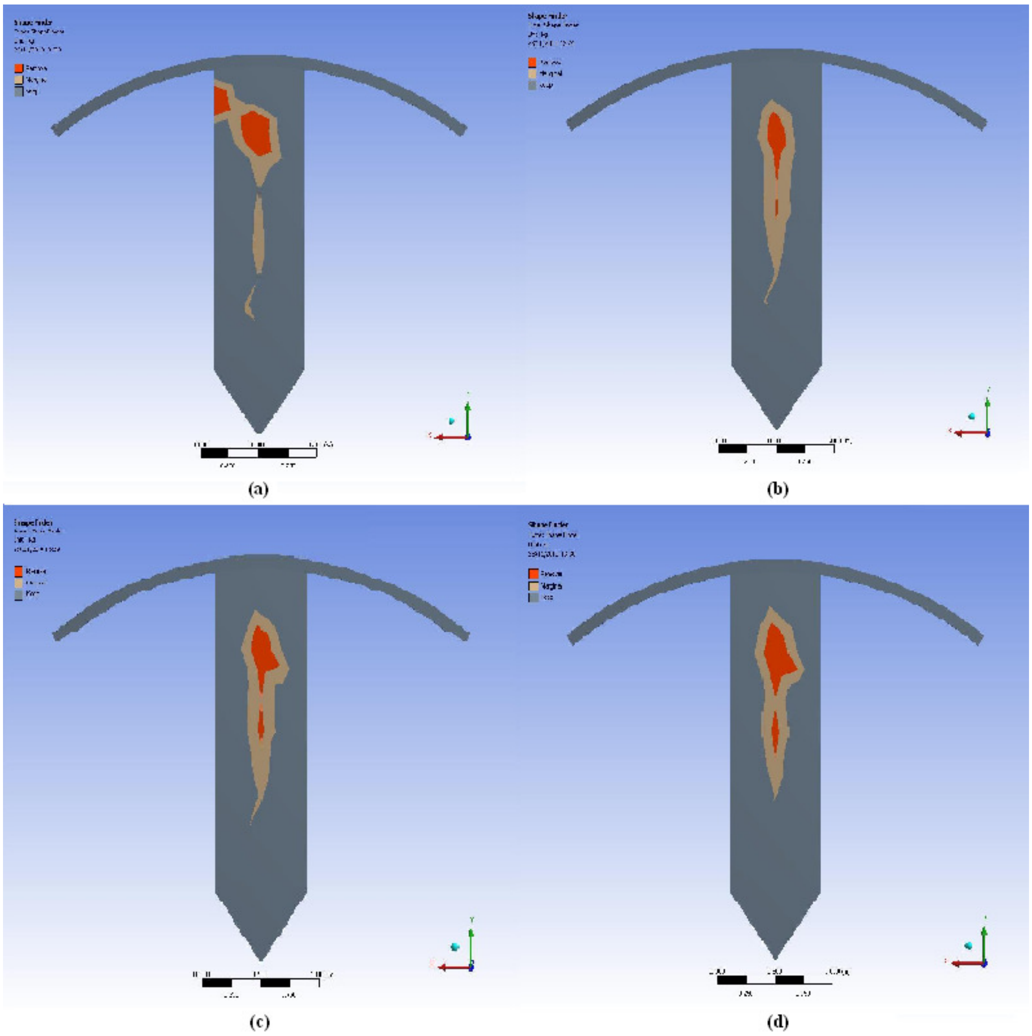

Figure 13 - (a) 2.42MNm, (b) 4.42MNm, (c) 6.42MNm, (d) 8.42MNm

Figure 13 shows that when both forces are taken into consideration, the part that could be removed changes in shape as the moment increases. For a small moment the unnecessary part is rather round but as the moment increases it becomes more elliptical. In all cases, the removable part was located in the upper-middle part of the arm.

This can be attributed to the fact that in order to withstand the increasing circumferential stress, the structure should be more solid on its sides. These are quite the opposite results from the ones in before where the Maxwell stress increased and shows that these two forces need different parts of the structure in order to remain robust enough.

Apart from the forces that apply, another important factor that can drive the outcome of the structural optimisation tool is the structural variables of the tested structure. The variables that were tested during this research were the radius and the depth of the arm of the structure. Each time that a parameter was tested, values of the rest remained the same as described in "Introduction".

2.2.3 Increasing Radius (*R*)

The radius of the shape varied from 1.5m up to 5m. In each case the axial length of the rotor's back varied accordingly in order to retain the aspect ratio of the structure static and equal to 0.3 ($K_{rad}=l/2R$). Figure 14 illustrates some of the resulting outputs of the shape optimisation tool.

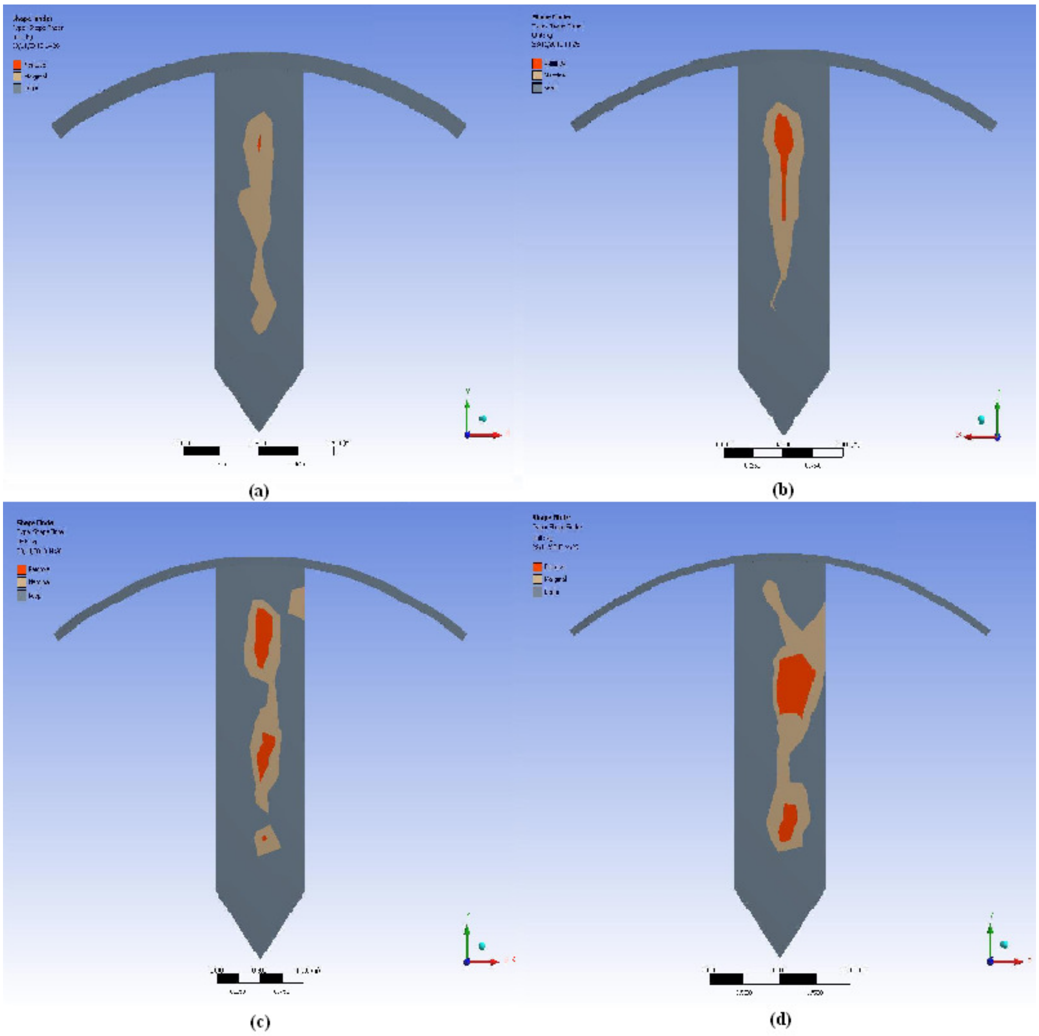

Figure 14 - (a) *R*=2m, (b) *R*=3m, (c) *R*=4m, (d) *R*=5m

For a small radius there is almost nothing that could be removed from the arm of the structure. As the radius increases, the unnecessary part that is outlined on the arm appears on the upper-middle part. For larger radiuses a second part that could be removed appears in the lower-middle section of the arm. Finally, for the larger radius tested, the two unnecessary parts, become bigger in size and "move" lower near the rotor's shaft.

This leads to the conclusion that as the radius increases but the arm depth remains the same, the structure becomes more resistant against the structural stresses, thus larger parts of it could be removed without any risk to the stiffness of the complete structure.

2.2.4 Increasing Arm Depth (*d*)

The depth of the structure's arm varied from 0.4m up to 0.7m. Figure 15 illustrates some of the resulting outputs of the shape optimisation tool.

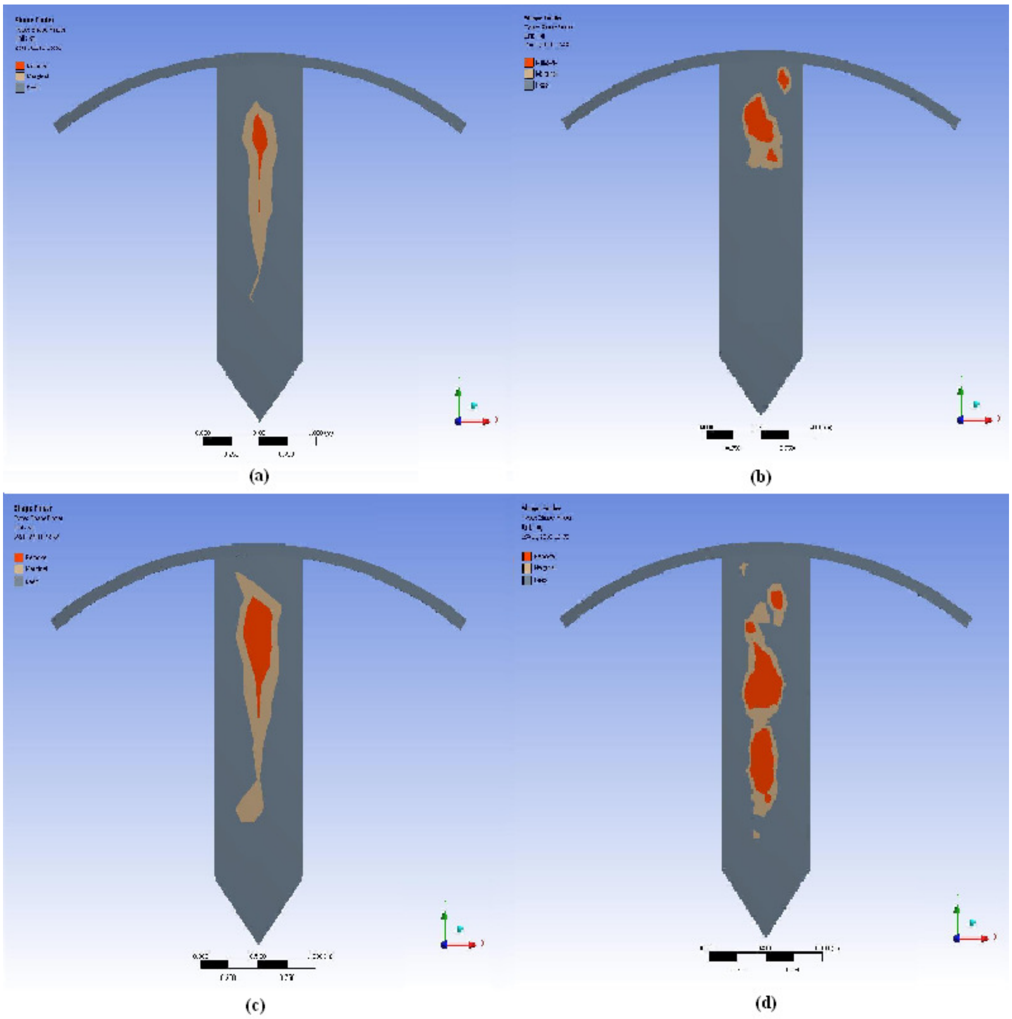

Figure 15 - (a) *d*=0.4m, (b) *d*=0.5m, (c) *d*=0.6m, (d) *d*=0.7m

As the thickness increases, the originally small elliptical red part that could be removed increases in size. In the final optimisation with the larger tested arm thickness, the removable part becomes even larger in size and "moves" closer to the centre of the arm.

As the arm's thickness increases, the structure becomes more robust thus more resistant to both structural forces that apply on it. Therefore greater part of its mass could be removed from the rotor's arm without the danger of the structure losing its shape due to the radial or circumferential deflection.

2.2.5 Increasing Arm Breadth (b)

As described in (16), b is inversely proposal to the number of arms of the structure. In other words, by decreasing the arm's breadth the number of arms on the rotor's structure is increased. Figure 16 illustrates some of the resulting outputs of the shape optimisation tool.

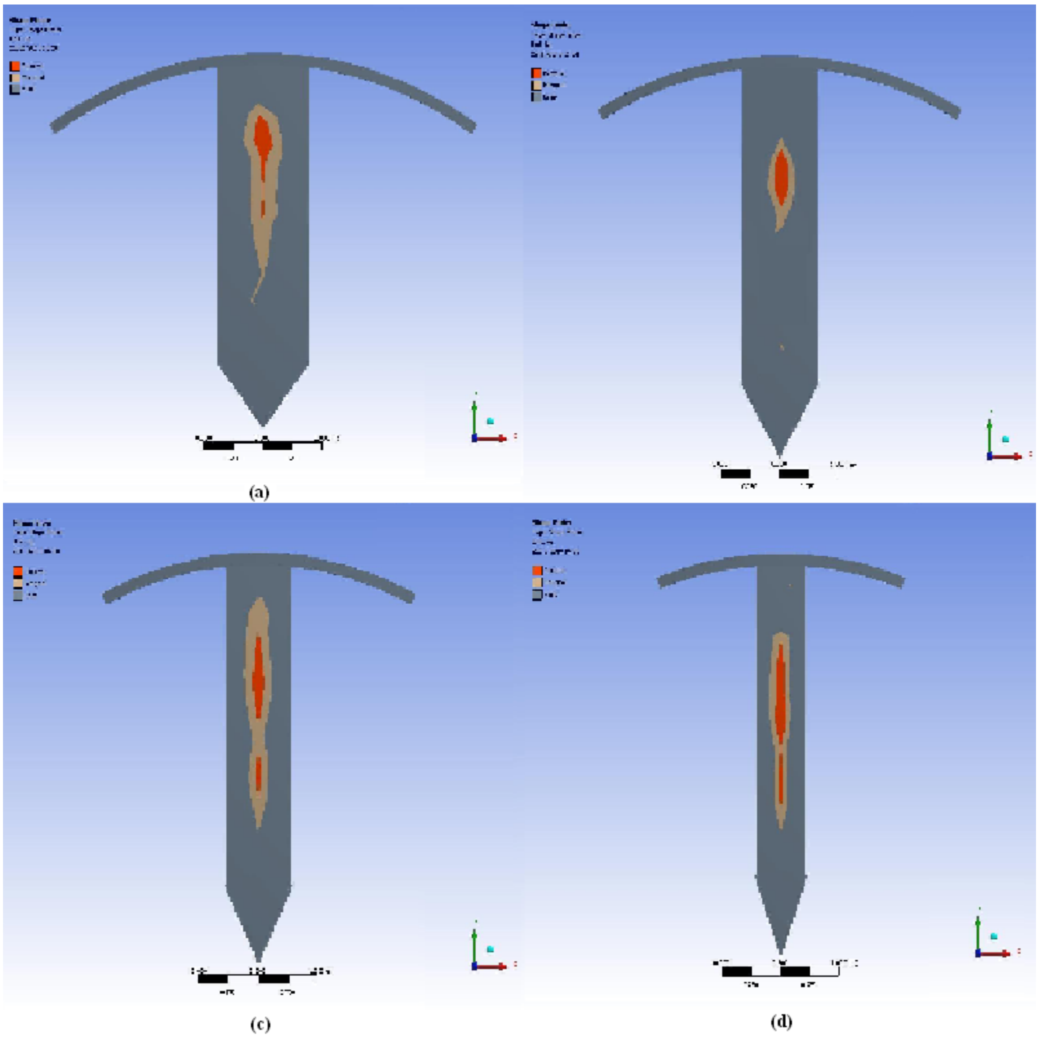

Figure 16 - (a) b=0.628m – 5arms, (b) b=0.524m – 6arms, (c) b=0.449m – 7arms, (d) b=0.349m – 9arms

As Figure 16 indicates, for small number of arms (n<7) the removable part on the rotor's arm is rounder and located on the upper section of the arm. For larger number of arms (n≥7) the unnecessary part is longer and narrower and is spread along the centre of the rotor's arm.

2.2.6 Increasing target reduction (%)

The final parameter that was tested was the target reduction of the structure. This is not a reliable parameter though since the higher the target reduction the less stiff and robust the final structure would be, leading to unreliable results. Nonetheless, it was tested in order to understand the trend with which the marginal part and the part that should be removed are changing. The target reduction varied from 10% up to 40%. Figure 17 illustrates some of the resulting outputs of the shape optimisation tool.

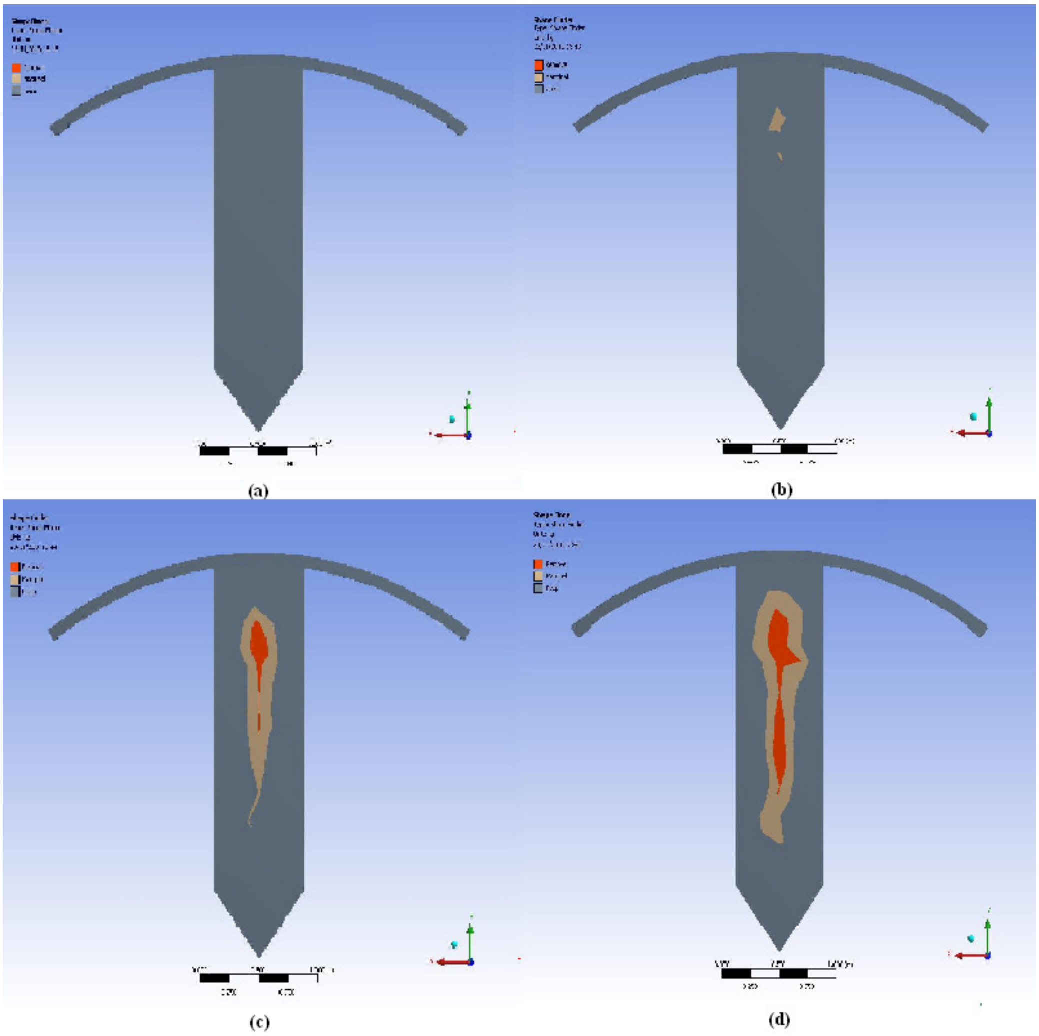

Figure 17 - (a) 10%, (b) 20%, (c) 30%, (d) 40%

As it should have been expected, the area of the red coloured part of the tested structure increased together with the percentage of the target reduction.

Originally, there is no outlined area that should be removed. As the target reduction increases, a marginal area appears in the upper-middle part of the arm which then turns into the part that could be removed from the rotor's arm. In the final stage, the removable area becomes longer and extends across most of the arm's length. It is unknown though at which point the remaining structure stops being robust enough and becomes unable to maintain the airgap clearance.

2.2.7. Conclusions

According to the research described in the previous sections, in order to optimise the structure of a direct drive rotor with arms, the greatest concern should be the number of arms of the structure.

Although the part that could be removed is affected by the Maxwell stress that acts on the rotor and the moment that gives rice to the circumferential stress, their magnitudes are static and can be calculated beforehand. Thus there can be no practical variation of the removable part due to these parameters.

Finally, although the radius length and the arm's thickness give greater removable areas, these parameters should be kept in minimum possible values because they add a lot of structural mass on the rotor.

The next step of this research would be the creation of the structural model of a complete rotor with arms bearing the new pattern that was outlined with the help of the shape optimisation tool. Since there is quite a variation among the patterns depending on the number of arms n, a large number of different models should be created in order to find which case returns the most lightweight structure but also to make sure that the radial and circumferential deflections are within limitations.

2.3 Rotor Modelling

For the second part of this research, a number of structural models of a rotor with arms were created. Each model differs from the others according to its number of arms.

In each case the different structures are structurally optimised according to the output of the shape optimisation tool. The new optimised models are then compared to the original structures in order to find out in what degree the structure's mass has been decreased and how much the radial and circumferential deflection have changed.

2.3.1 Rotor with 5 arms

A model of a rotor with five arms was created in order to compare its structural mass and its radial and circumferential deflection with the ones of the new design. The mass of the rotor with 5 arms was 58700kg. Its dimensions were: R=3m, l=1.717m, b=0.628m, d=0.4m and h_{yr}=0.09m (Figure 18).

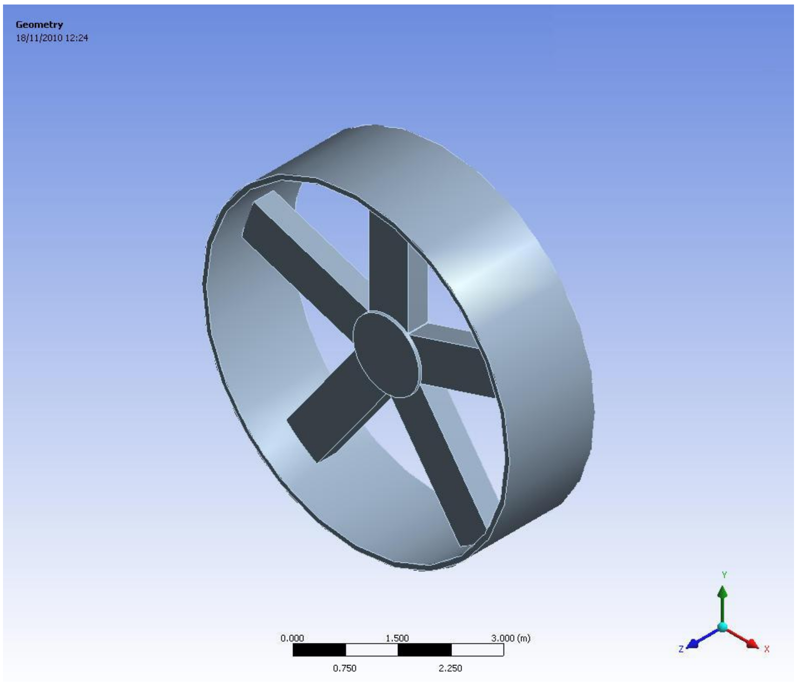

Figure 18 - Rotor with 5 arms

The radial deflection was $u_A = 2.88\times10^{-4}$ m ($u_{A\_max} = 3\times10^{-4}$ m) and the circumferential deflection due to rotation was $z_A = 5.57\times10^{-4}$ m ($z_{A\_max} = 6\times10^{-4}$ m) (Figure 19)

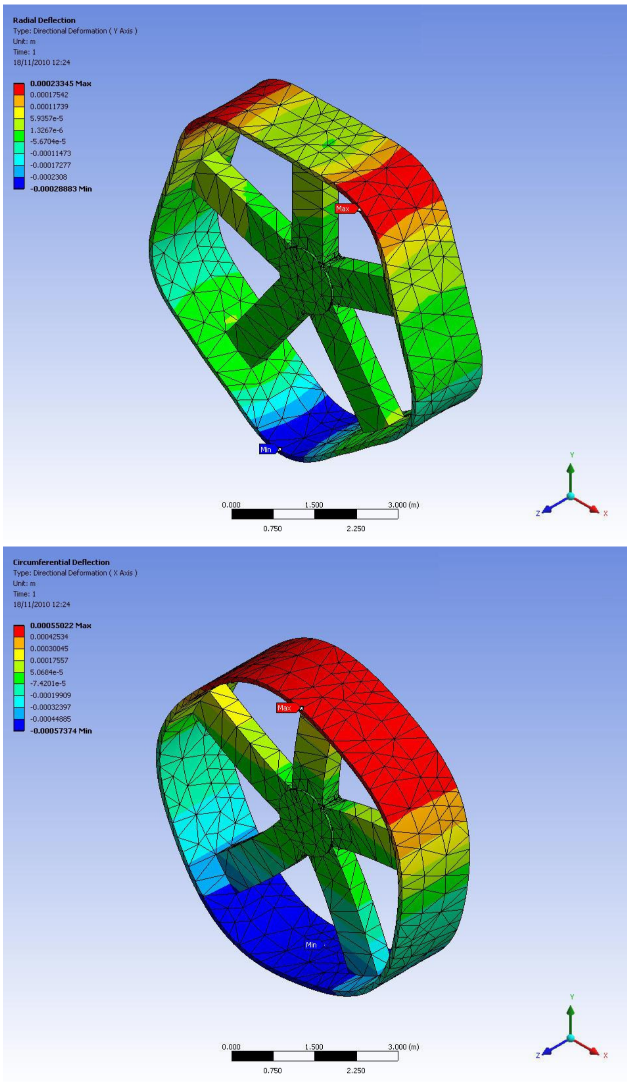

Figure 19 – Radial and Circumferential deflection of 5-armed structure

A model of this structure's arm was introduced into the shape optimisation tool with a 30% target reduction. The output of the shape finder can be seen in Figure 20 .

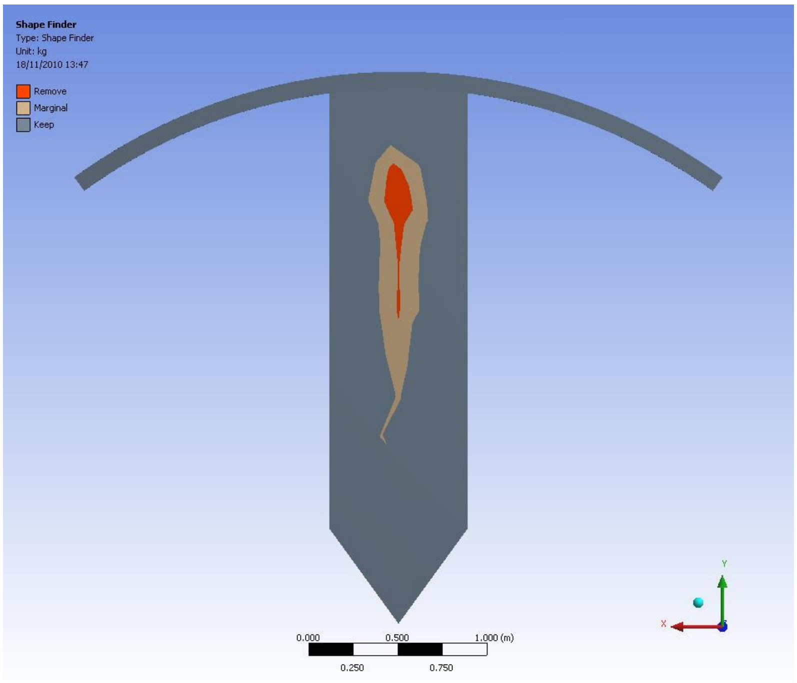

Figure 20 - Shape Finder output

The next step was an attempt to remove the portion of the arm's mass that the shape finder outlined as unneeded. The new geometry that was created is illustrated in Figure 21 .

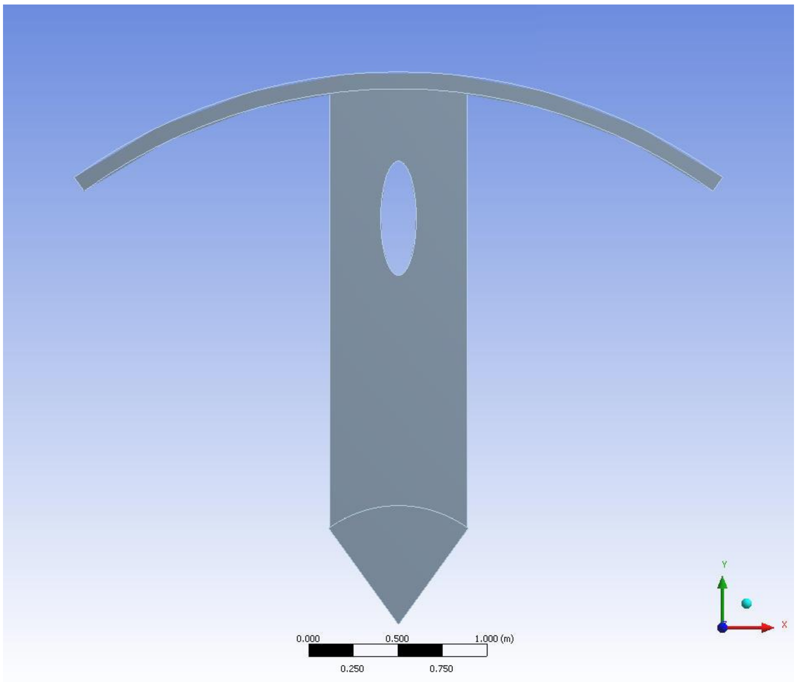

Figure 21 - Structure after shape optimisation

A comparison between the two shapes is given below (Figure 22).

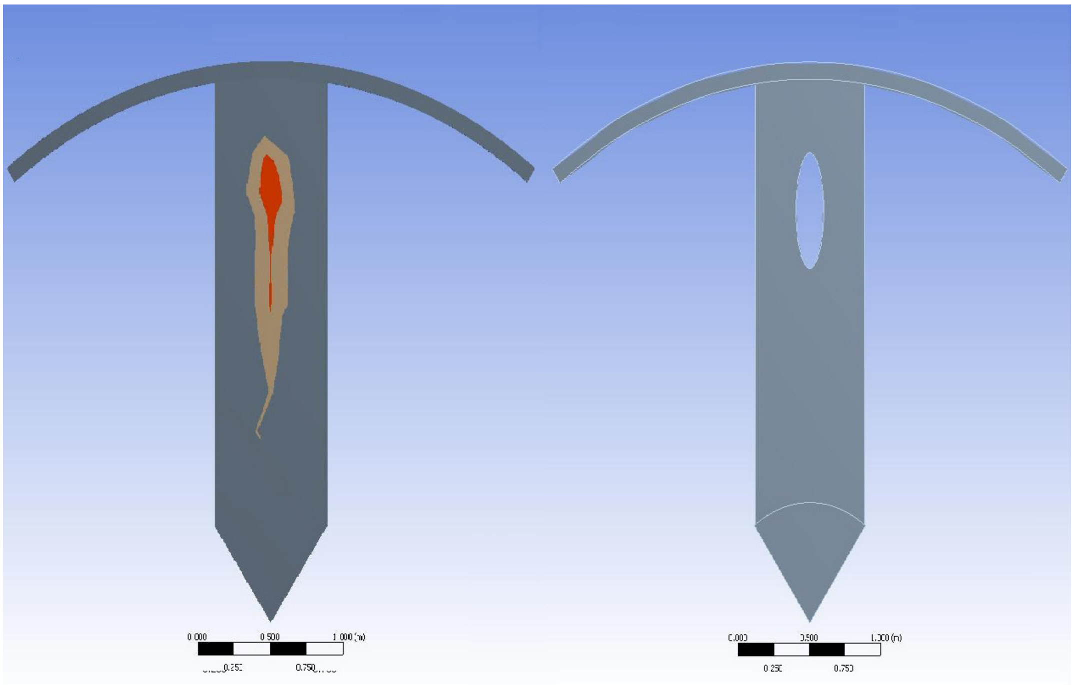

Figure 22 - On the left the shape finder's output. On the right the designed geometry

The new geometry was introduced as a pattern in the design tool in order to create a complete rotor with five arms and the desired pattern on its arms (Figure 23).

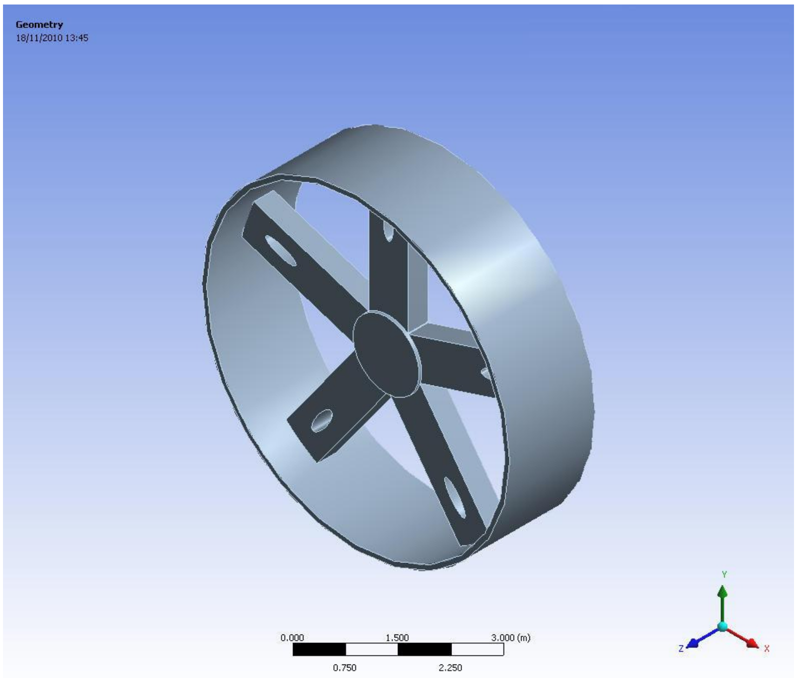

Figure 23 - Shape optimised rotor with 5 arms

The total mass of the rotor was reduced compared to the original design from 58700kg to 57100kg (3% mass reduction). This rotor design was tested for its stiffness against the two major deflections. The radial deflection was $u_A = 2.87\times10^{-4}$ m and the circumferential deflection due to rotation was $z_A = 5.96\times10^{-4}$ m (Figure 24).

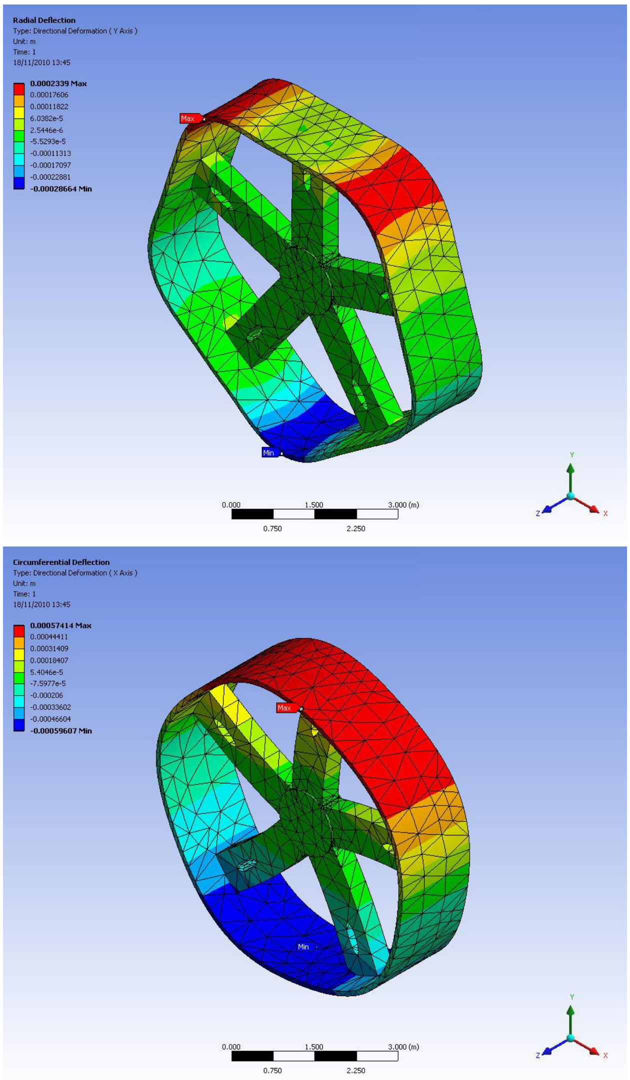

Figure 24 – Radial and Circumferential deflection for shape optimised rotor with 5 arms

The radial deflection remained the same as the original structure. The circumferential deflection increased by 0.39×10-4m compared to the original 5-armed rotor structure but remained within limitations.

2.3.2 Rotor with 6 arms

A structural model of a rotor with six arms was created in order to compare its structural mass and its radial and circumferential deflection with the ones of the new design. The mass of the rotor with 6 arms was 64200kg. Its dimensions were: R=3m, l=1.717m, b=0.524m, d=0.500m and h_{yr}=0.085m (Figure 25).

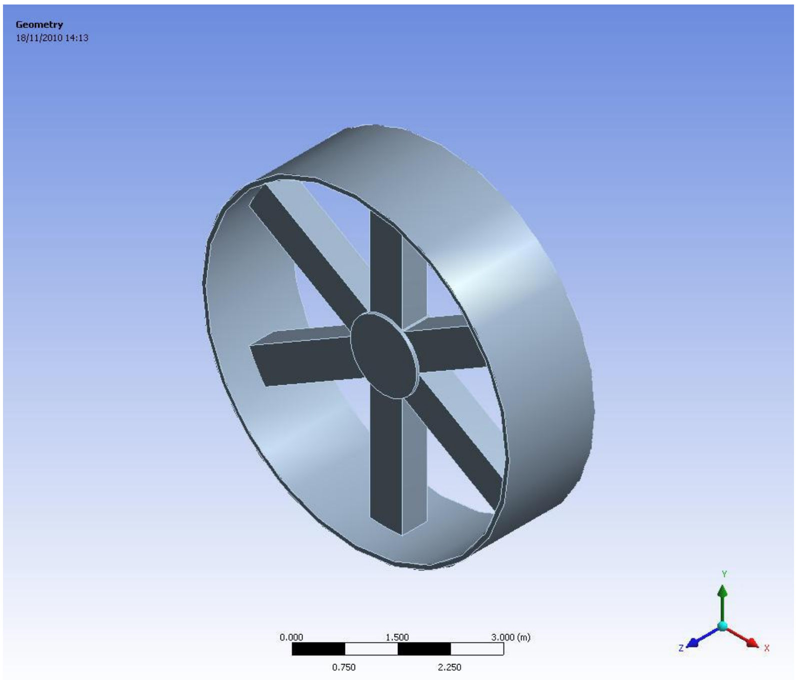

Figure 25 - Rotor with 6 arms

The radial deflection was u_A = 2.70×10^{-4} m (u_{A_max} = 3×10^{-4} m) and the circumferential deflection due to rotation was z_A = 5.83×10^{-4}m (z_{A_max} = 6×10^{-4} m) (Figure 26)

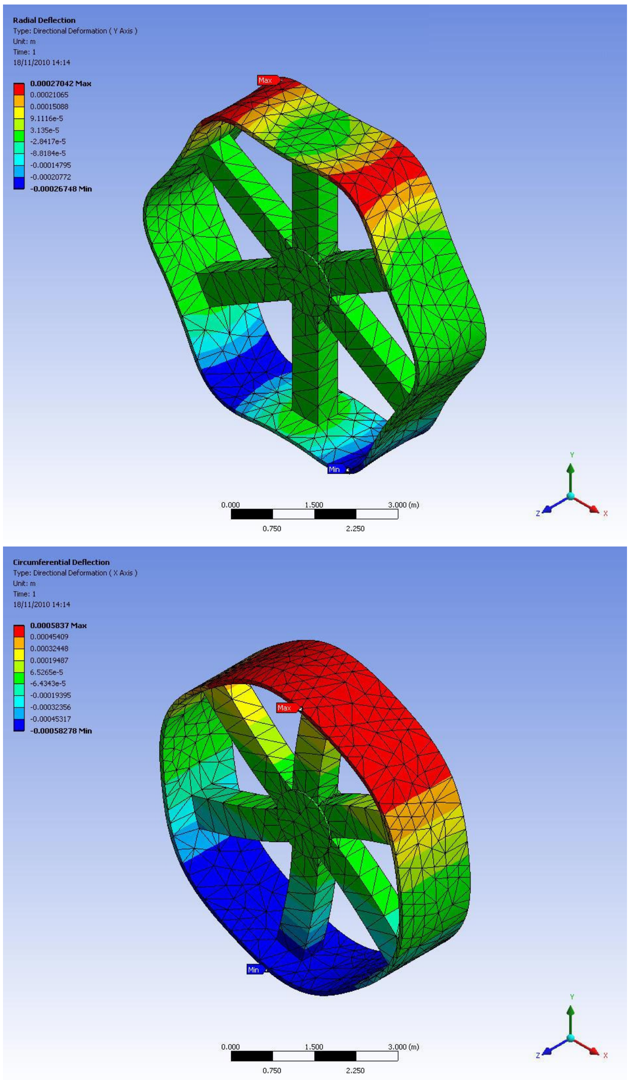

Figure 26 – Radial and Circumferential deflection of 6-armed structure

Same as before, a model of this structure's arm was introduced into the shape optimisation tool. The target reduction for the given body was set to 30%. The output of the shape finder can be seen in Figure 27 .

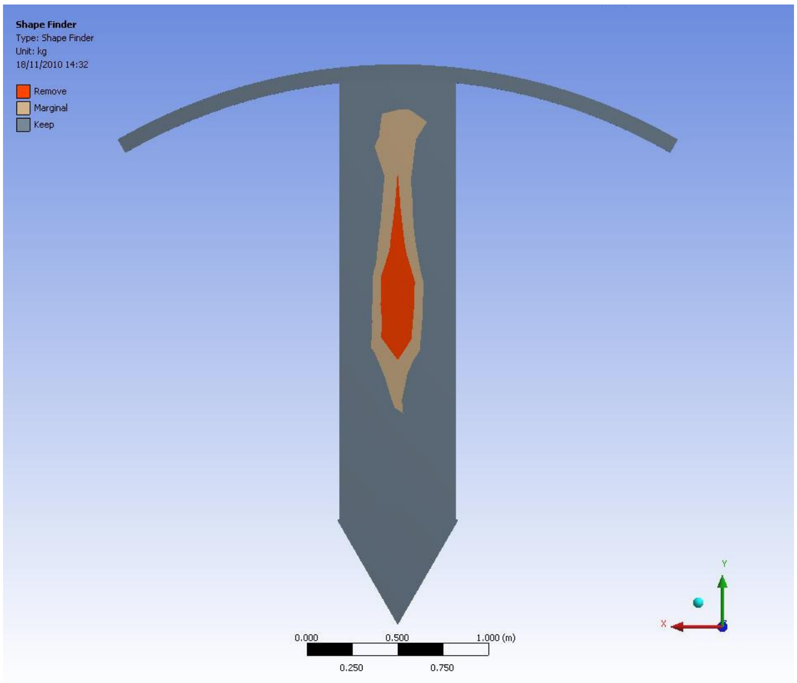

Figure 27 - Shape Finder output

The outlined part of the arm was removed. A comparison between the two shapes is given below (Figure 28). An optimised rotor with 6 such arms is depicted in Figure 29 .

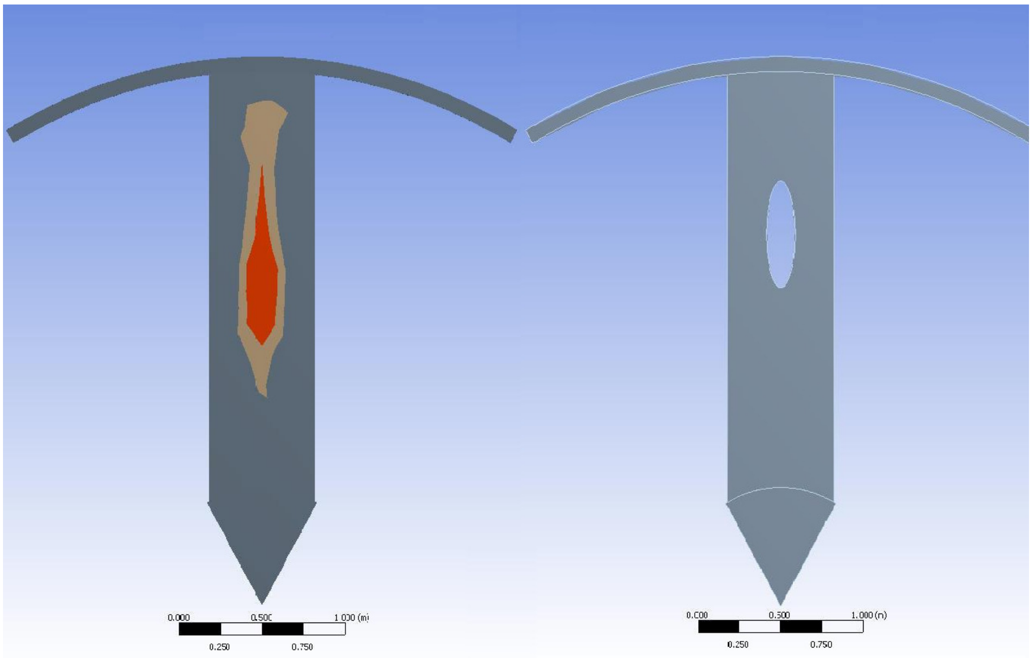

Figure 28 - On the left the shape finder's output. On the right the designed geometry

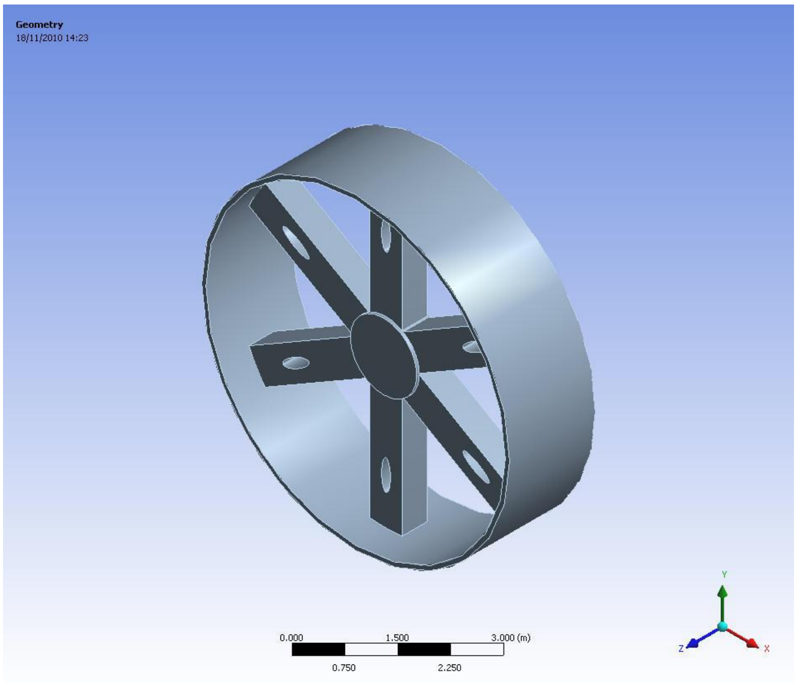

Figure 29 - Shape optimised rotor with 6 arms

The total mass of the rotor was reduced compared to the original design from 64200kg to 62200kg (3.1% mass reduction). This rotor design was tested for its stiffness against the two major deflections. The radial deflection was $u_A = 2.75\times10^{-4}$ m and the circumferential deflection due to rotation was $z_A = 6.05\times10^{-4}$ m (Figure 30).

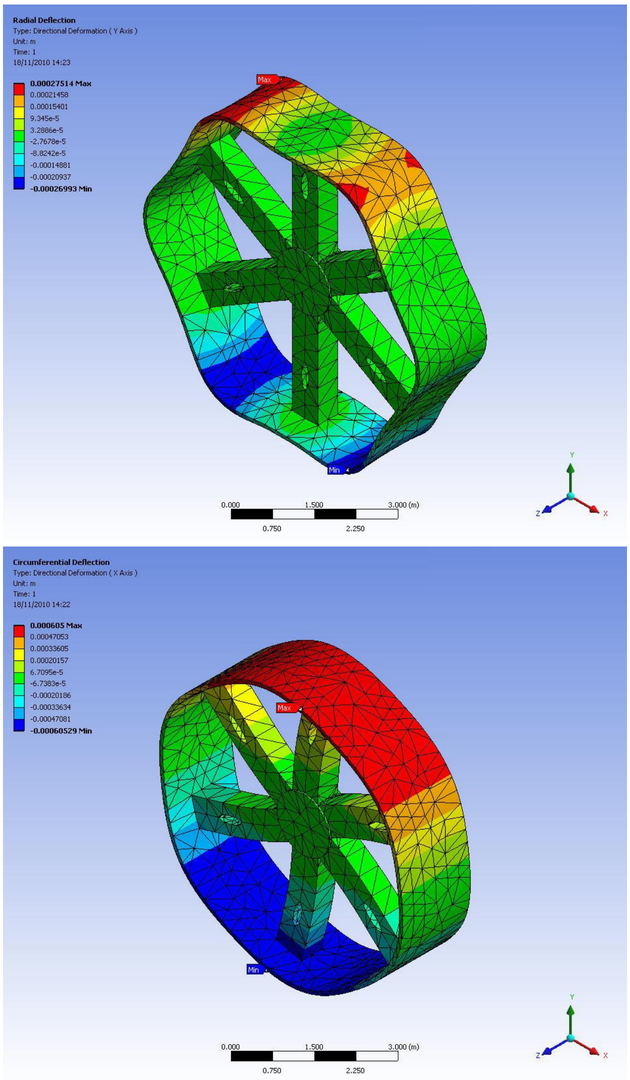

Figure 30 – Radial and Circumferential deflection for shape optimised rotor with 6 arms

The radial deflection increased by 0.05×10-4m compared to the original 6-armed rotor structure. The circumferential deflection also increased by 0.22×10-4m but remained within limitations.

2.3.3 Rotor with 7 arms

Following the same procedure once again, a structural model of a rotor with seven arms was created in order to compare its structural mass and its radial and circumferential deflection with the ones of the new design. The mass of this rotor was 72200kg. Its dimensions were: R=3m, l=1.717m, b=0.449m, d=0.580m and h_{yr}=0.085m (Figure 31).

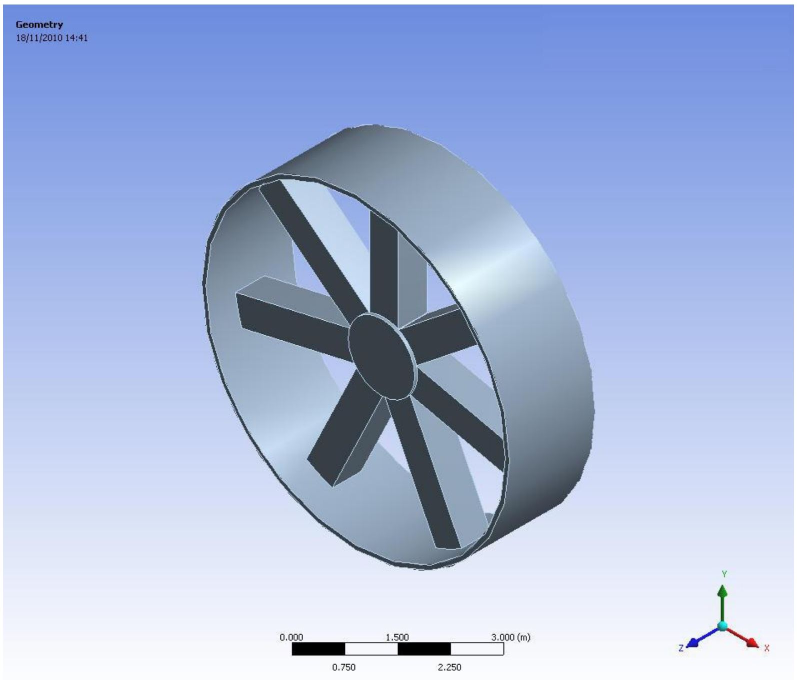

Figure 31 - Rotor with 7 arms

The radial deflection was u_A = 2.75×10^{-4} m (u_{A_max} = 3×10^{-4} m) and the circumferential deflection due to rotation was z_A = 5.77××10^{-4} m (z_{A_max} = 6×10^{-4} m) (Figure 32)

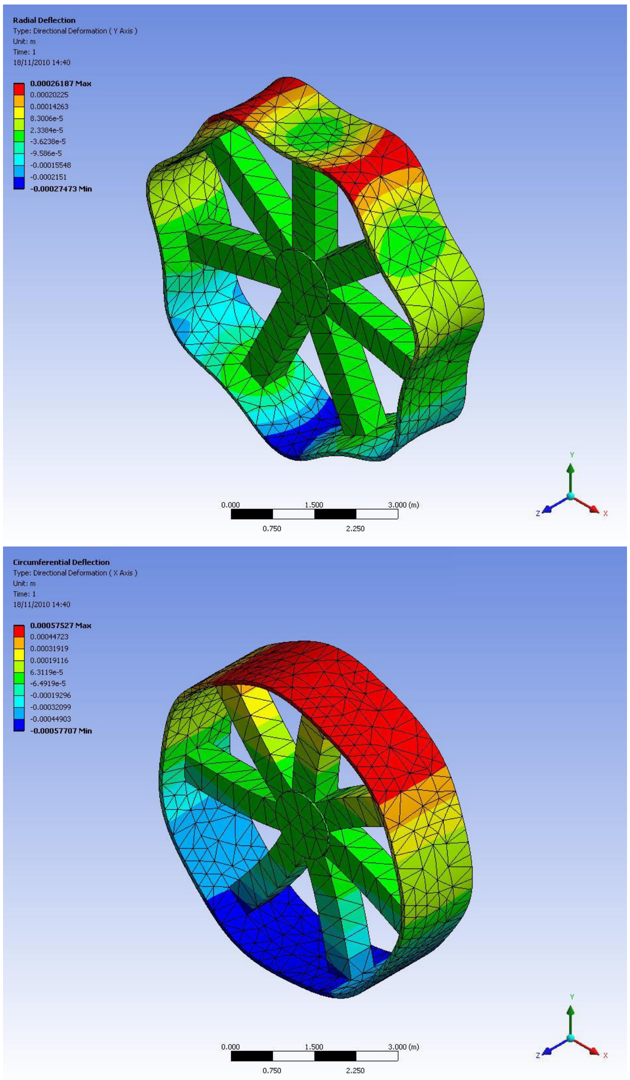

Figure 32 – Radial and Circumferential deflection of 7-armed structure

Same as before, a model of this structure's arm was introduced into the shape optimisation tool. The target reduction for the given body was set to 30%. The output of the shape finder can be seen in Figure 33 .

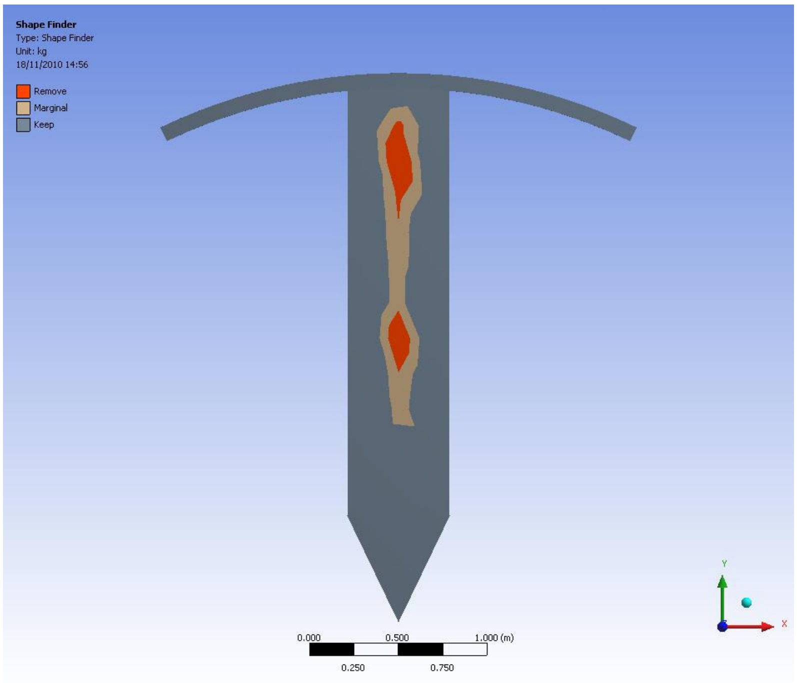

Figure 33 - Shape Finder output

The outlined part of the arm was removed. A comparison between the two shapes is given below (Figure 34). The optimised rotor with 7 such arms is depicted in Figure 35 .

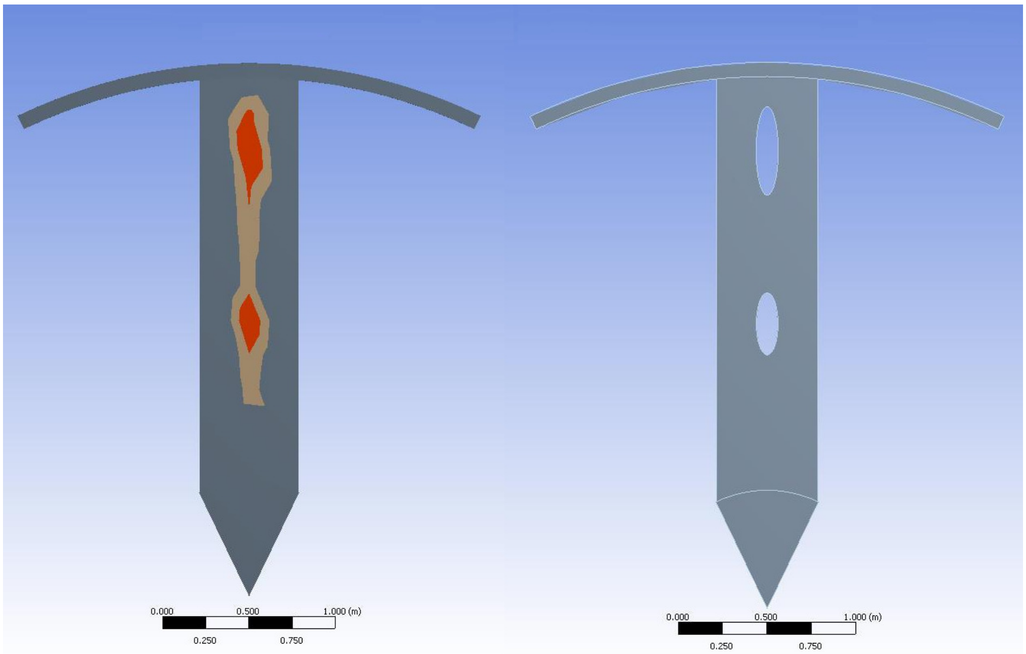

Figure 34 - On the left the shape finder's output. On the right the designed geometry

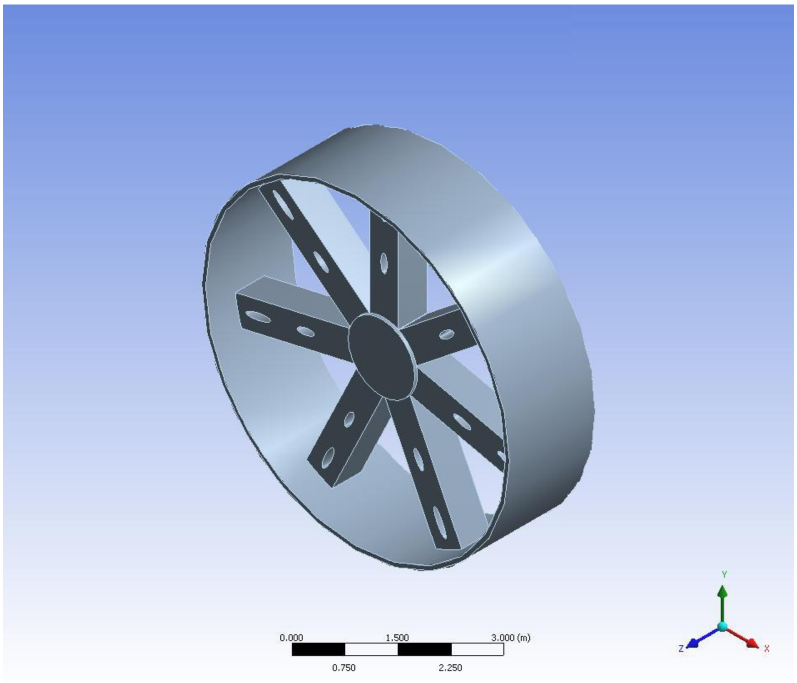

Figure 35 - Shape optimised rotor with 7 arms

The total mass of the rotor was reduced compared to the original design from 72200kg to 68200kg (5.5% mass reduction). This rotor design was tested for its stiffness against the two major deflections. The radial deflection was $u_A = 2.96 \times 10^{-4}$ m and the circumferential deflection due to rotation was $z_A = 5.97 \times 10\text{-}4$m (Figure 36).

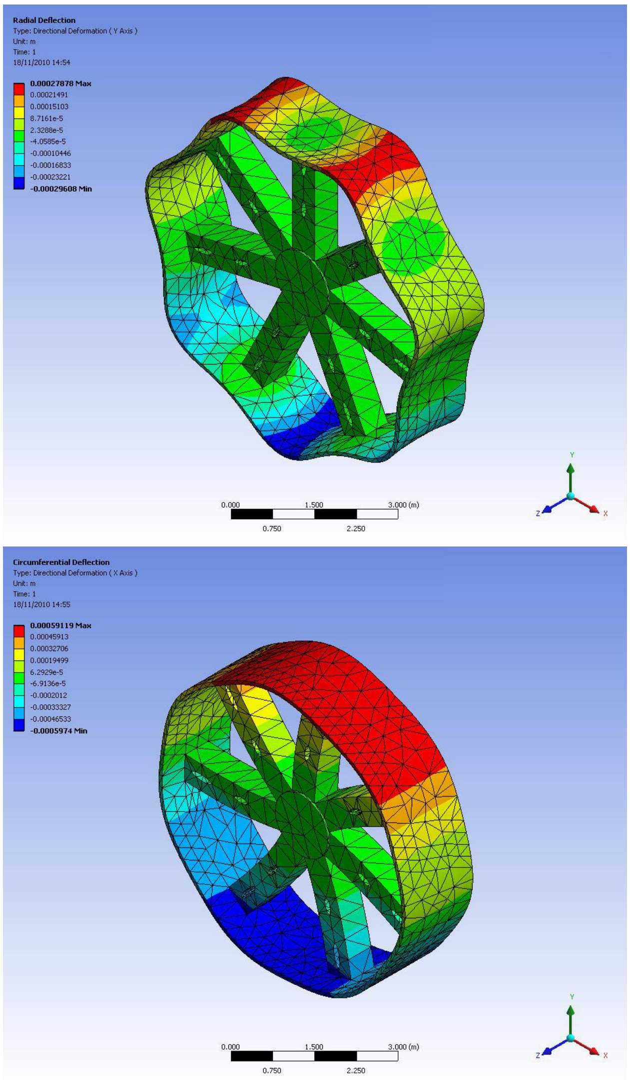

Figure 36 – Radial and Circumferential deflection for shape optimised rotor with 7 arms

The radial deflection increased by 0.21×10^{-4}m compared to the original 7-armed rotor structure and the circumferential one also increased by 0.20×10^{-4}m. Both deflections remained within limitations.

2.3.4 Rotor with 8 arms

Following the same procedure, a structural model of a rotor with eight arms was created. The mass of this rotor was 79000kg. Its dimensions were: R=3m, l=1.717m, b=0.393m, d=0.650m and h_{yr}=0.080m (Figure 37).

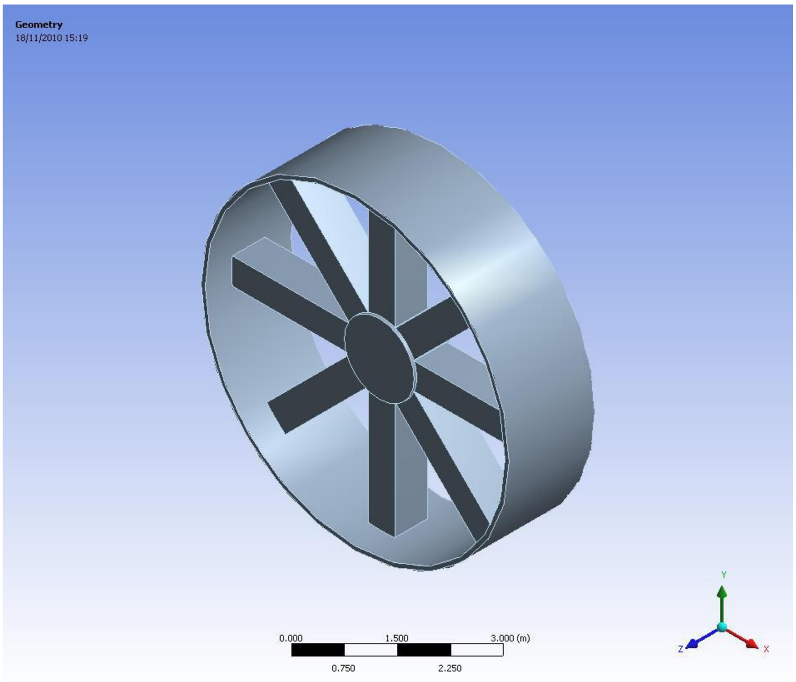

Figure 37 - Rotor with 8 arms

The radial deflection was $u_A = 2.66\times10^{-4}$ m ($u_{A\_max} = 3\times10^{-4}$ m) and the circumferential deflection due to rotation was $z_A = 5.62\times10^{-4}$ m ($z_{A\_max} = 6\times10^{-4}$ m) (Figure 38).

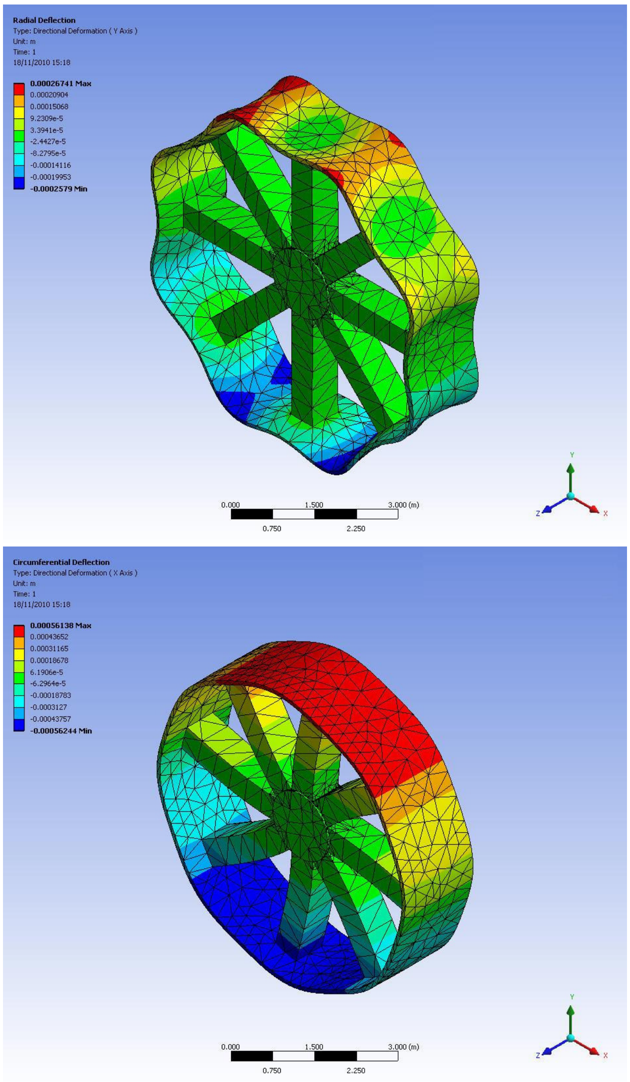

Figure 38 – Radial and Circumferential deflection of 8-armed structure

A model of this structure's arm was introduced into the shape optimisation tool. The target reduction for the given body was set to 30%. The output of the shape finder is illustrated in Figure 39 .

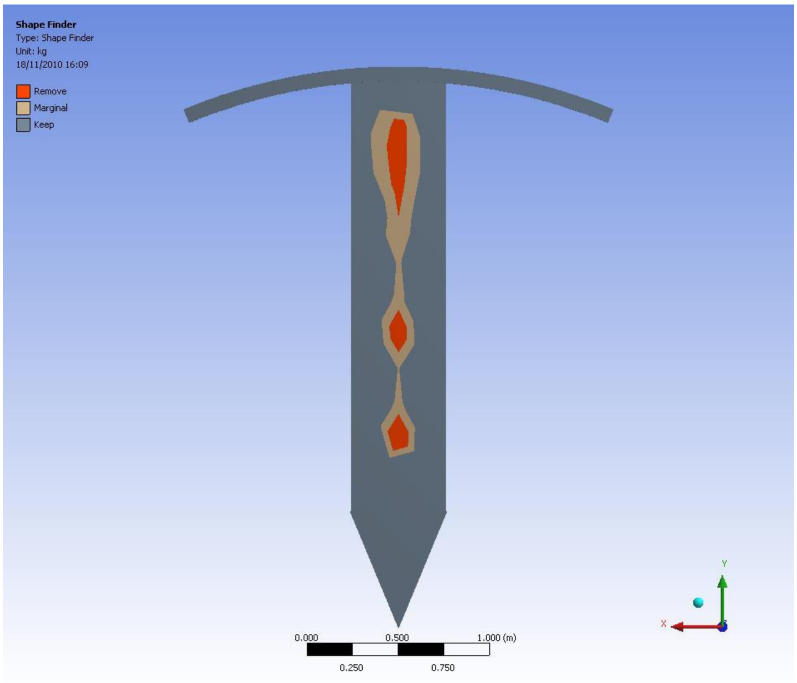

Figure 39 - Shape Finder output

The outlined part of the arm was removed. A comparison between the two shapes is given below (Figure 40). The optimised rotor with 8 such arms is depicted in Figure 41 .

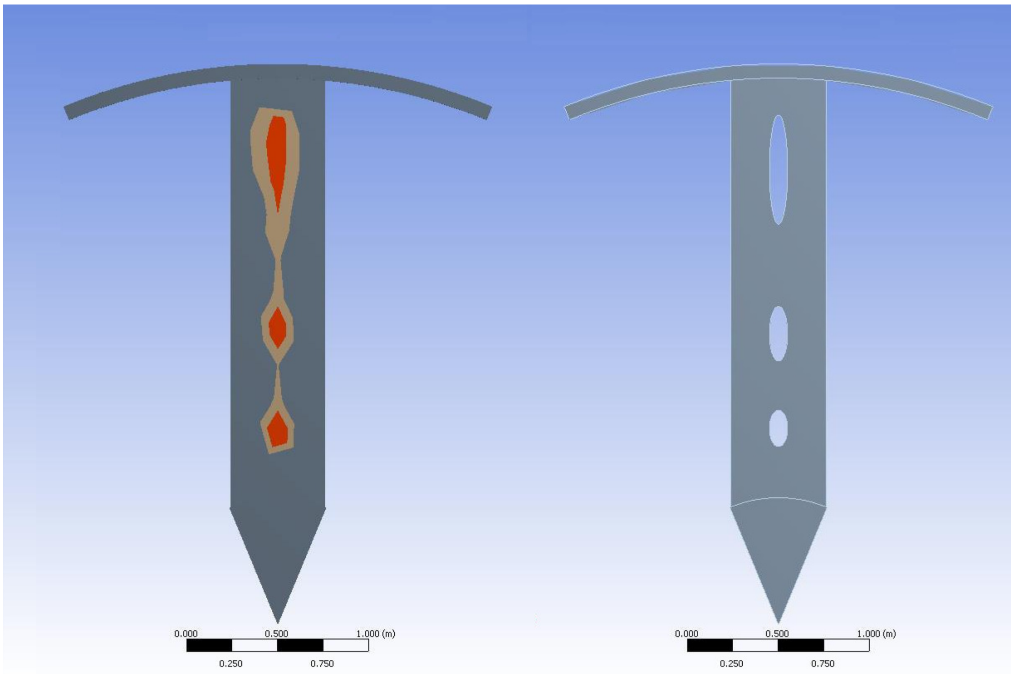

Figure 40 - On the left the shape finder's output. On the right the designed geometry

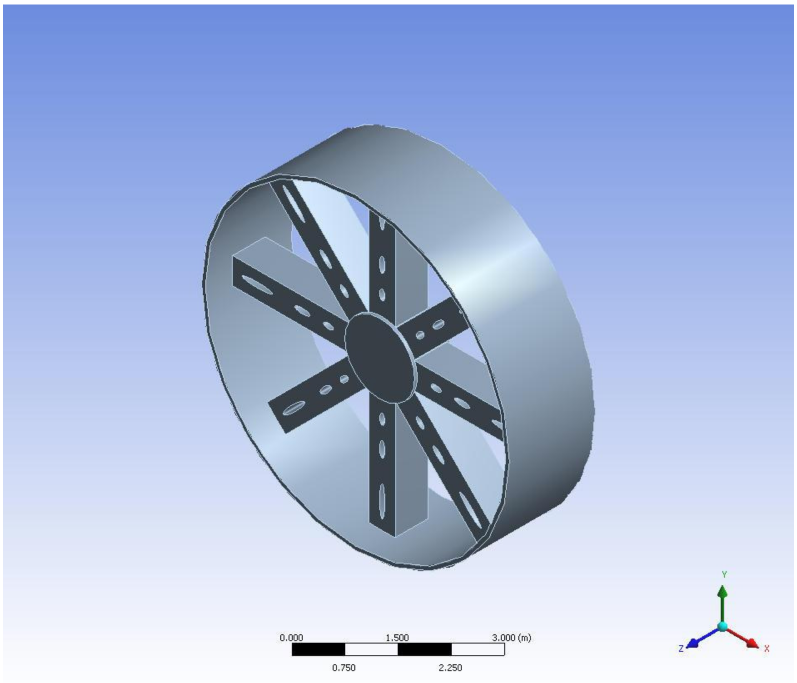

Figure 41 - Shape optimised rotor with 8 arms

The total mass of the rotor was reduced compared to the original design from 79000kg to 75000kg (5.1% mass reduction). This rotor design was tested for its stiffness against the two major deflections. The radial deflection was $u_A = 2.66\times10^{-4}$m and the circumferential deflection due to rotation was $z_A = 6.00\times10^{-4}$m (Figure 42).

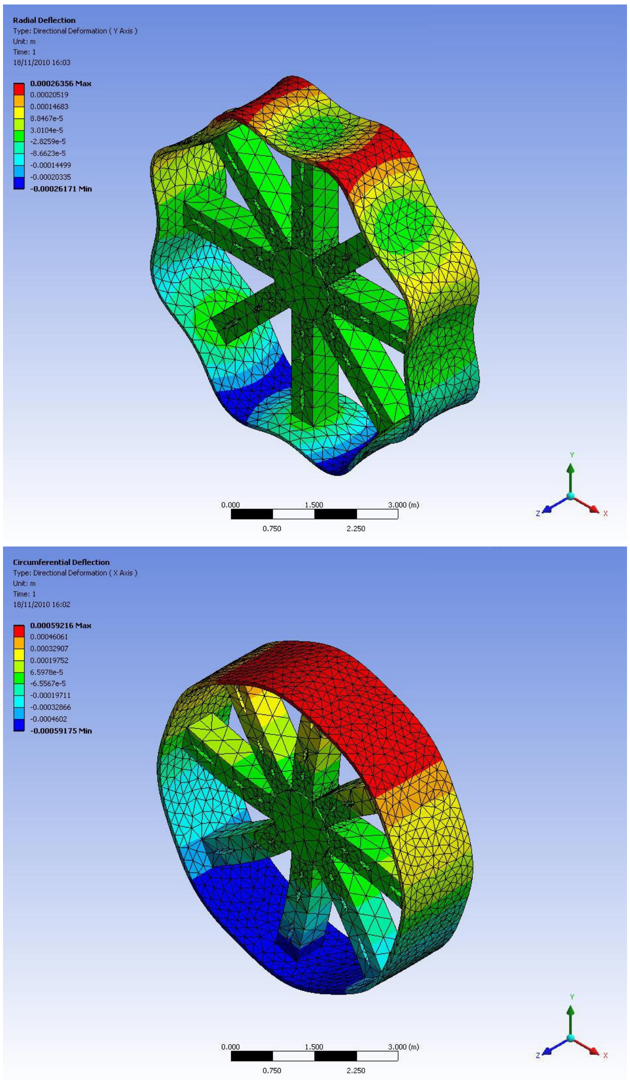

Figure 42 – Radial and Circumferential deflection for shape optimised rotor with 8 arms

The radial deflection increased by 0.03×10^{-4}m compared to the original 8-armed rotor structure and the circumferential one also increased by 0.30×10^{-4}m. Both deflections remained within limitations.

2.3.5 Rotor with 9 arms

Following the same procedure, a structural model of a rotor with nine arms was created. The mass of this rotor was 83400kg. Its dimensions were: R=3m, l=1.717m, b=0.349m, d=0.700m and h_{yr}=0.075m (Figure 43).

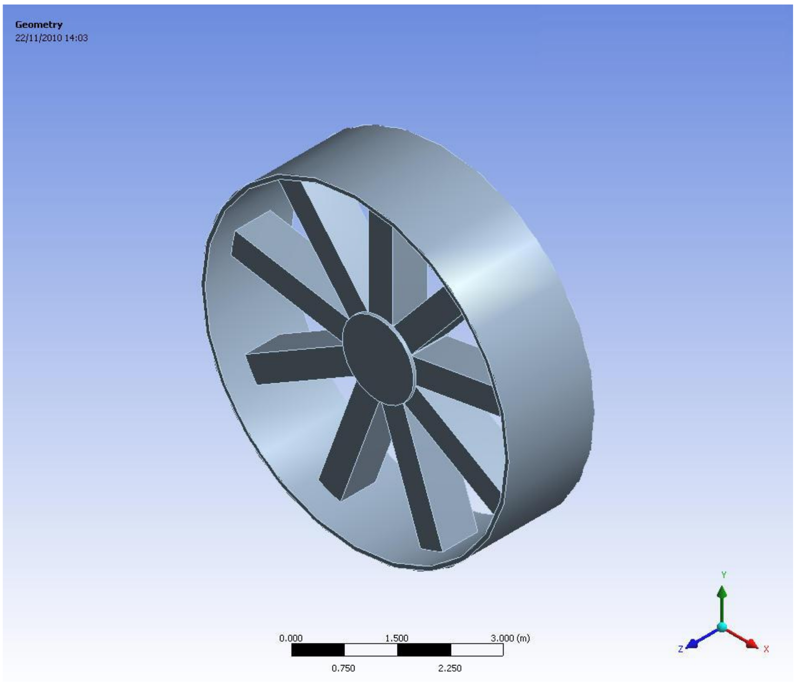

Figure 43 - Rotor with 9 arms

The radial deflection was $u_A = 2.66\times10^{-4}$m ($u_{A_max} = 3\times10^{-4}$m) and the circumferential deflection due to rotation was $z_A = 5.52\times10^{-4}$ m ($z_{A\_max} = 6\times10^{-4}$ m) (Figure 44).

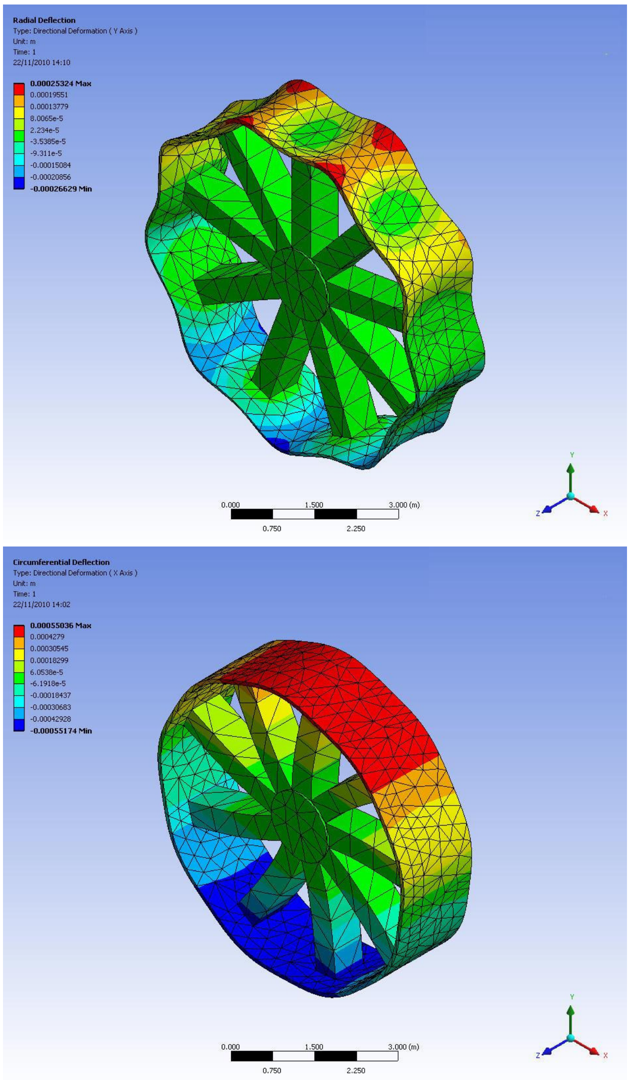

Figure 44 – Radial and Circumferential deflection of 9-armed structure

A model of this structure's arm was introduced into the shape optimisation tool. The target reduction for the given body was set to 30%. The output of the shape finder is illustrated in Figure 45 .

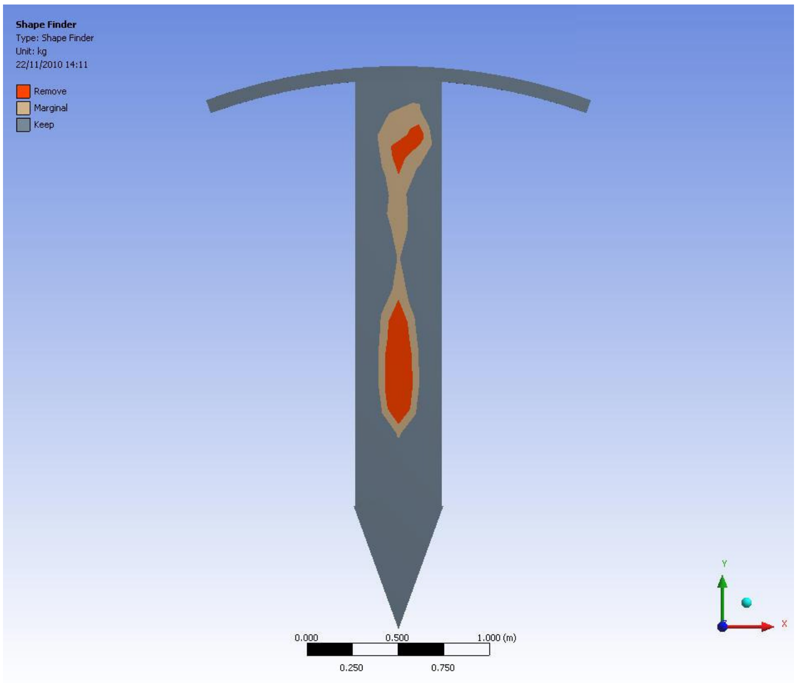

Figure 45 - Shape Finder output

The outlined part of the arm was removed. A comparison between the two shapes is given below (Figure 46). The optimised rotor with 9 such arms is depicted in Figure 47 .

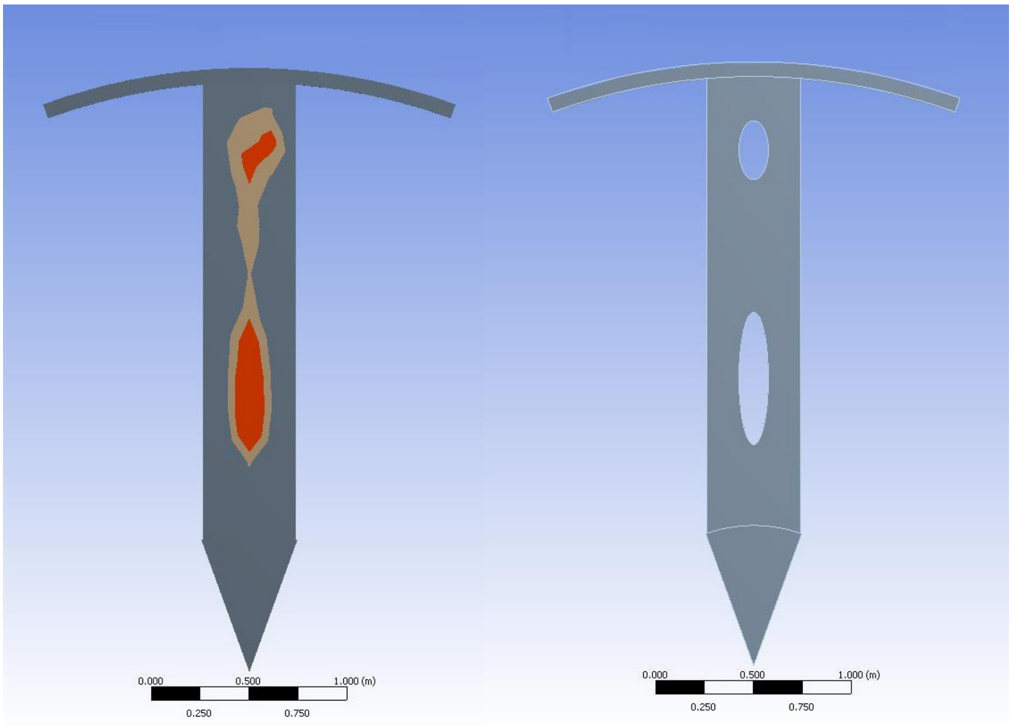

Figure 46 - On the left the shape finder's output. On the right the designed geometry

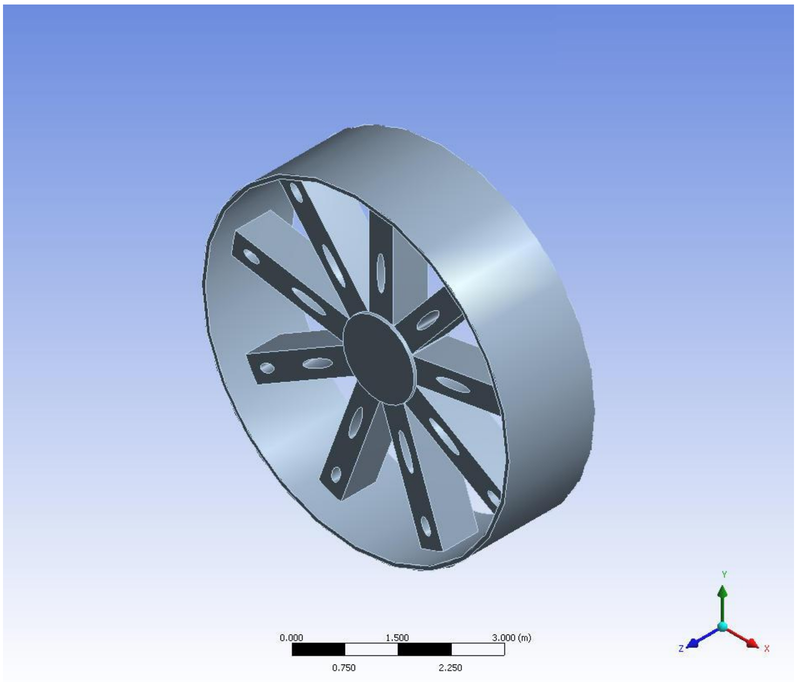

Figure 47 - Shape optimised rotor with 9 arms

The total mass of the rotor was reduced compared to the original design from 83400kg to 77700kg (6.8% mass reduction). This rotor design was tested for its stiffness against the two major deflections. The radial deflection was $u_A = 2.67\times10^{-4}$ m and the circumferential deflection due to rotation was $z_A = 6.00\times10^{-4}$m (Figure 48).

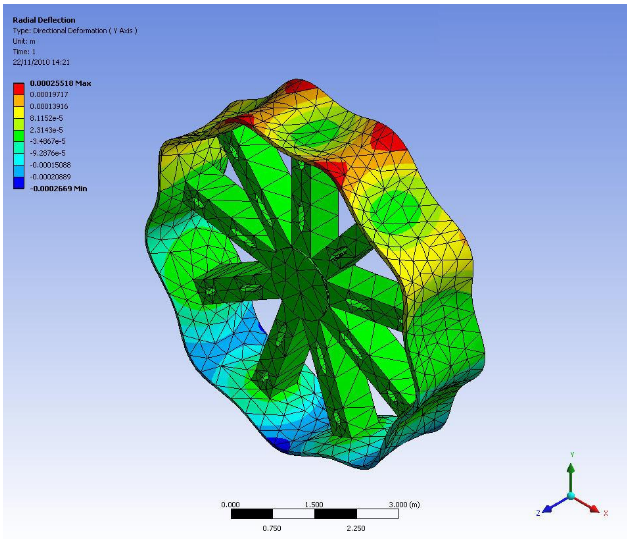

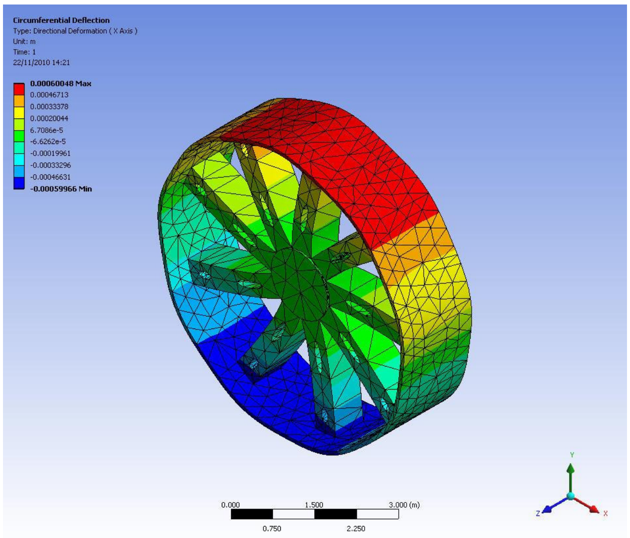

Figure 48 – Radial and Circumferential deflection for shape optimised rotor with 9 arms

The radial deflection increased by 0.01×10^{-4}m compared to the original 9-armed rotor structure and the circumferential one also increased by 0.48×10^{-4}m. Both deflections remained within limitations.

2.3.6 Rotor with 10 arms

Following the same procedure, a structural model of a rotor with ten arms was created. The mass of this rotor was 88800kg. Its dimensions were: R=3m, l=1.717m, b=0.314m, d=0.750m and h_{yr}=0.070m (Figure 49).

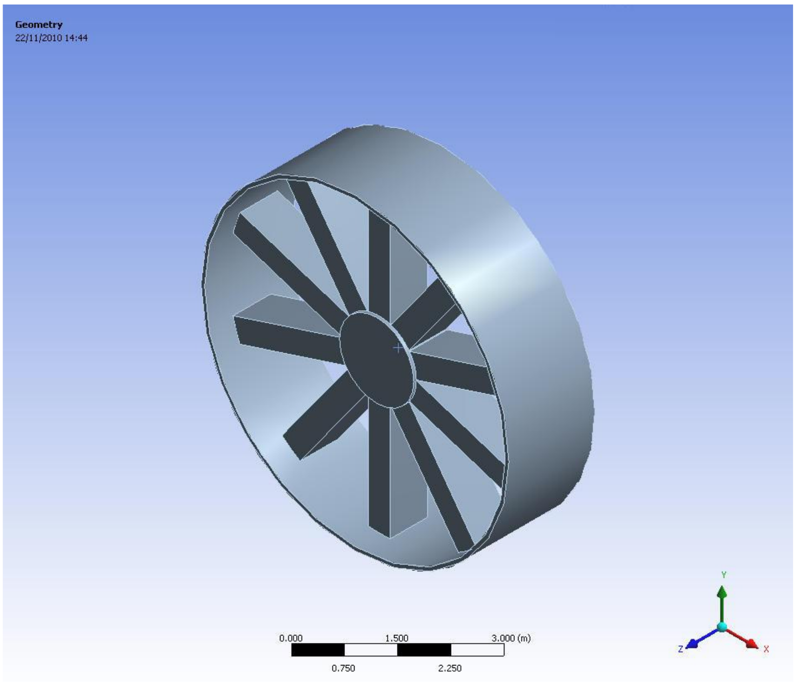

Figure 49 - Rotor with 10 arms

The radial deflection was $u_A = 2.61 \times 10^{-4}$ m ($u_{A\_max} = 3 \times 10^{-4}$ m) and the circumferential deflection due to rotation was $z_A = 5.63 \times 10^{-4}$m ($z_{A\_max} = 6 \times 10^{-4}$ m) (Figure 50).

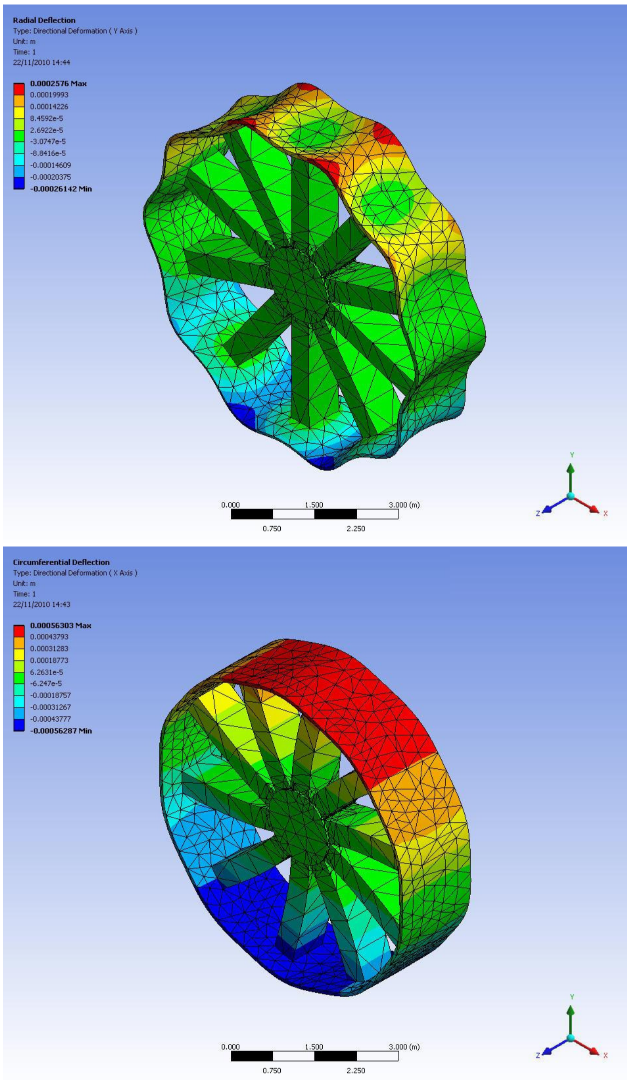

Figure 50 – Radial and Circumferential deflection of 10-armed structure

A model of this structure's arm was introduced into the shape optimisation tool. The target reduction for the given body was set to 30%. The output of the shape finder is illustrated in Figure 51 .

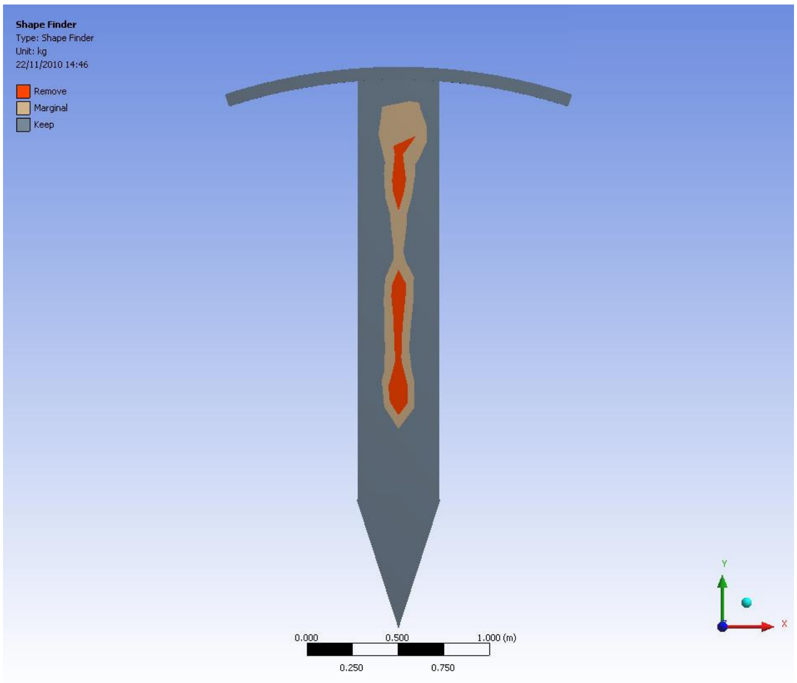

Figure 51 - Shape Finder output

The outlined part of the arm was removed. A comparison between the two shapes is given below (Figure 52). The optimised rotor with 10 such arms is depicted in Figure 53 .

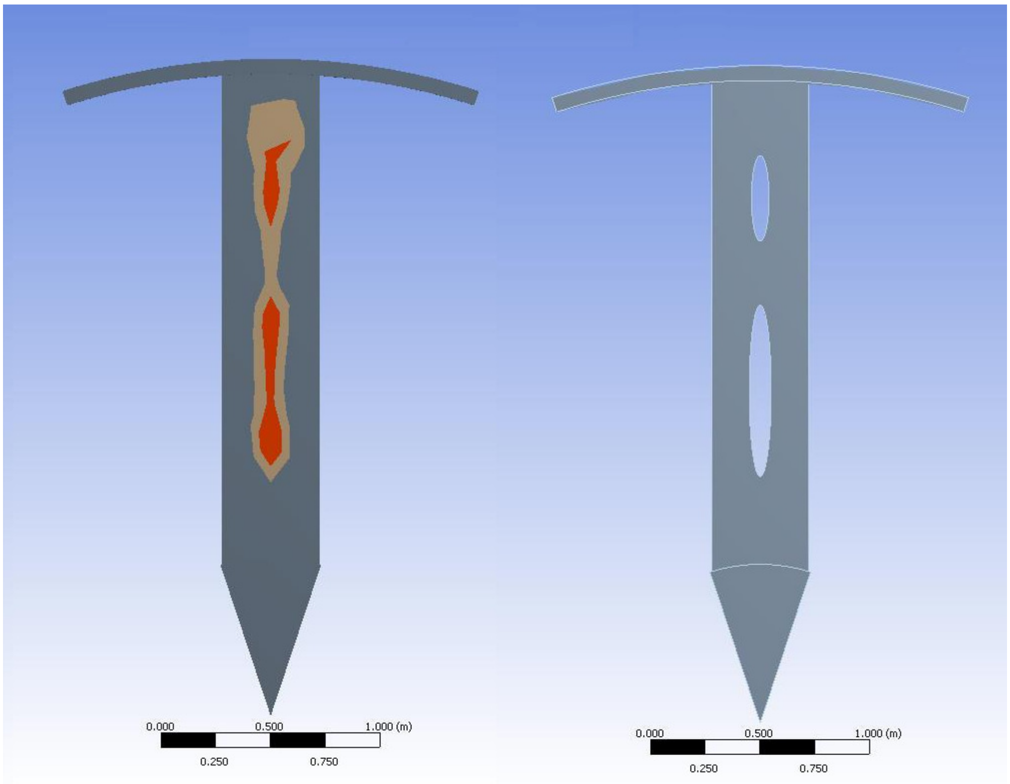

Figure 52 - On the left the shape finder's output. On the right the designed geometry

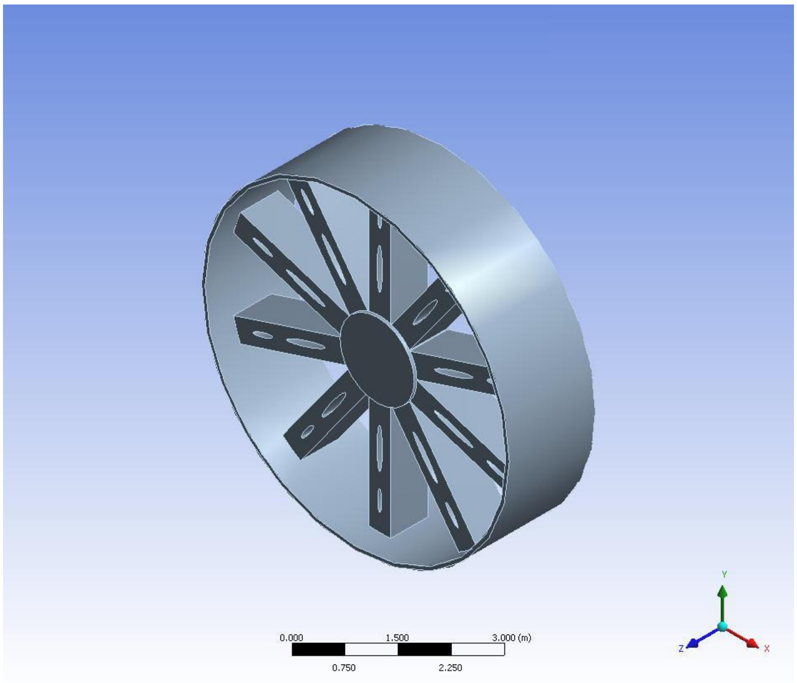

Figure 53 - Shape optimised rotor with 10 arms

The total mass of the rotor was reduced compared to the original design from 88800kg to 82900kg (6.7% mass reduction). This rotor design was tested for its stiffness against the two major deflections. The radial deflection was $u_A = 2.71\times10^{-4}$ m and the circumferential deflection due to rotation was $z_A = 6.08\times10^{-4}$m (Figure 54).

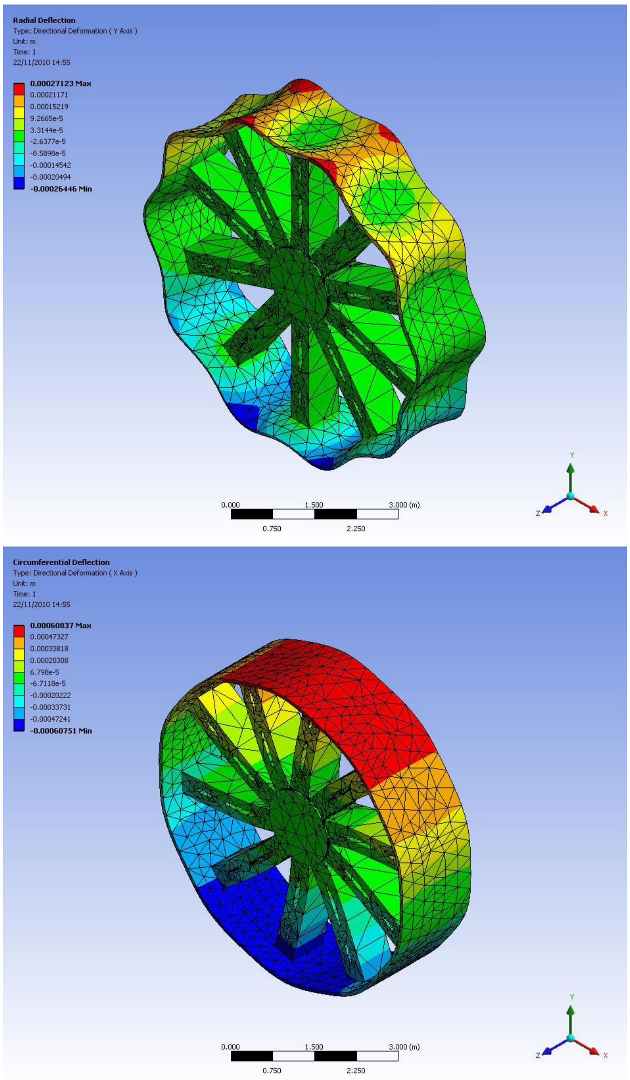

Figure 54 – Radial and Circumferential deflection for shape optimised rotor with 10 arms

The radial deflection increased by 0.10×10^{-4}m compared to the original 10-armed rotor structure and the circumferential one also increased by 0.45×10^{-4}m. Both deflections remained within limitations.

2.3.7 Conclusions
After conducting a large number of experiments the best results occurred for structures with the minimum number of arms (Figure 55).

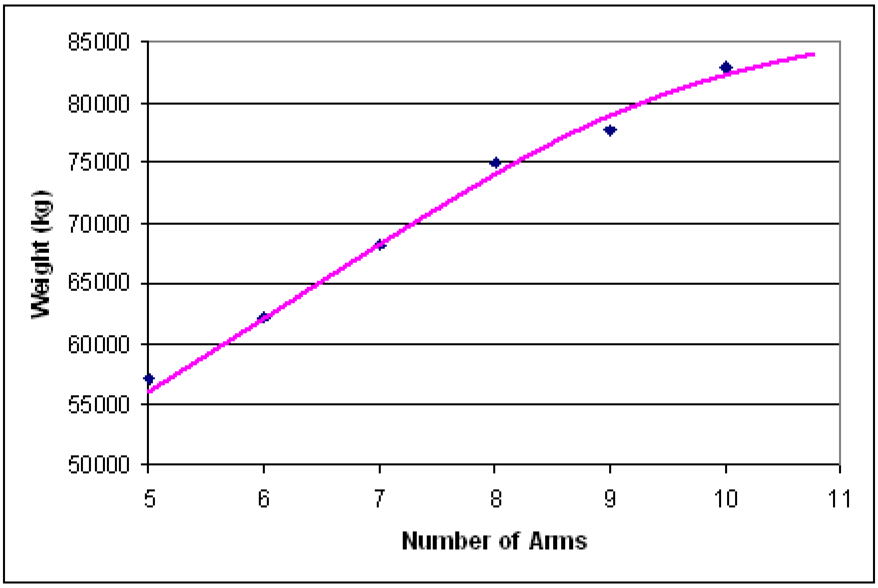

Figure 55 – Weight comparison of optimised structures

The following general conclusions can be outlined:

- Structures with small numbers of arms are lighter and more robust compared to structures with a large number of arms.
- The most lightweight structure was the optimised rotor with 5 arms (57100kg). This can be attributed to the fact that as the number of arms increased, the breadth of each arm (b) decreased according to (1). That made the total structure much more vulnerable towards the circumferential deflections. In order to compensate for this effect, the depth of the arm (d) had to be increased leading to heavier arms and heavier structures.
- As the number of arms increased, the structures were more resistant against the radial deflection. Therefore the rotor's back thickness could be decreased.
- The maximum mass reduction that was achieved was 6.8% for heavier structures with 9 or 10 arms.

Another suggested topology to reduce the total weight of a rotor with arms is to create a structure with hollow arms (Figure 56). In this concept the arms of the structure are hollow on the inside as it can be seen in more detail in Figure 57 . The thickness of the arms was t_w from each side of the arm.

The new structure that was modelled was much lighter that the original 5-armed structure with solid arms but was more vulnerable to the circumferential deflection. In order to make the new design more robust the depth of the arms (d) was increased. Its final dimensions were: R=3m, l=1.717m, b=0.628m, d=0.550m, h_{yr}=0.090m and t_w=0.095m.

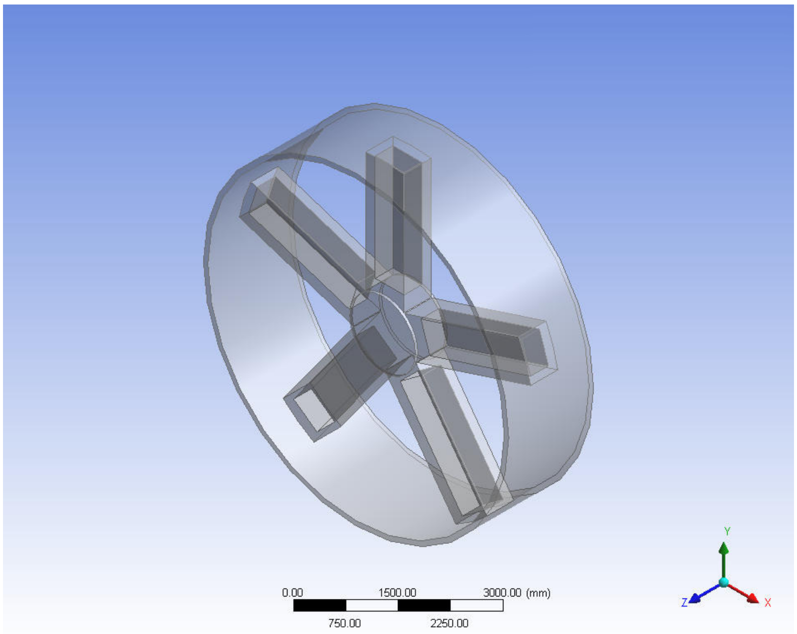

Figure 56 – 5-armed rotor with hollow arms

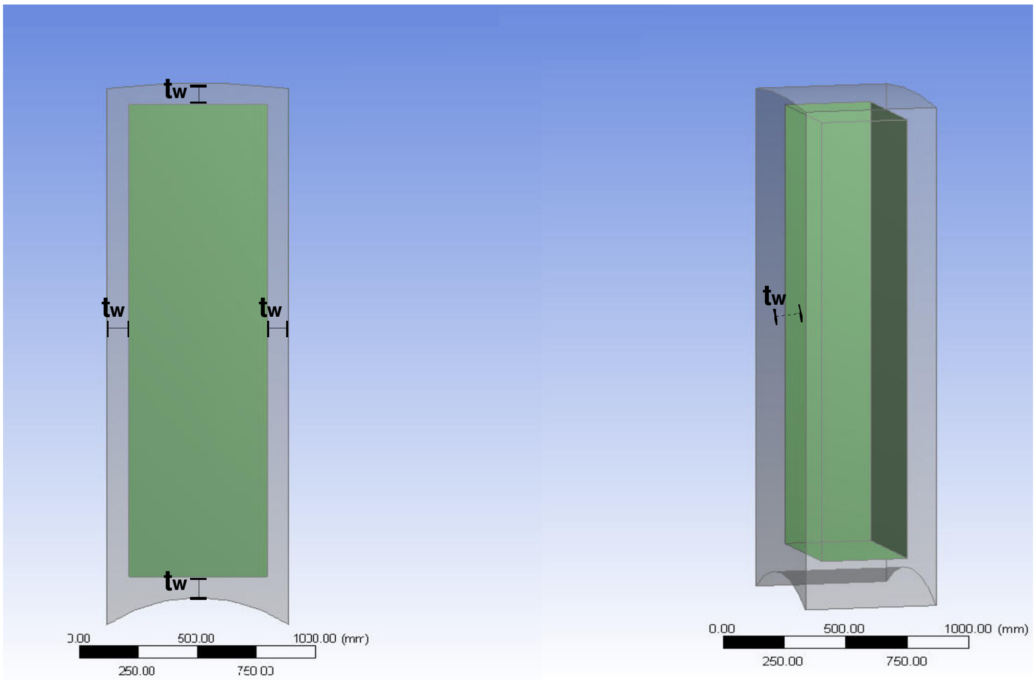

Figure 57 – Transparent view of rotor's arm. The hollow part is outlined with green colour

The final structure was once again tested for its stiffness against the two major deflections. The radial deflection was $u_A = 2.92\times10^{-4}$ m and the circumferential deflection due to rotation was $z_A = 5.90\times10^{-4}$m (Figure 58).

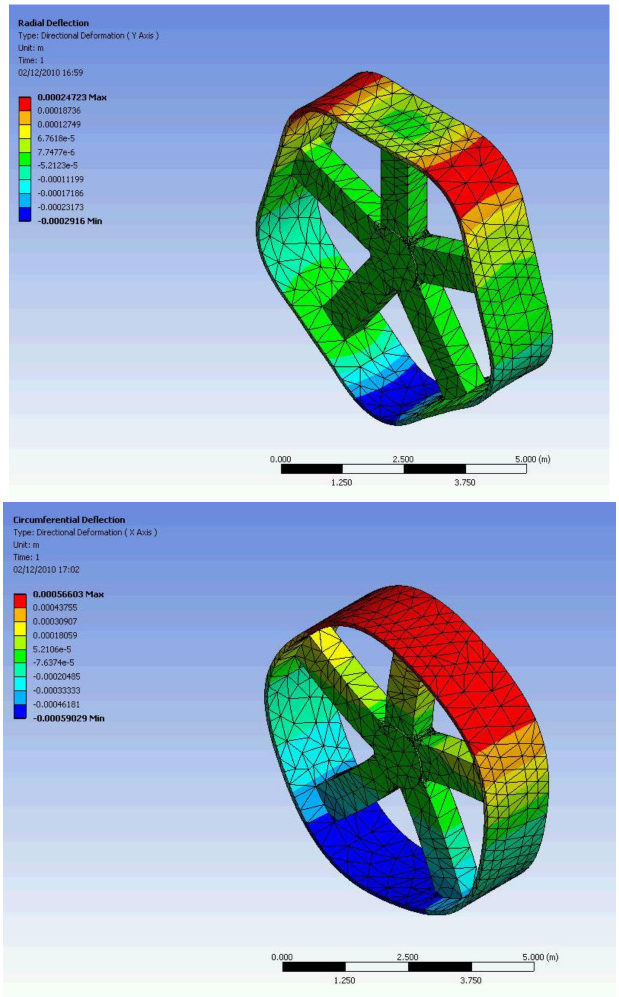

Figure 58 – Radial and Circumferential deflection for 5-armed rotor with hollow arms

Although the depth of the arms increased a lot it did not affect the total weight of the structure due to its hollow design.

The total weight of the structure was 52100g, almost 7 tonnes lighter than the original 5-armed design (11.24% mass reduction) and 5 tonnes lighter than the optimised 5-armed design (9% lighter). This design is the most lightweight of all the tested designs until now. It is not possible to know why the shape optimisation tool of the FEA program [8] did not come up with this solution during the previous experiments that took place. This can be attributed either to the way that the tool is programmed to optimise the given models or to the fact that even if it can come up with such solution there is way to depict it to the user.

The results of this research could be of great use in the designing of a novel lightweight rotor topology. The same shape and weight optimisation could be made for the stator of a direct drive generator with discs of the same power output.

The same optimization procedure was applied to stator structures with arms, giving similar results.

Section 3 Shape Optimisation of generator structures with discs

3.1 Introduction

The shape optimization tool in ANSYS program [8] is a structural analysis that seeks to find the best use of material for a body. This involves optimizing the distribution of material so that the given structure will have the maximum stiffness for a set of loads. The output is a plot that outlines the portions of the geometry that least contribute to the stiffness of the structure for a number of given loads. The marginal portions are outlined with brown colour while the mass that could be removed from the given geometry is outlined with red colour (Figure 59).

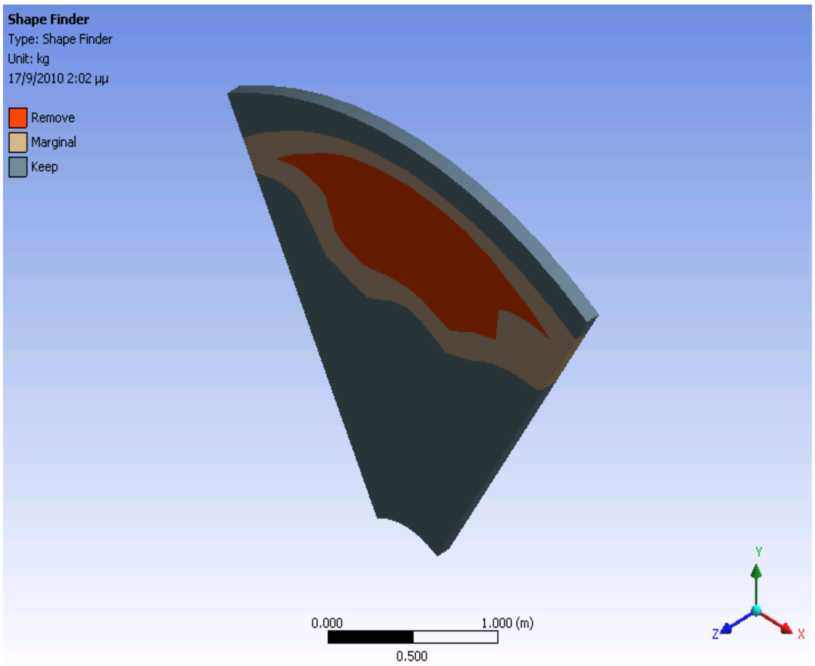

Figure 59 - Shape Finder output

This tool could be a great asset regarding the shape optimisation and the structural mass reduction of a direct drive generator as it could provide the guidelines for the production of a lightweight generator topology. The resulting novel topology should be capable of producing the needed torque while being robust enough to withstand the great structural forces that apply on the generator's structure at the same time.

For this research a geometry that could be part of the structure of a disc rotor was designed including part of the rotor back, the disc and the shaft of the rotor. Symmetry regions were added on both sides of the structural model so that the FEA tool would "think" that this model is part of a whole (Figure 60). The Y-axis of each symmetry region was used as a symmetry normal in the shape optimisation program.

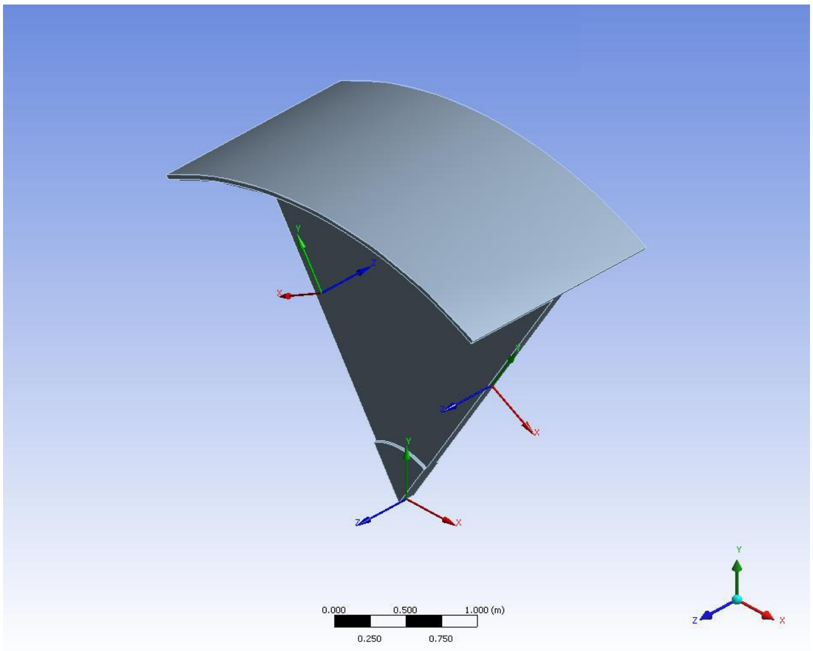

Figure 60 - Original shape and symmetry regions

The dimensions of the structure were:

- R = 3m (the radius of the disc)
- l = 1.717m (axial length)
- K_{rad} = 0.3
- t_d = 0.1m (the disc thickness)
- h_{yr} = 0.06m (rotor back thickness)
- arc = 60^o

This structural design was chosen to model a 5MW generator. The dimensions of the machine (radius and axial length) are great enough to provide the necessary torque needed for the nominal power output of such a generator. At the same time, the rotor back and the disc thickness were chosen to be great enough to maintain the necessary airgap clearance against the structural forces that act on the generator's structure (Maxwell stress – gravitational stress – circumferential stress).

The geometry mentioned above was then introduced to the shape optimisation tool. The loads that applied on this geometry were chosen to be the same that would apply on the rotor of a 5MW direct drive generator:

- The radial pressure on the surface of the rotor due to the normal component of the Maxwell stress (q = 280 kPa).
- A moment that gives rise to a stress in the tangential direction (circumferential stress), which represents the force that the magnetic field of the stator applies to the rotor and vice versa as the stator acts like a "brake" to the circular movement of the rotor (M_o = 4.42 MNm).

The target reduction for the given body that should be stiff enough to withstand the above mentioned loads was set to 25%. The output of the shape finder can be seen in Figure 61.

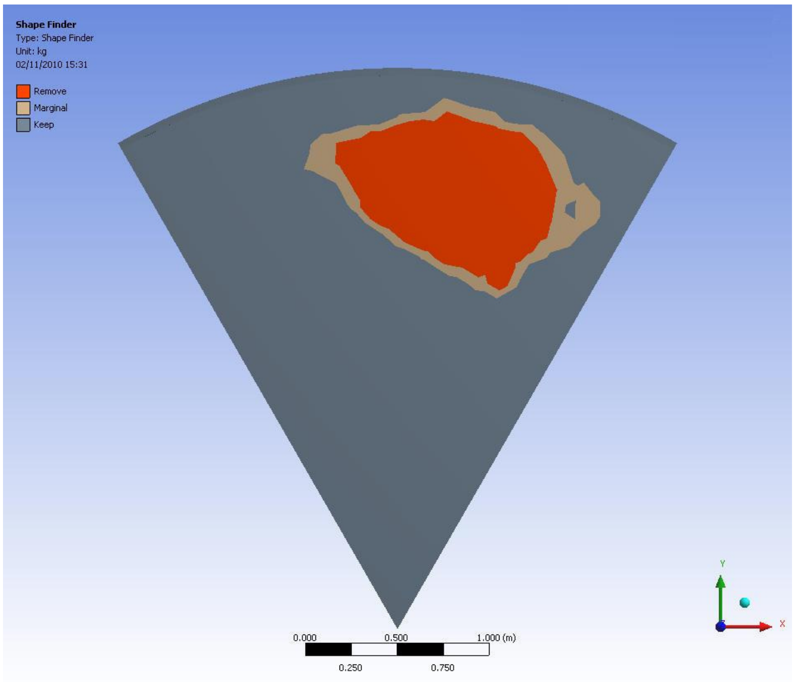

Figure 61 - Structure after shape optimisation

It seems that the major part that could be removed from the structure illustrated above is an elliptical part in the upper-middle section of the structure (resembles a water-drop). In order to understand how this shape changes according to all the possible variables, a number of experiments took place in order to specify how and in what degree each parameter affects the outcome of the shape optimisation tool.

The possible parameters that were tested were:

- The radial stress (normal component of Maxwell stress – Pa)
- The circumferential moment (Nm)
- The radius of the structure (R)
- The structure's thickness (t_d)
- The angle of the arc (°)
- The percentage of target reduction (%)

In each case, only one of the parameters varies when all the others are kept to their original values which are K_{rad}=0.3, R=3m, t_d=0.1m, h_{yr}=0.06m, arc angle=60°, radial stress q=280kPa, moment M_o=4.42MNm and target optimisation=25%. The axial length of the structure varies when the radius varies in order to retain the same K_{rad}.

The first step to take in order to understand why the shape optimisation tool comes up with specific results would be to experiment on the two major forces that apply on the given model (Radial & Circumferential stress).

3.2 Testing the Different Parameters

3.2.1 Increasing Radial Stress

For the first stage of this research, the tested structure was subjected to optimisation taking under consideration only the radial deflection that is applied on it – a moment was not included in this case. This happened in order to understand how the Maxwell stress affects the given structure. The Maxwell stress increased from 80kPa up to 680kPa. Figure 62 illustrates some of the resulting outputs of the shape optimisation tool for this case.

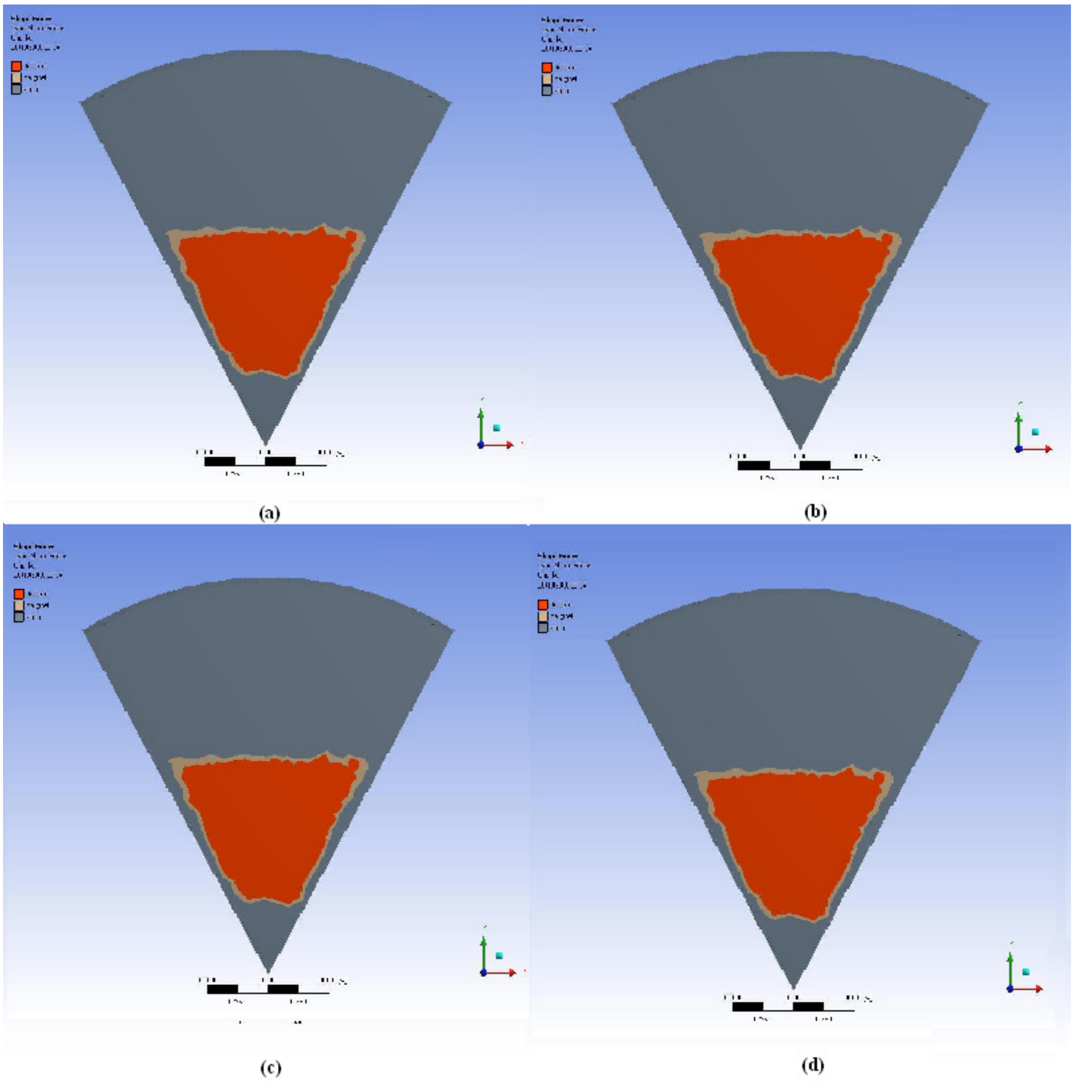

Figure 62 - (a) 80kPa, (b) 280kPa, (c) 480kPa, (d) 680kPa

As Figure 62 suggests, the part near the centre of the structure could be removed if just the radial stress was to be taken under consideration. Furthermore, it seems like the unnecessary part of the structure remains the same in all tested cases.

In a second stage the moment that gives rise to the circumferential stress was introduced as well. Figure 63 illustrates the same results for the given structure including the circumferential stress.

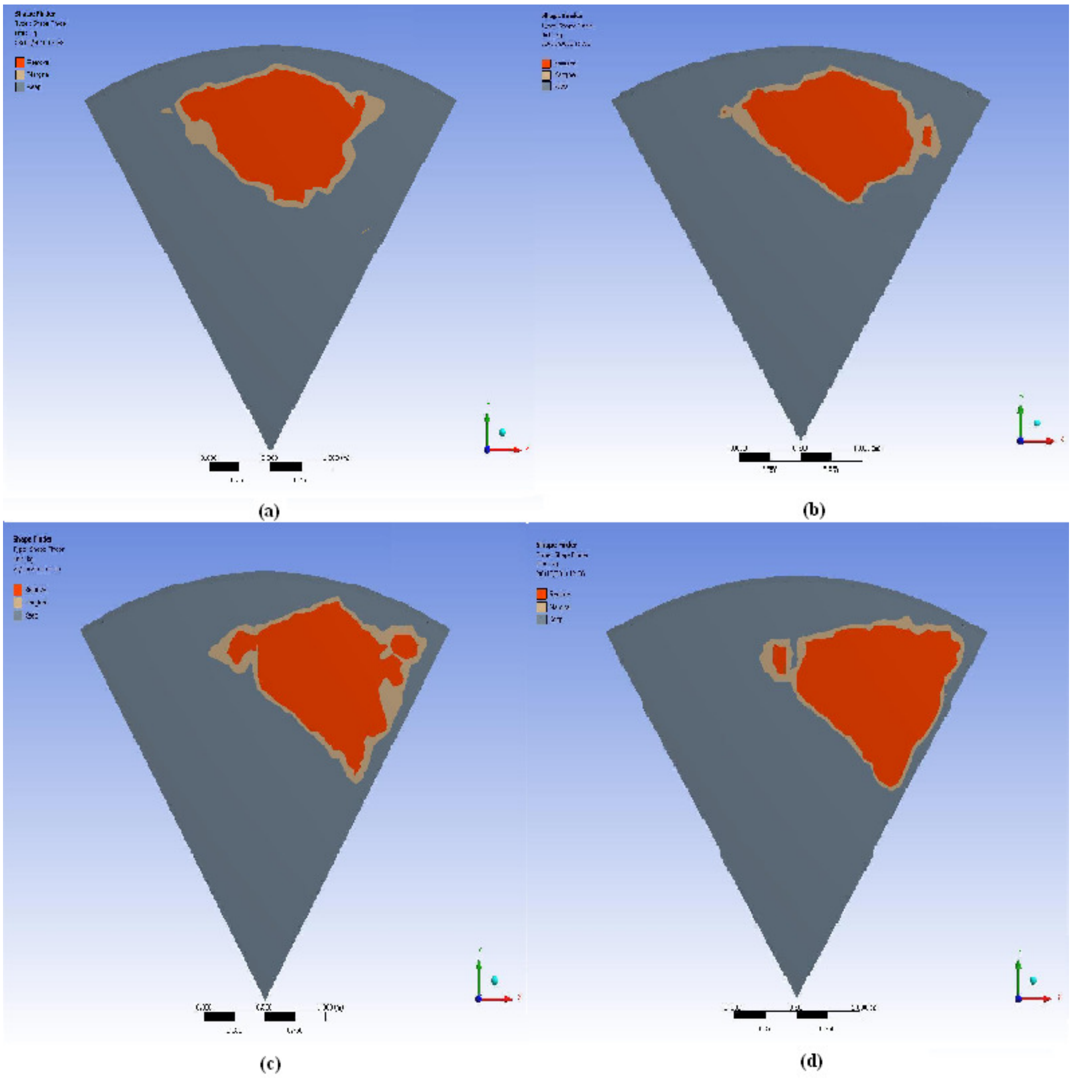

Figure 63 - (a) 80kPa, (b) 280kPa, (c) 480kPa, (d) 680kPa

Figure 63 shows that when the torque is taken into consideration as well, the part that could be removed changes dramatically in shape and location. For a small radial stress the unnecessary part is located in the middle of the structure and as the radial stress increases it “moves” towards the right part of the shape. Another observation is that as the Maxwell stress increases the removable part turns from a radial-like shape to a triangular one.

This can be attributed to the fact that in order to withstand the increasing radial stress, the structure should be more solid in its centre, directly under the centre of the arc.

3.2.2 Increasing Torque

Using the same procedure as before, a rising moment was introduced in the program on its own without any radial stress acting on the structure. The moment increased from 2.42MNm up to 8.42MNm. Figure 64 illustrates some of the resulting outputs of the shape optimisation tool for this case.

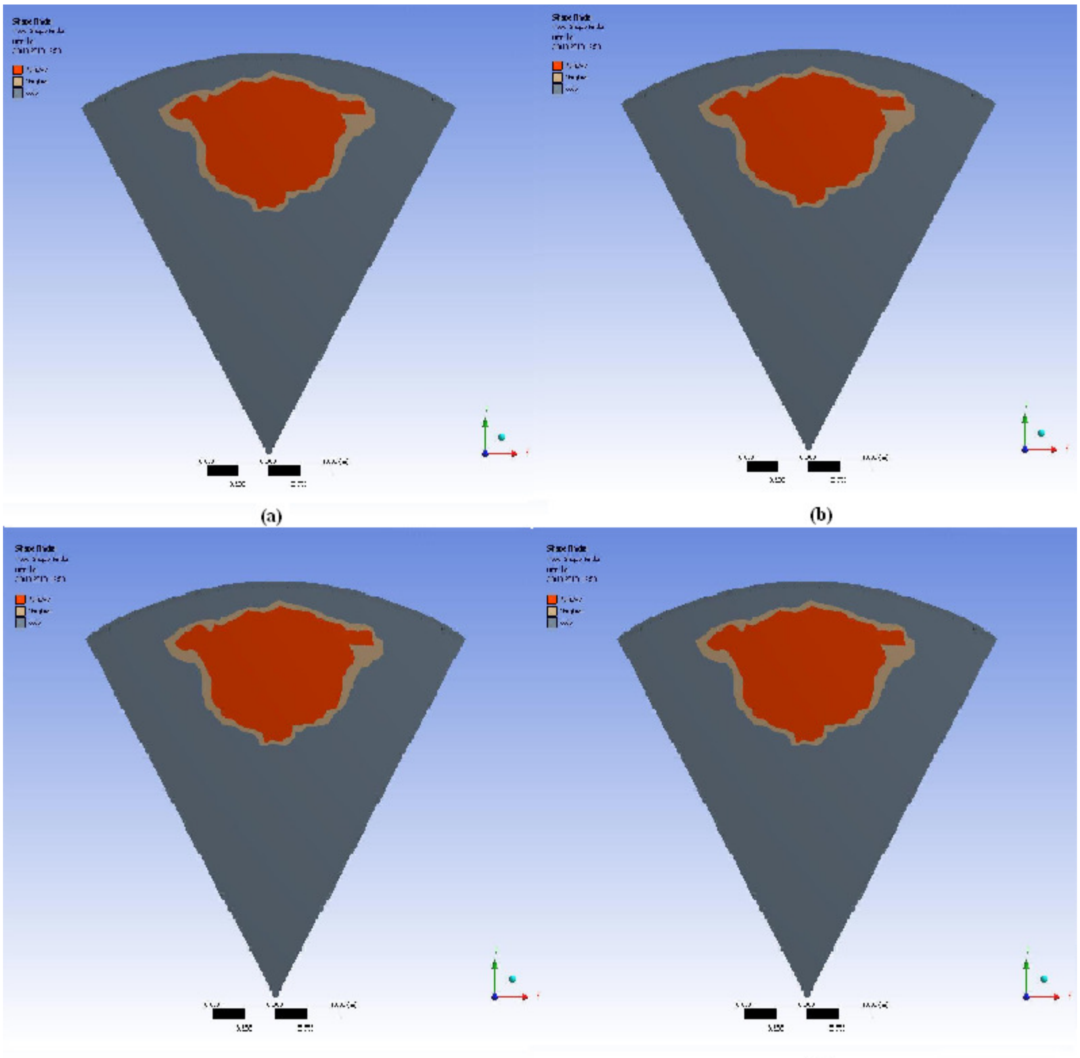

(a) (b) (c) (d)

Figure 64 - (a) 2.42MNm, (b) 4.42MNm, (c) 6.42MNm, (d) 8.42MNm

As Figure 64 suggests, the part near the top of the structure could be removed if just the circumferential stress applied on the tested structure. Same as the first tested in 3.2.1 the unnecessary part of the structure remains the same as the moment increases.

In a second stage the radial stress was introduced as well. Figure 65 illustrates the same results for the given structure including the stress on the radial direction.

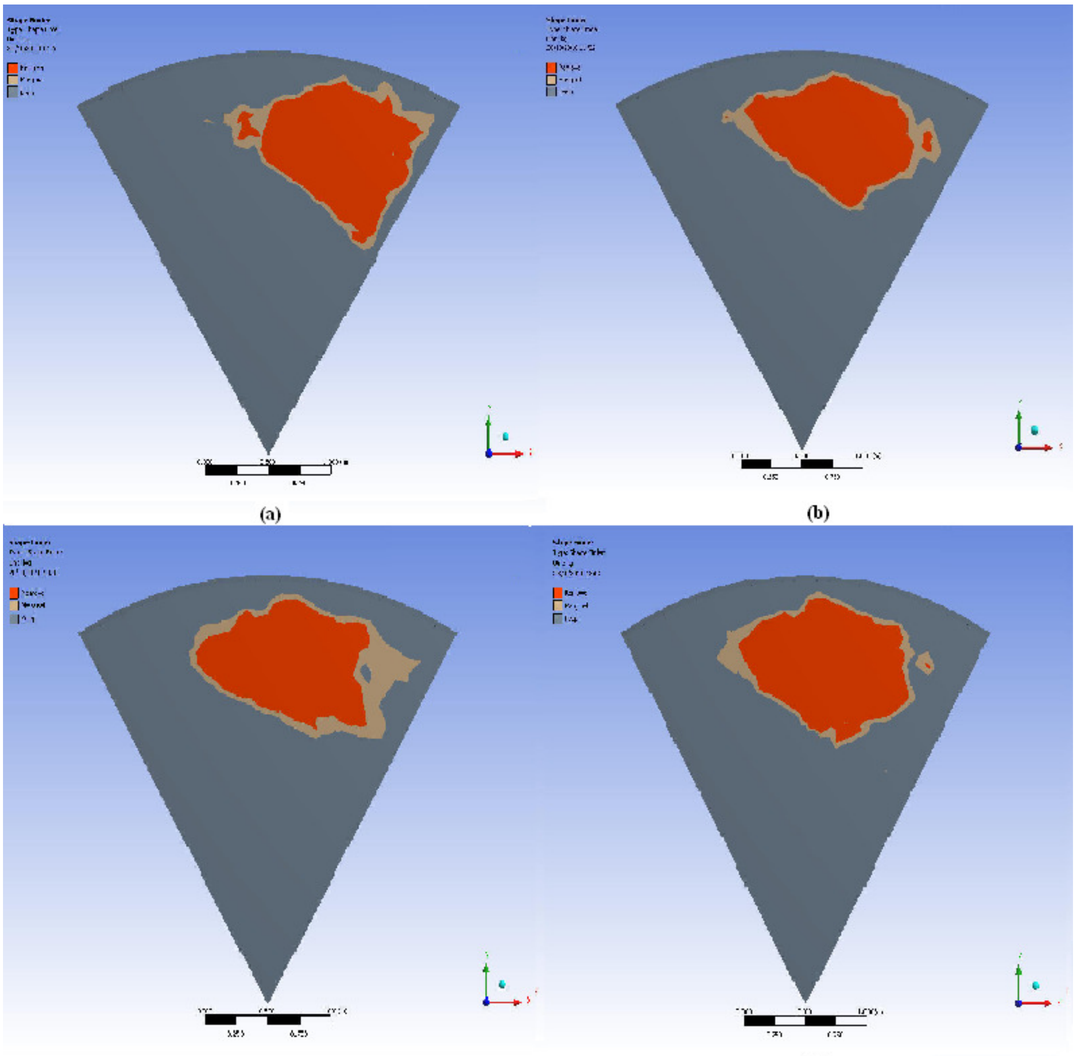

(a) (b) (c) (d)

Figure 65 - (a) 2.42MNm, (b) 4.42MNm, (c) 6.42MNm, (d) 8.42MNm

Figure 65 shows that when both forces are taken into consideration, the part that could be removed changes dramatically in shape and location as the moment increases. For a small moment the unnecessary part is located in the right-upper part of the structure and as the moment increases it "moves" towards the centre of the shape. Another observation is that as the moment increases the removable part becomes more circular.

This can be attributed to the fact that in order to withstand the increasing circumferential stress, the structure should be more solid in its two sides and towards its centre. These are quite the opposite results from the ones in 3.2.1 where the Maxwell stress increased and show that these two forces need different parts of the structure in order to remain robust enough.

Apart from the forces that apply, another important factor that can drive the outcome of the structural optimisation tool is the structural variables of the tested structure. The variables that were tested during this research were the radius, the back thickness and the angle of the arc of the structure. Each time that a parameter was tested, values of the rest remained the same as described in "Introduction".

3.2.3 Increasing Radius (*R*)

The radius of the shape varied from 1.5m up to 5m. In each case the axial length of the rotor's back varied accordingly in order to retain the aspect ratio of the structure static and equal to 0.3 ($K_{rad}=l/2R$). Figure 66 illustrates some of the resulting outputs of the shape optimisation tool.

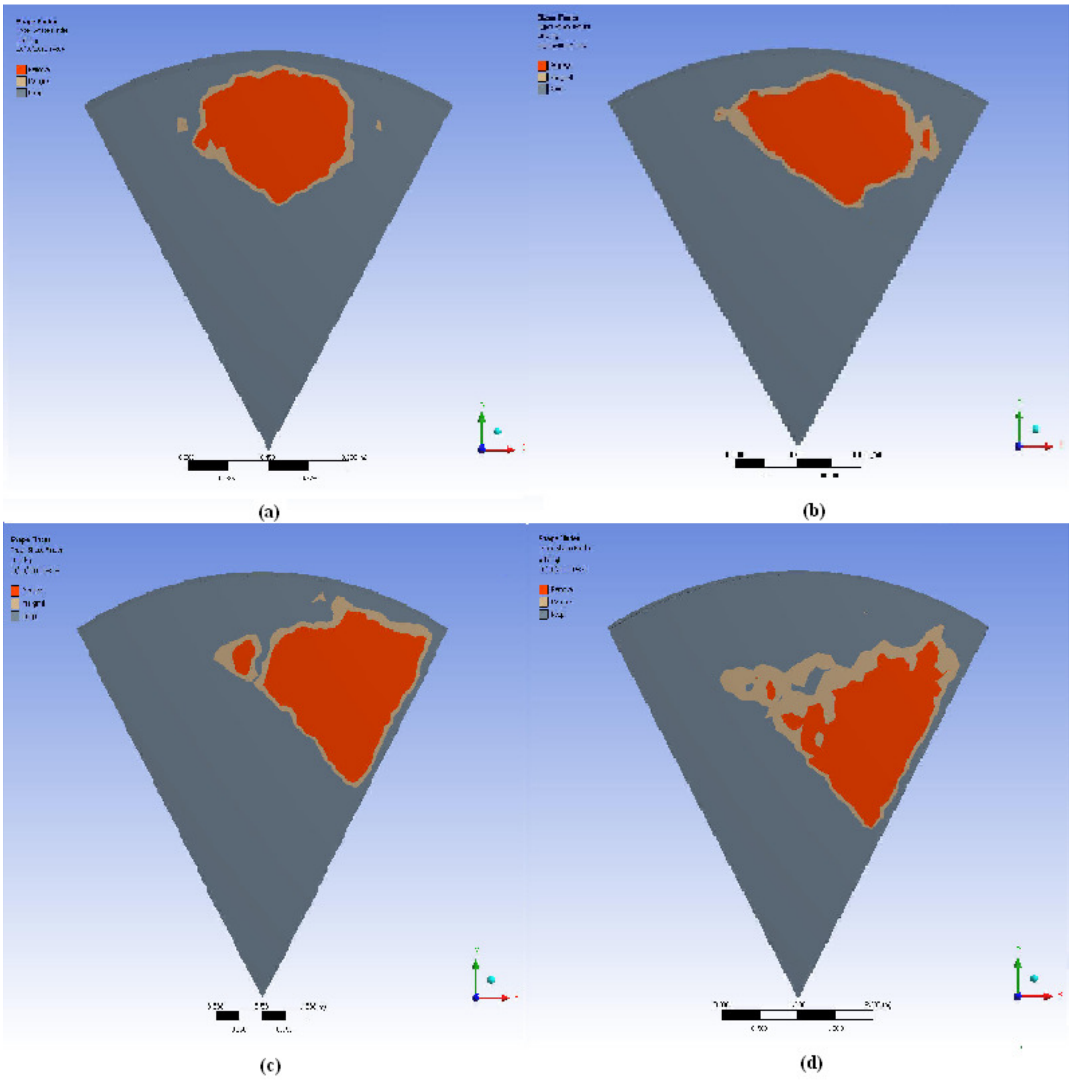

(a) (b) (c) (d)

Figure 66 - (a) *R*=2m, (b) *R*=3m, (c) *R*=4m, (d) *R*=5m

For a small radius the unnecessary part is more circular and located in the middle of the structure, but as the radius increases its shape turns into a triangle "moves" towards the right part of the structure. These results resemble the ones of 3.2.1 where the Maxwell stress increased in magnitude.

This leads to the conclusion that as the radius increases but the thickness of the disc remains the same, the structure becomes less resistant against the stress in the radial direction but more resistant against the circumferential stress.

3.2.4 Increasing Disc Thickness (t_d)

The thickness of the shape varied from 0.02m up to 0.14m. Figure 67 illustrates some of the resulting outputs of the shape optimisation tool.

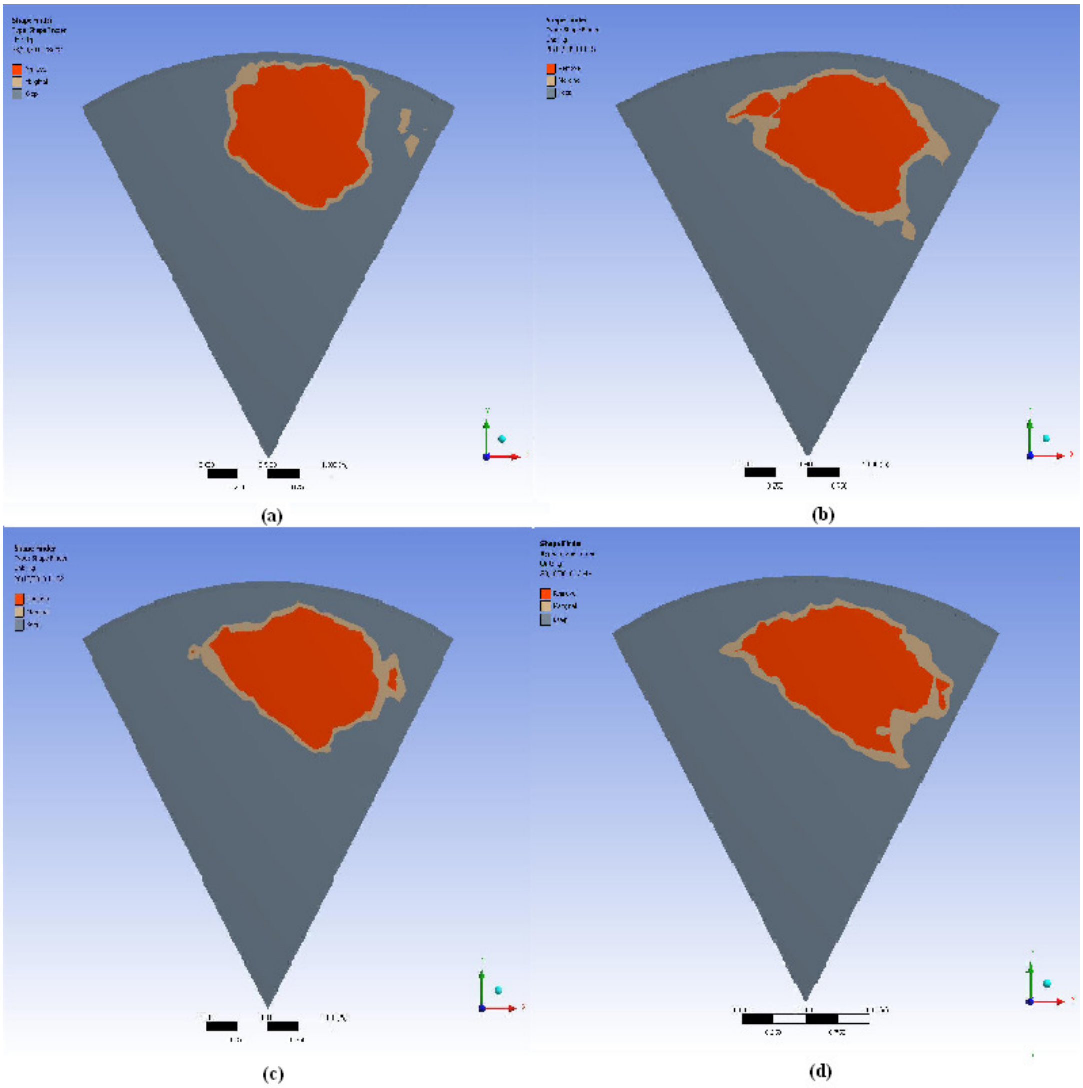

Figure 67 - (a) t_d=0.02m, (b) t_d=0.06, (c) t_d=0.1m, (d) t_d=0.14m

As the thickness increases, the originally round red part that could be removed from the structure loses its shape and becomes bigger and more elliptical.

The reason for the increase of the red coloured area is directly connected to the increase of the disc thickness. As the disc thickness increases, the structure becomes more robust thus more resistant to both structural forces that apply on it. Therefore greater part of its mass could be removed without the danger of the structure losing its shape due to the radial or circumferential deflection.

3.2.5 Increasing arc angle (°)

The arc angle of the shape varied from 30° up to 180°, representing the number of pattern repeats that could be used in order to create a full circle (from 2 to 12). Figure 68 illustrates some of the resulting outputs of the shape optimisation tool.

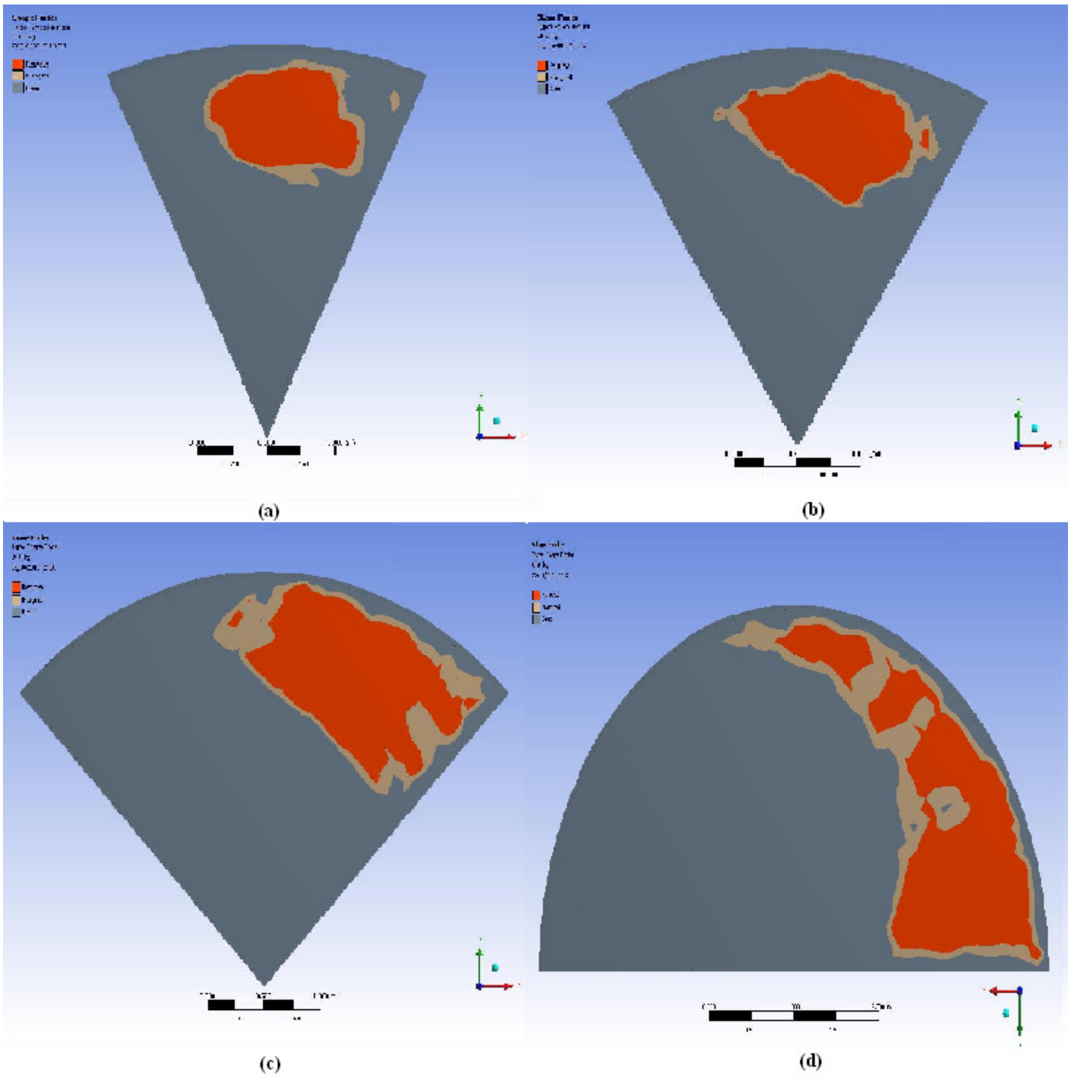

Figure 68 - (a) 45°, (b) 60°, (c) 90°, (d) 180°

As the angle of the structure increases, the originally round red part that could be removed from the structure becomes bigger and more elliptical and "moves" to the right side of the structure.

3.2.6 Increasing target reduction (%)

The final parameter that was tested was the target reduction of the structure. This is not a reliable parameter though since the higher the target reduction the less stiff and robust the final structure would be, leading to unreliable results. Nonetheless, it was tested in order to understand the trend with which the marginal part and the part that should be removed are changing. The target reduction varied from 5% up to 35%. Figure 69 illustrates some of the resulting outputs of the shape optimisation tool.

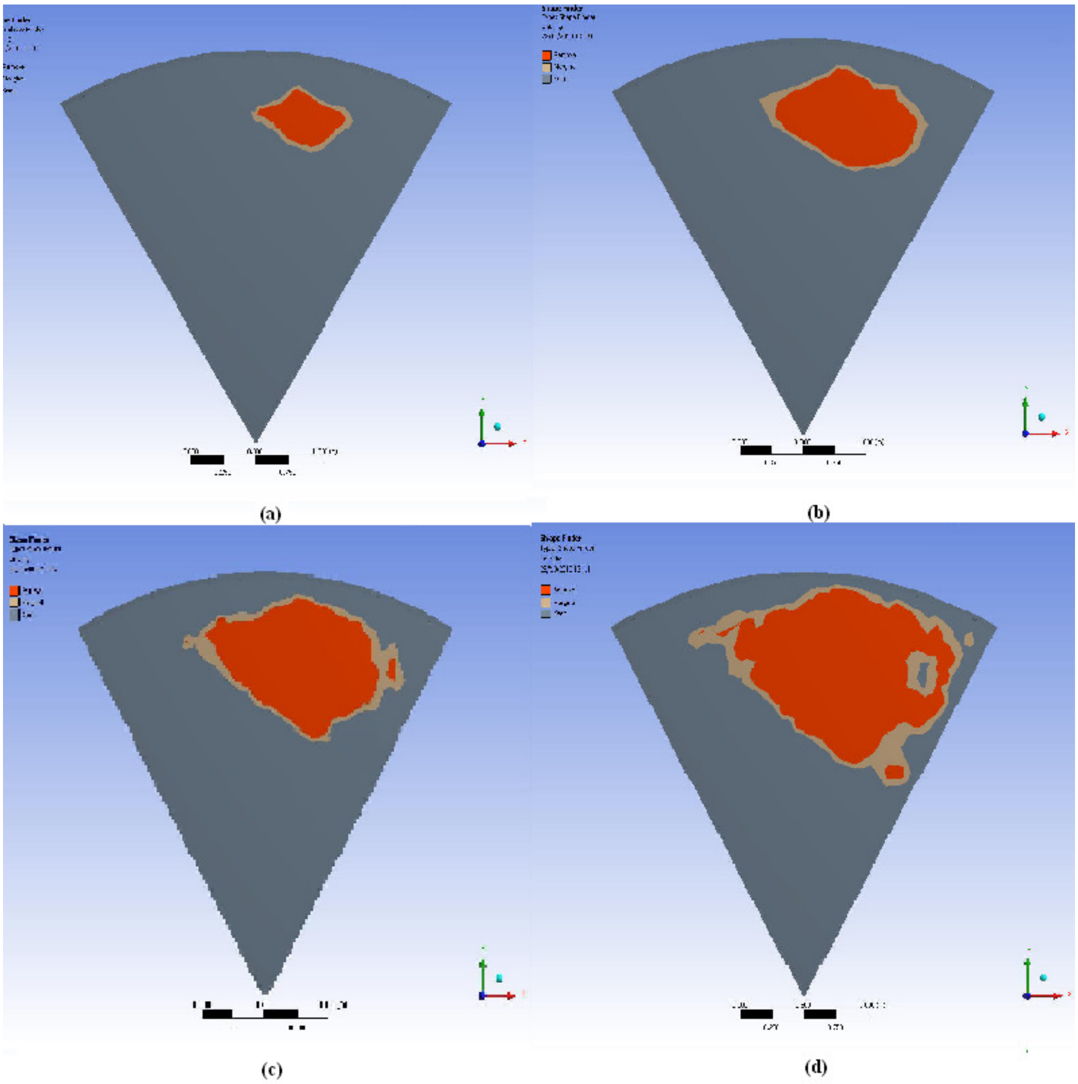

Figure 69 - (a) 5%, (b)15%, (c) 25%, (d) 35%

As it should have been expected, the area of the red coloured part of the tested structure increased together with the percentage of the target reduction.

The originally small round shape extends towards the centre and the right side of the structure for greater target reduction. It is unknown though at which point the remaining structure stops being robust enough and becomes unable to maintain the airgap clearance.

3.2.7 Conclusions

It seems that in order to optimise the structure of a direct drive rotor with disc, the greatest concern should be the number of times that the pattern would be repeated (arc angle).

Although the part that could be removed is affected by the Maxwell stress that acts on the rotor and the moment that gives rice to the circumferential stress, their magnitudes are static and can be calculated beforehand. Thus there can be no practical variation of the removable part due to these parameters.

Finally, although the radius length and the disc thickness give greater removable areas, these parameters should be kept in minimum possible values because they add a lot of structural mass on the rotor.

The next step of this research would be the creation of the structural model of a complete rotor with disc bearing the new pattern that was outlined with the help of the shape optimisation tool. Since there is quite a variation among the patterns depending on the number of the pattern repetitions (arc angle), a large number of different models should be created in order to find which case returns the most lightweight structure but also to make sure that the radial and circumferential deflections are within limitations.

3.3 Rotor Modelling

3.3.1 Introduction

For the second part of this research, a number of structural models of a rotor with disc were created. The different models were missing a portion of their mass according to the output of the shape optimisation tool. Each model can be characterised according to the number of pattern repetitions on the rotor disc.

A model of a rotor with disc was created in order to compare its structural mass and its radial and circumferential deflection with the new designs. The mass of the rotor with disc was 37900kg. Its dimensions were the same as the base case of section 3.2: R=3m, l=1.717m, t_d=0.1m and h_{yr}=0.06m (Figure 70).

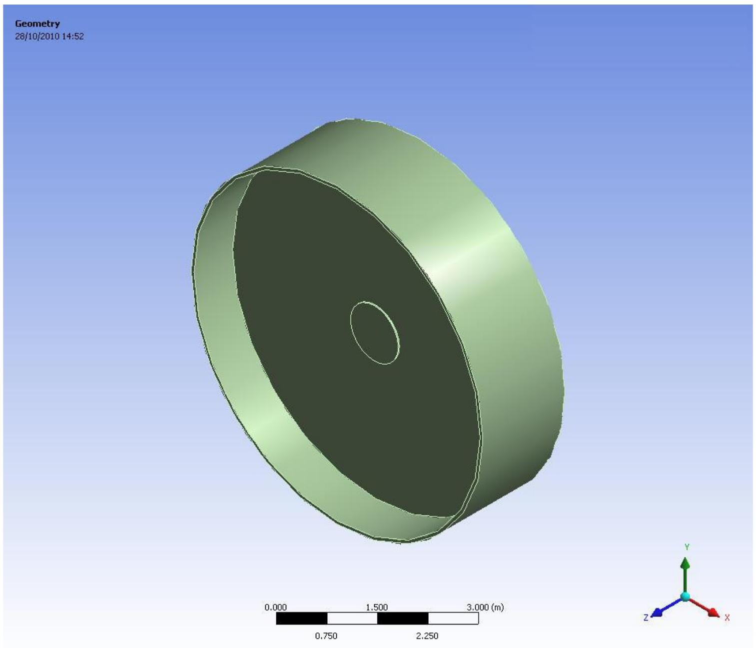

Figure 70 - Rotor with disc

The radial deflection was $u_A = 2.77\times10^{-4}$ m ($u_{A\_max} = 3\times10^{-4}$ m) and the circumferential deflection due to rotation was $z_A = 5.58\times10^{-4}$ m ($z_{A\_max} = 6\times10^{-4}$ m) (Figure 71)

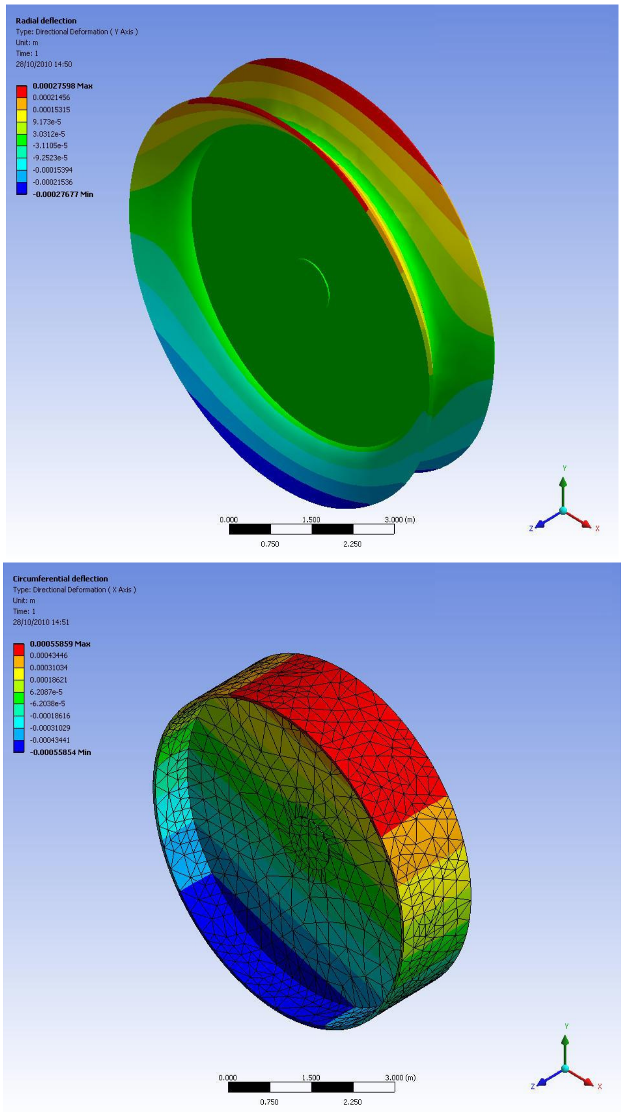

Figure 71 – Radial and Circumferential deflection

3.3.2 12 pattern repetitions

A model with 30° arc was introduced into the shape optimisation tool to create a disc geometry with 12 pattern repetitions. The target reduction for the given body was set to 30%. The output of the shape finder can be seen in Figure 72.

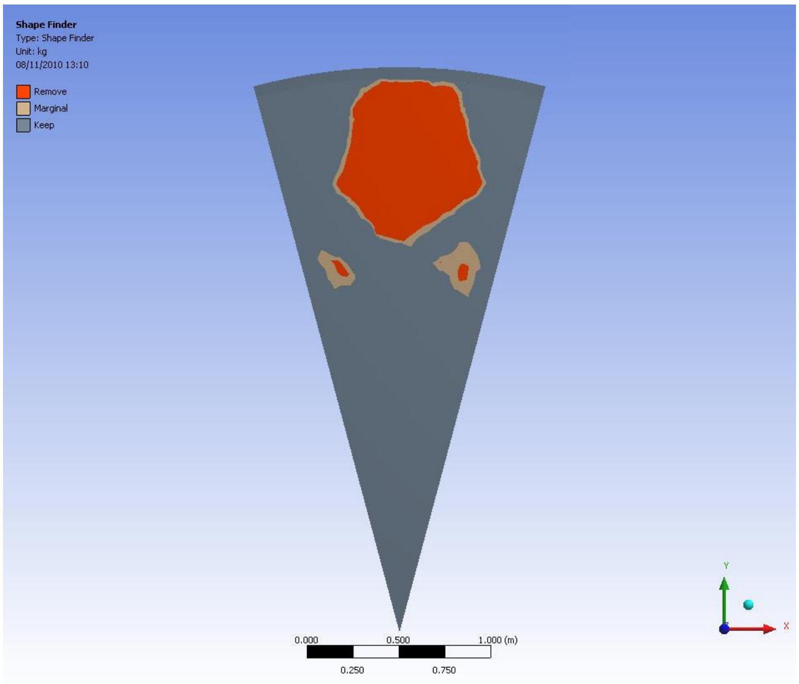

Figure 72 - Shape Finder output

The next step was an attempt to remove the portion of the mass that the shape finder outlined as unneeded. The new geometry is illustrated in Figure 73.

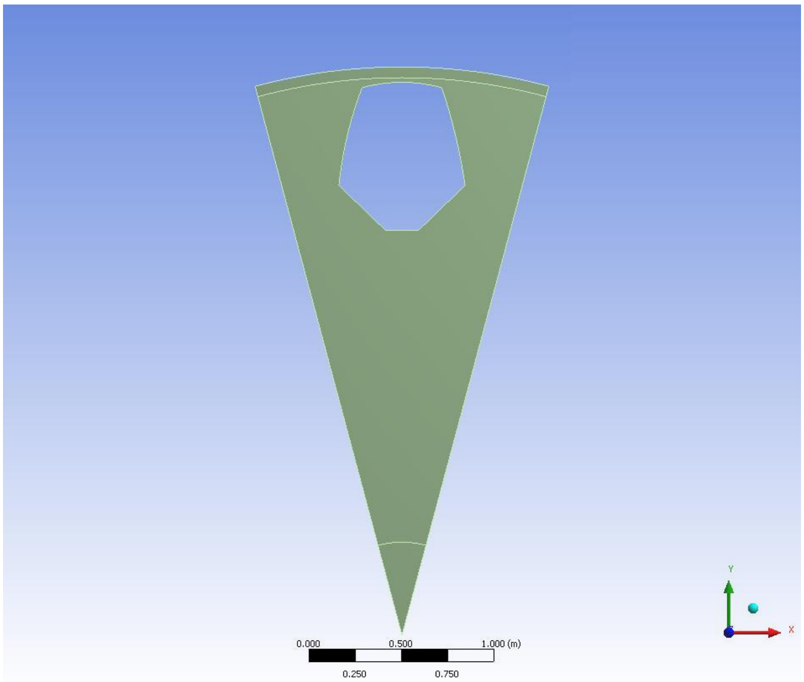

Figure 73 - Structure after shape optimisation

A comparison between the two shapes is given below (Figure 74).

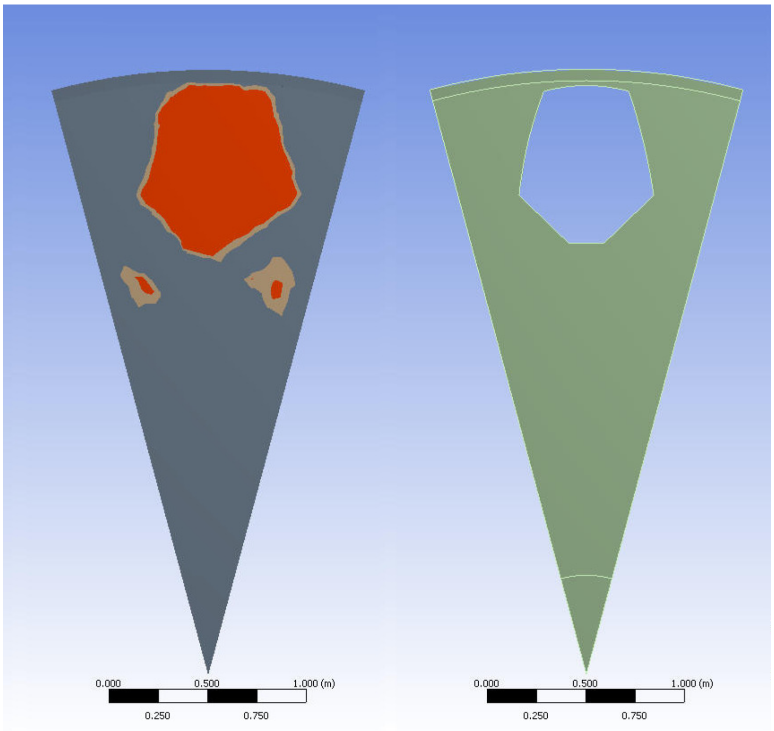

Figure 74 - On the left the shape finder's output. On the right the designed geometry

The new geometry was introduced as a pattern in the design tool in order to create a complete rotor with disc with the desired shape (Figure 75).

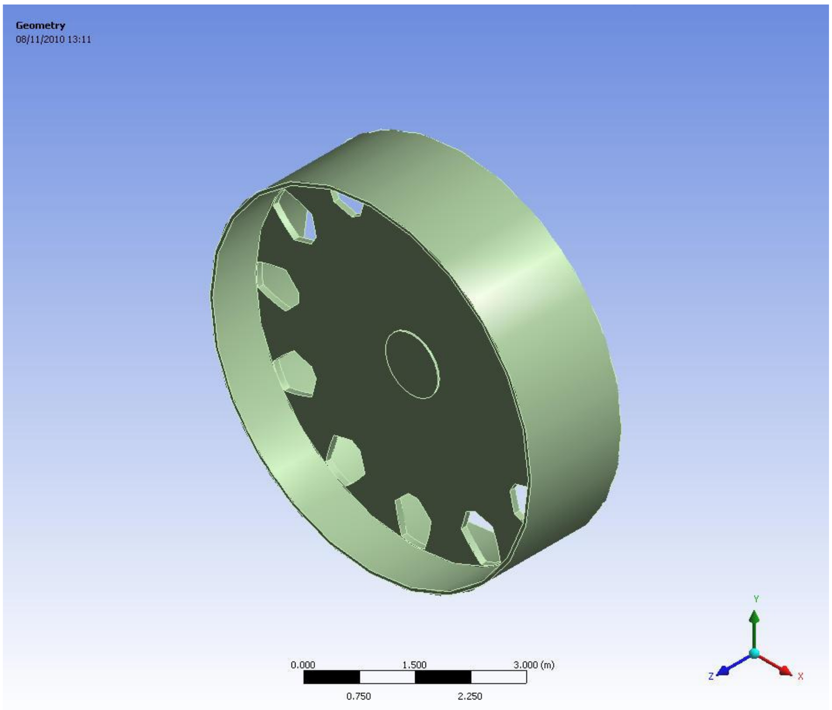

Figure 75 - Full rotor with 12 pattern repetitions

The total mass of the disc rotor was reduced compared to the original disc rotor design from 37900kg to 33500kg (11.7% mass reduction). This rotor design was tested for its stiffness against the two major deflections. The radial deflection was $u_A = 2.90\times10^{-4}$ m ($u_{A\_max} = 3\times10^{-4}$ m) and the circumferential deflection due to rotation was $z_A = 6.01\times10^{-4}$m ($z_{A\_max} = 6\times10^{-4}$ m) (Figure 76).

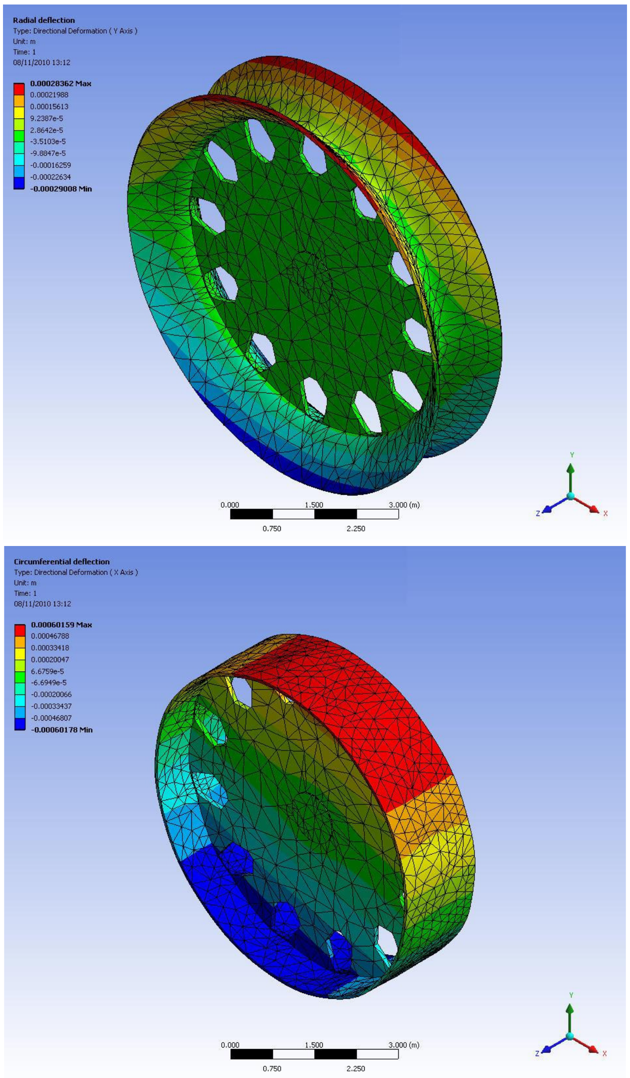

Figure 76 – Radial and Circumferential deflection for 12 pattern repetitions

The radial deflection increased slightly compared to radial deflection that the full disc structure experienced, only 0.13×10^{-4} m. The circumferential deflection increased by 0.43×10^{-4} m but remained within limitations.

3.3.3 8 pattern repetitions

Following the same procedure described in 3.3.1, a structural model for a rotor was created based on the output of the shape optimisation program for a structure with a 45º arc (Figure 77). The target reduction for the given body was set to 30%.

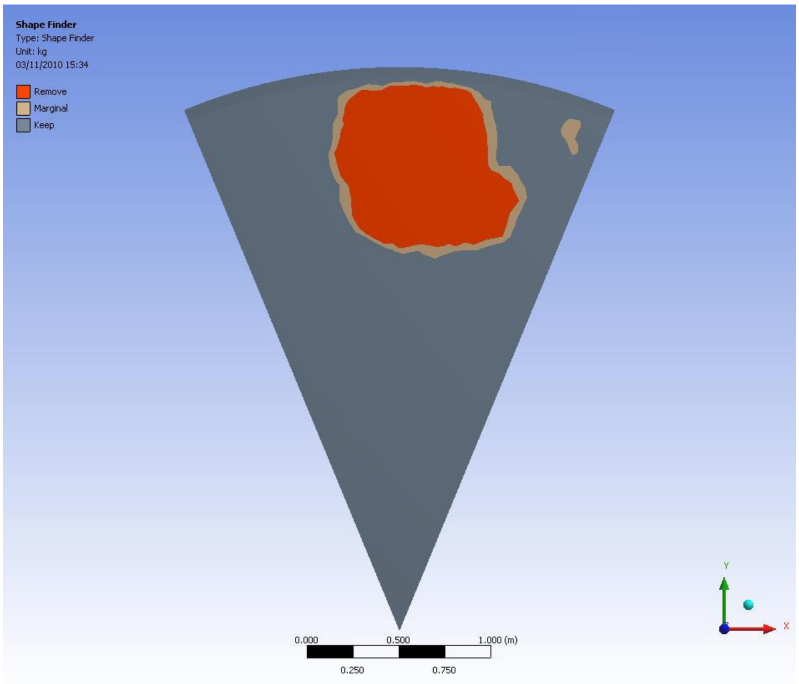

Figure 77 - Shape Finder output

Once the outlined part was removed (Figure 78) the new geometry was introduced as a pattern in the design tool in order to create a complete rotor with disc with the desired shape (Figure 79).

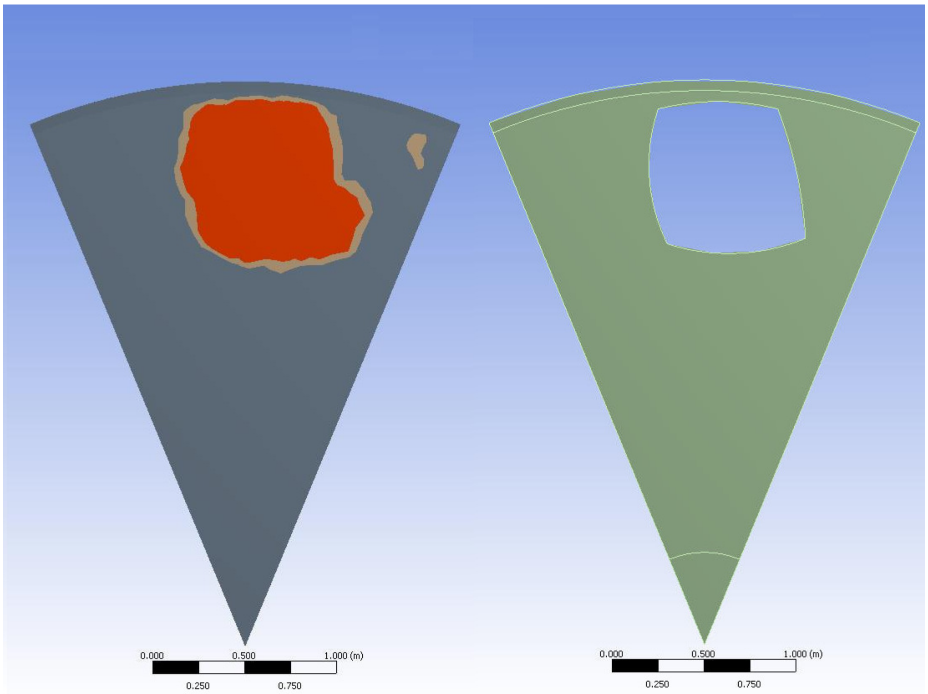

Figure 78 - On the left the shape finder's output. On the right the designed geometry

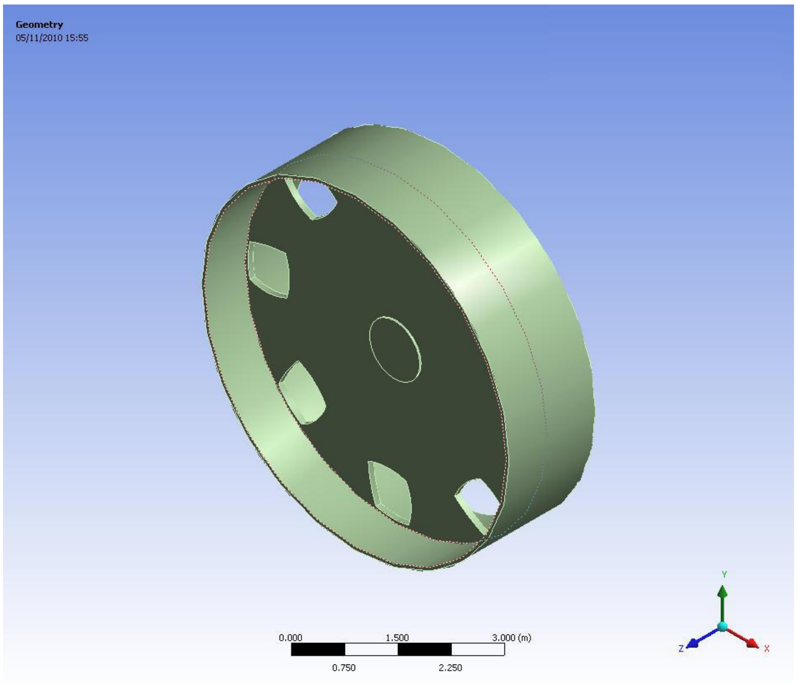

Figure 79 - Full rotor with 8 pattern repetitions

The total mass of the disc rotor was reduced compared to the original disc rotor design from 37900kg to 33600kg (11.3% mass reduction). This rotor design was tested for its stiffness against the two major deflections. The radial deflection was $u_A = 2.92\times10^{-4}$ m ($u_{A\_max} = 3\times10^{-4}$ m) and the circumferential deflection due to rotation was $z_A = 6.00\times10^{-4}$ m ($z_{A\_max} = 6\times10^{-4}$ m) (Figure 80).

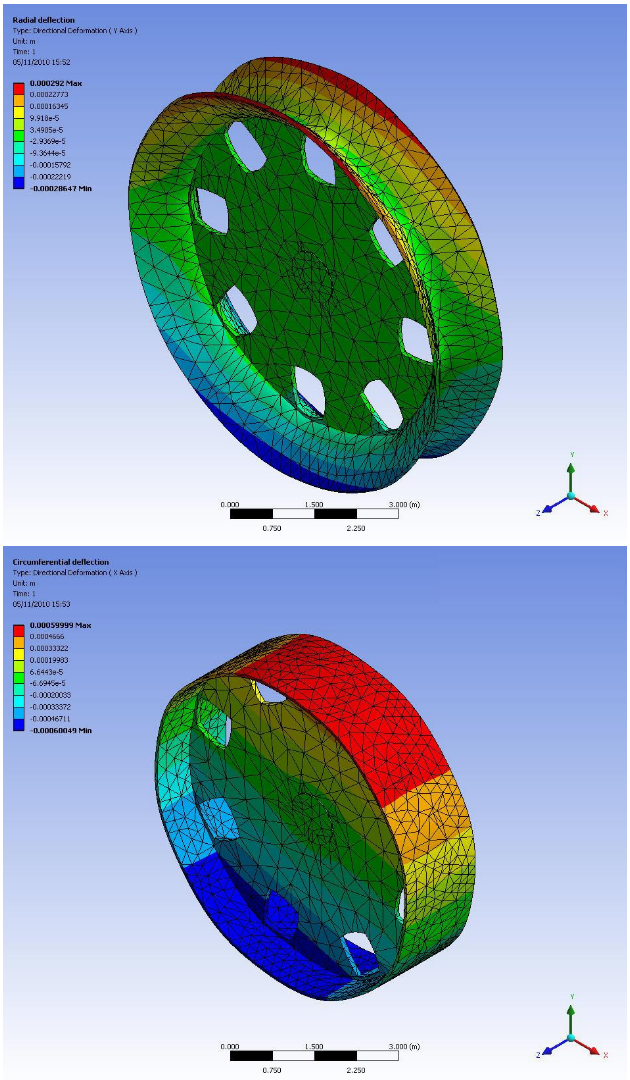

Figure 80 – Radial and Circumferential deflection for 8 pattern repetitions

The radial deflection increased compared to radial deflection that the full disc structure experienced, by 15×10^{-4} m. The circumferential deflection increased by 0.42×10^{-4} m.

3.3.4 6 pattern repetitions

Following the same procedure described in Chapter 3.3.1, a structural model for a rotor was created based on the output of the shape optimisation program for a structure with a 60° arc (Figure 81). The target reduction for the given body was set to 30%.

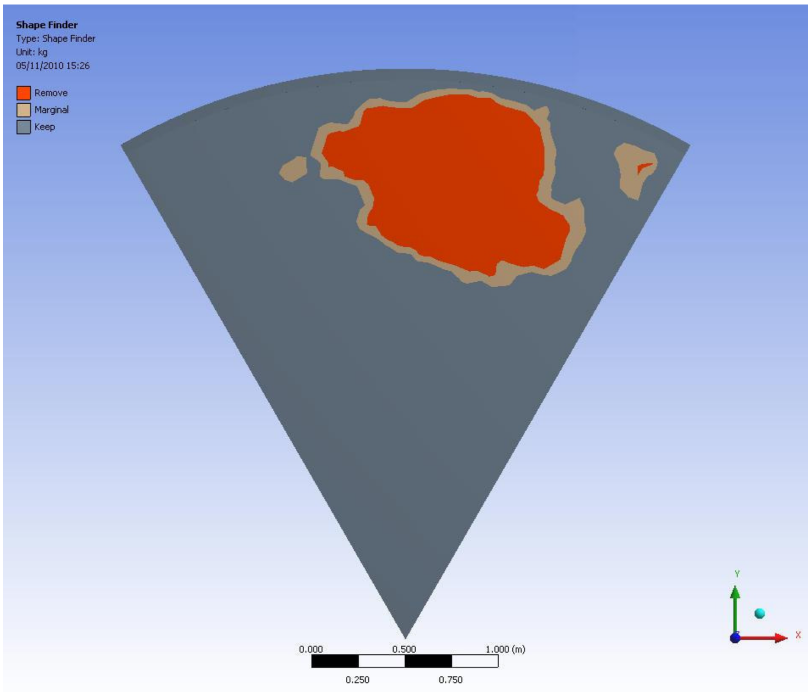

Figure 81 - Shape Finder output

Once the outlined part was removed (Figure 82) the new geometry was introduced as a pattern in the design tool in order to create a complete rotor with disc with the desired shape (Figure 83).

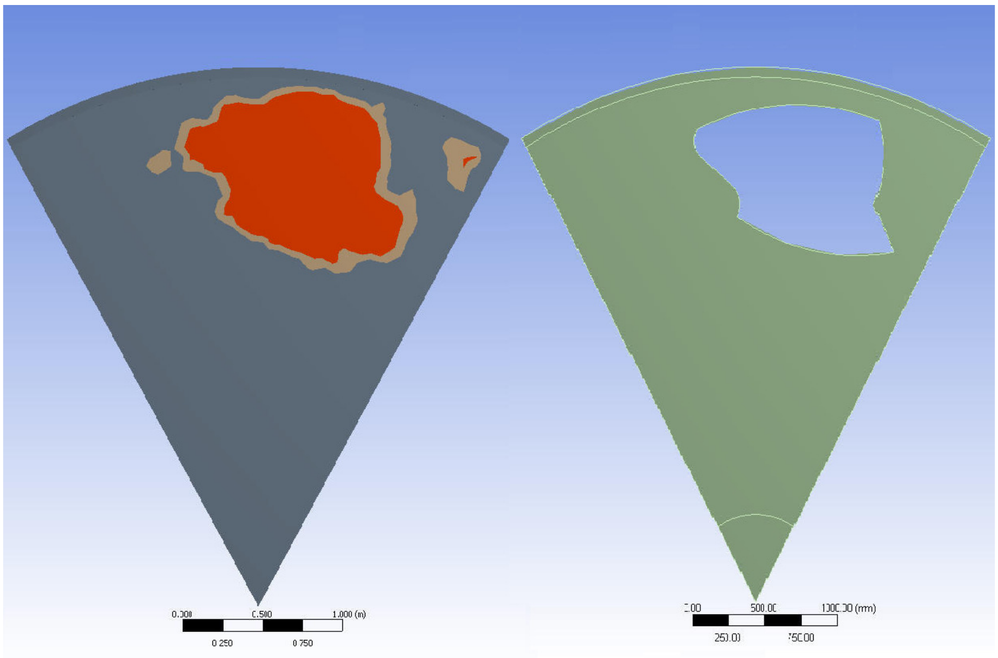

Figure 82 - On the left the shape finder's output. On the right the designed geometry

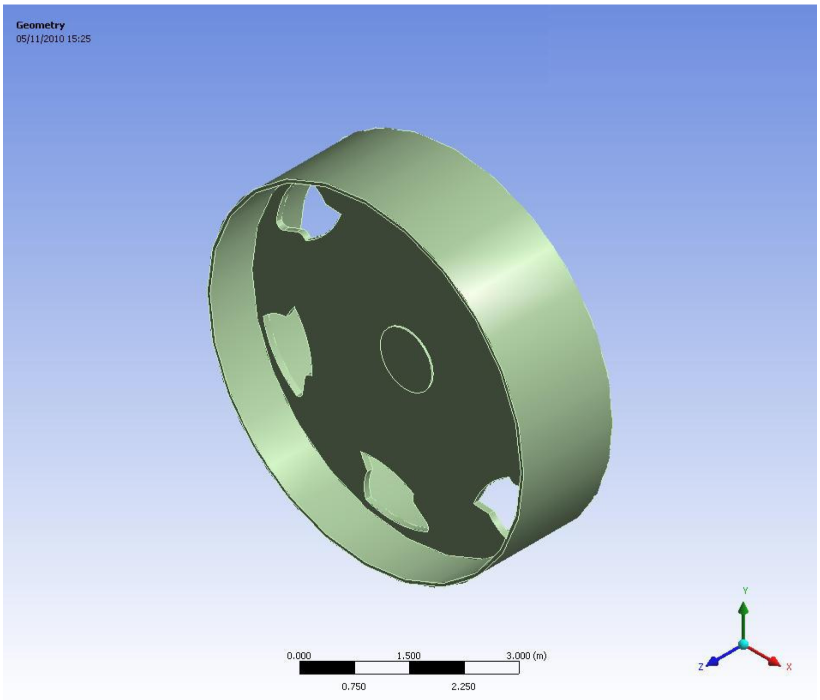

Figure 83 - Full rotor with 6 pattern repetitions

The total mass of the disc rotor was reduced compared to the original disc rotor design from 37900kg to 33500kg (11.6% mass reduction). This rotor design was tested for its stiffness against the two major deflections. The radial deflection was $u_A = 2.93\times10^{-4}$ m ($u_{A\_max} = 3\times10^{-4}$ m) and the circumferential deflection due to rotation was $z_A = 6.07\times10^{-4}$ m ($z_{A\_max} = 6\times10^{-4}$ m) (Figure 84).

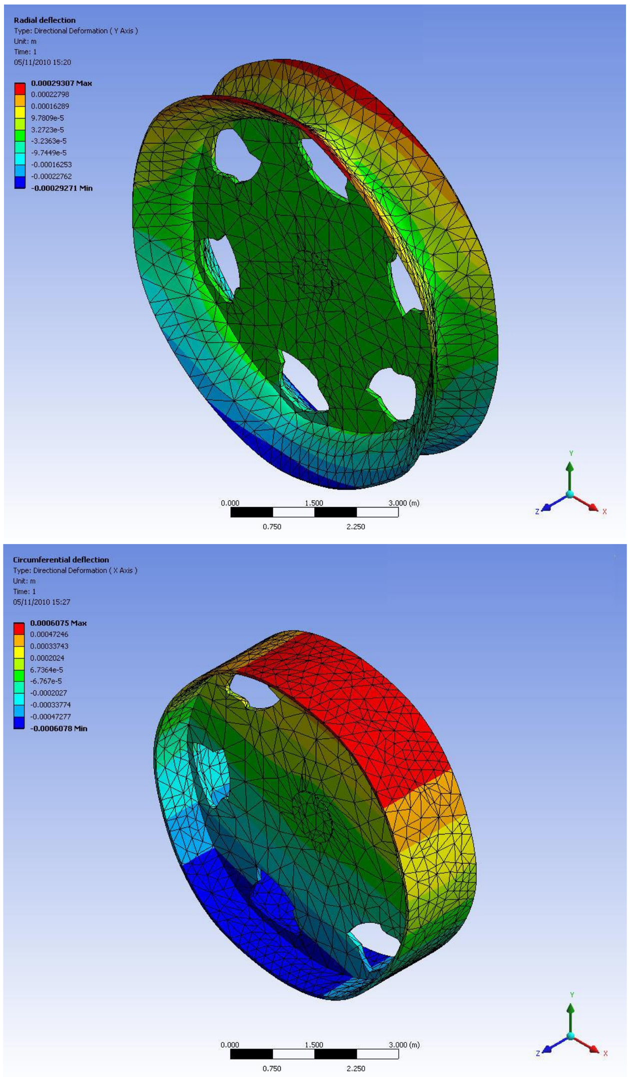

Figure 84 – Radial and Circumferential deflection for 6 pattern repetitions

The radial deflection increased by 0.16×10^{-4} m compared to the full disc structure, much more compared to the previous experiments. The circumferential deflection increased by 0.49×10^{-4} m.

3.3.5 4 pattern repetitions

Following the same procedure described in Chapter 3.3.1, a structural model for a rotor was created based on the output of the shape optimisation program for a structure with a 90° arc (Figure 85). The target reduction for the given body was set to 30%.

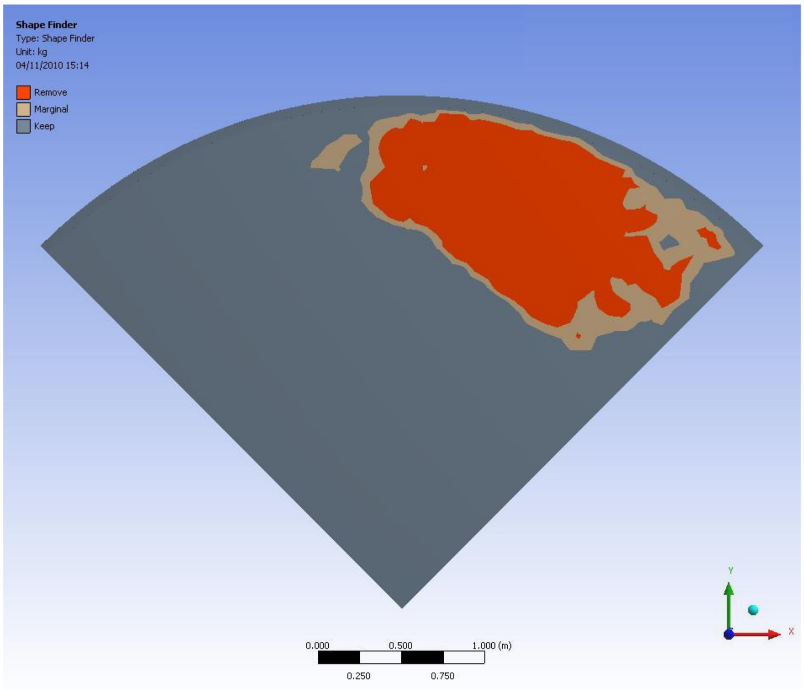

Figure 85 - Shape Finder output

Once the outlined part was removed (Figure 85) the new geometry was introduced as a pattern in the design tool in order to create a complete rotor with disc with the desired shape (Figure 86).

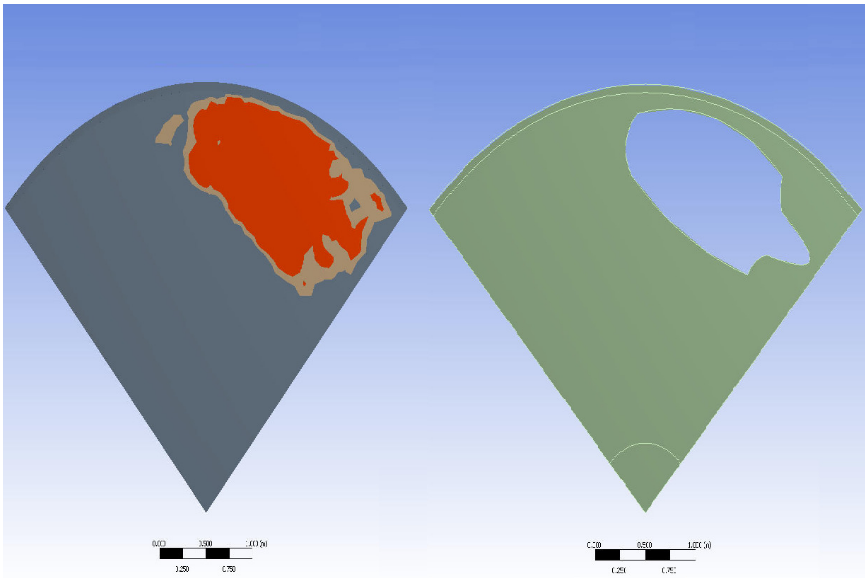

Figure 86 - On the left the shape finder's output. On the right the designed geometry

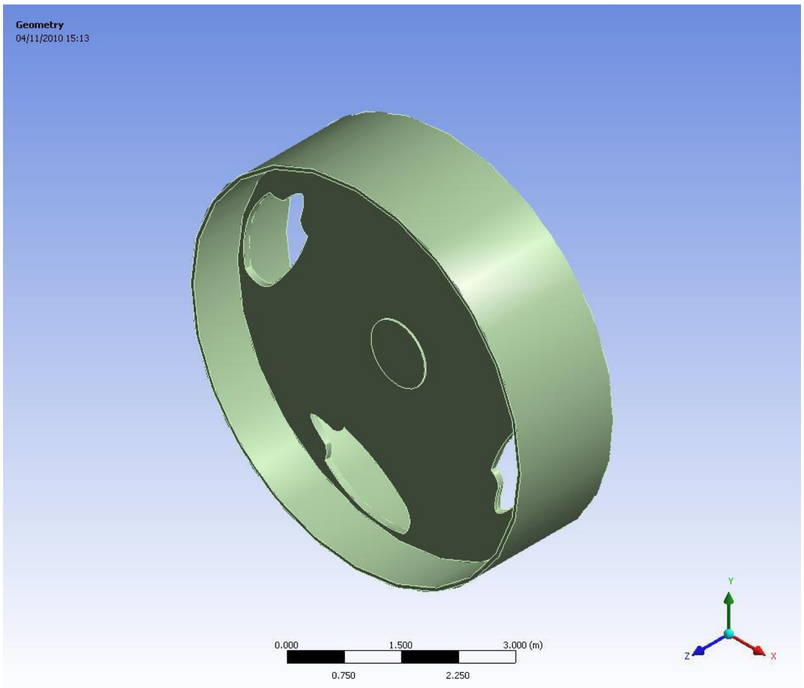

Figure 87 - Full rotor with 4 pattern repetitions

The total mass of the disc rotor was reduced compared to the original disc rotor design from 37900kg to 33650kg (11.2% mass reduction). This rotor design was tested for its stiffness against the two major deflections. The radial deflection was $u_A = 3\times10^{-4}$ m ($u_{A\_max} = 3\times10^{-4}$ m) and the circumferential deflection due to rotation was $z_A = 6.08\times10^{-4}$ m ($z_{A\_max} = 6\times10^{-4}$ m) (Figure 88).

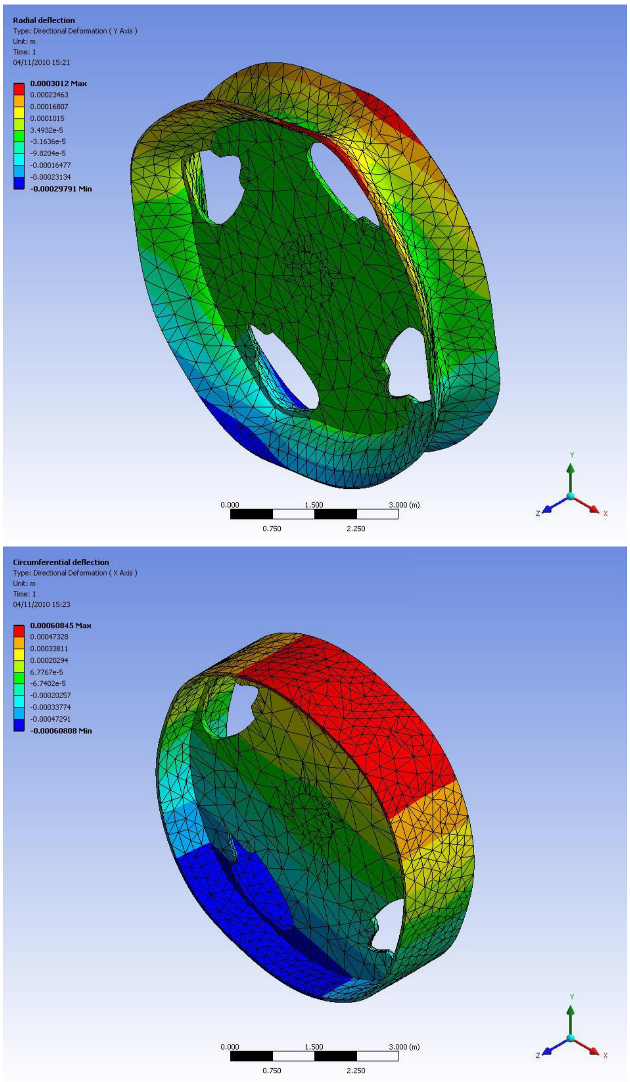

Figure 88 – Radial and Circumferential deflection for 4 pattern repetitions

The radial deflection increased by 0.23×10^{-4} m compared to the full disc structure, much more compared to the previous experiments. The circumferential deflection increased by 0.5×10^{-4} m.

3.3.6 3 pattern repetitions

Following the same procedure described in Chapter 3.3.1, a structural model for a rotor was created based on the output of the shape optimisation program for a structure with a 120° arc (Figure 89). The target reduction for the given body was set to 20% this time (instead of 30% like the previous experiments) because any higher target reduction than that gave rise to a radial deflection much greater that the specified upper limitation ($u_{A\_max} = R/10000 = 3 \times 10^{-4}$ m).

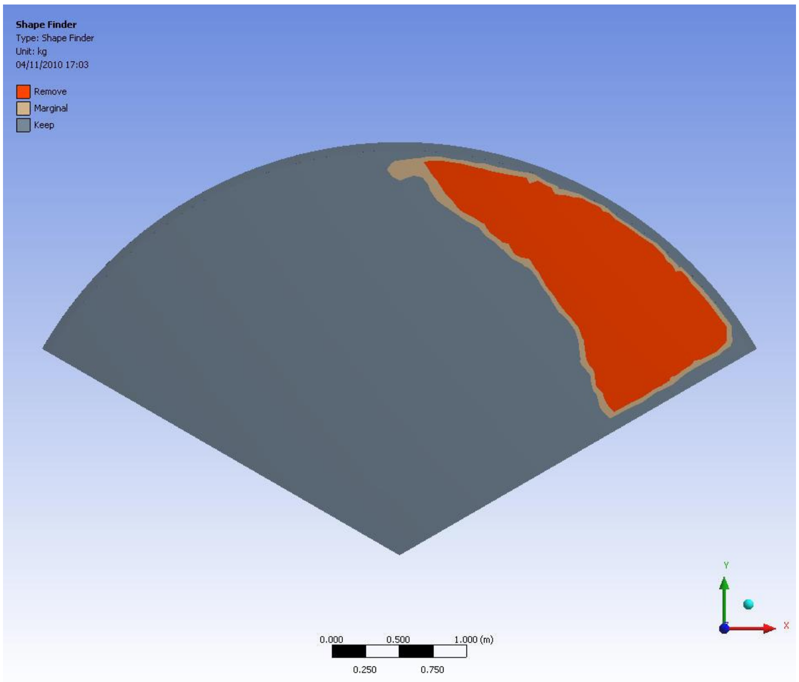

Figure 89 - Shape Finder output

Once the outlined part was removed (Figure 90) the new geometry was introduced as a pattern in the design tool in order to create a complete rotor with disc with the desired shape (Figure 91).

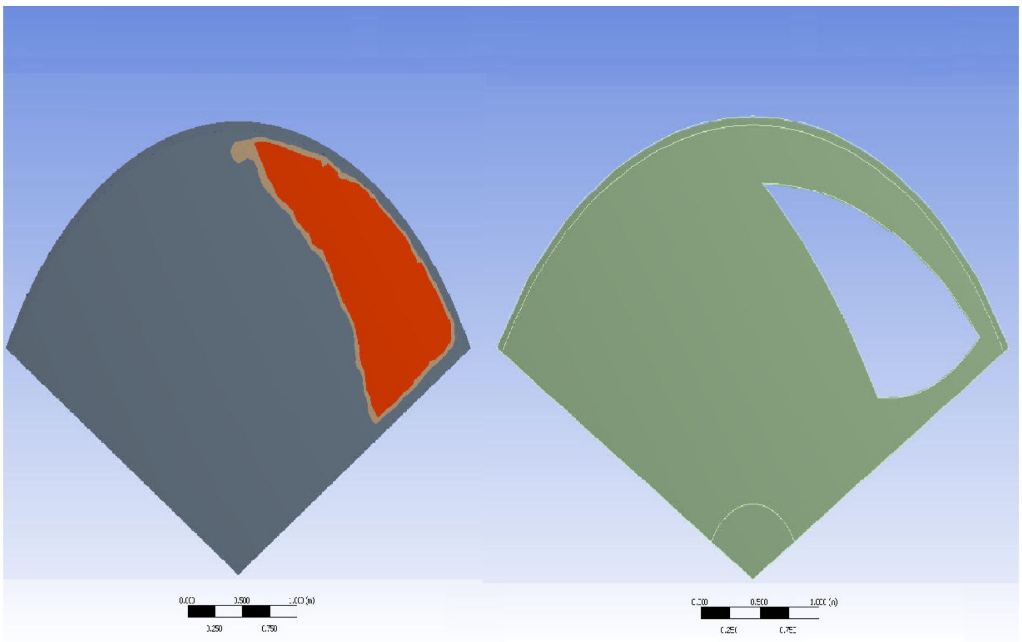

Figure 90 - On the left the shape finder's output. On the right the designed geometry

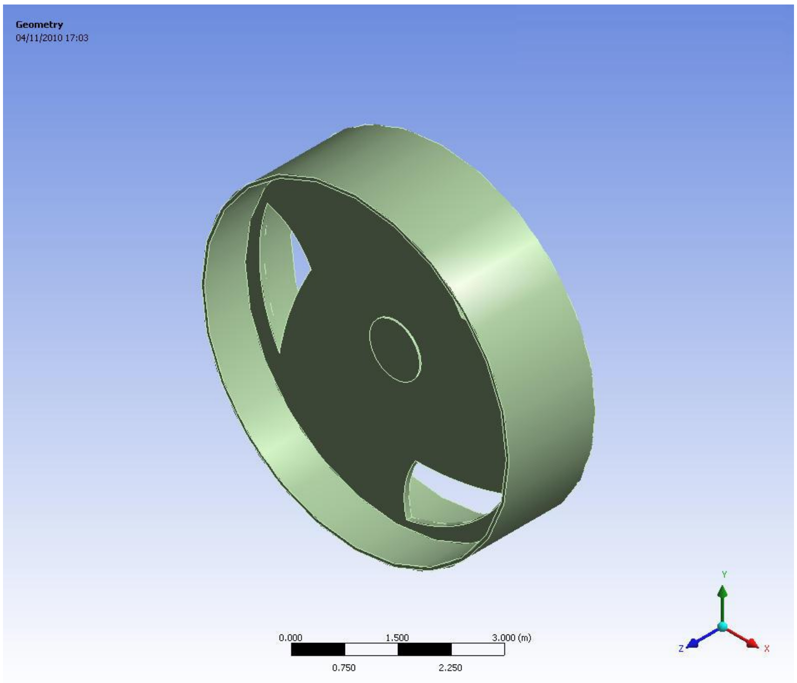

Figure 91 - Full rotor with 3 pattern repetitions

The total mass of the disc rotor was reduced compared to the original disc rotor design from 37900kg to 34500kg (9% mass reduction). This rotor design was tested for its stiffness against the two major deflections. The radial deflection was $u_A = 3.06\times10^{-4}$ m ($u_{A\_max} = 3\times10^{-4}$ m) and the circumferential deflection due to rotation was $z_A = 6.04\times10^{-4}$ m ($z_{A\_max} = 6\times10^{-4}$ m) (Figure 92).

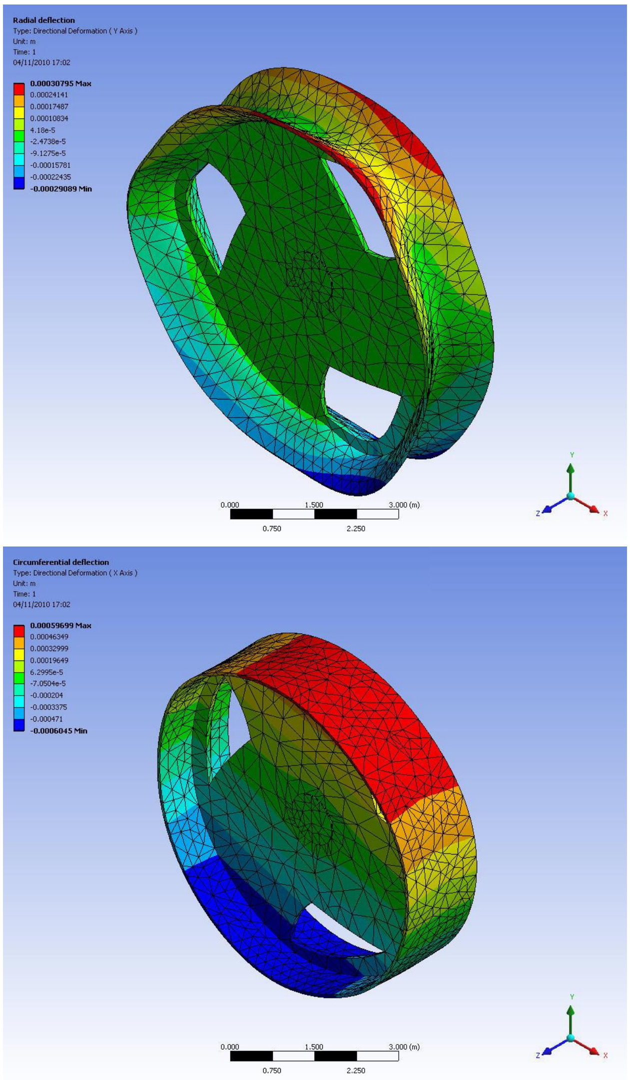

Figure 92 – Radial and Circumferential deflection for 3 pattern repetitions

The radial deflection increased by 0.29×10^{-4} m compared to the full disc structure. The circumferential deflection increased by 0.46×10^{-4} m.

3.3.7 2 pattern repetitions

Following the same procedure described in section 3.3.1, a structural model for a rotor was created based on the output of the shape optimisation program for a structure with a 180° arc (Figure 93). The target reduction for the given body was once again set to 20% (instead of 30% like the previous experiments) because any higher target reduction than that gave rise to a radial deflection much greater that the specified upper limitation ($u_{A\_max} = R/10000 = 3\times10^{-4}$ m).

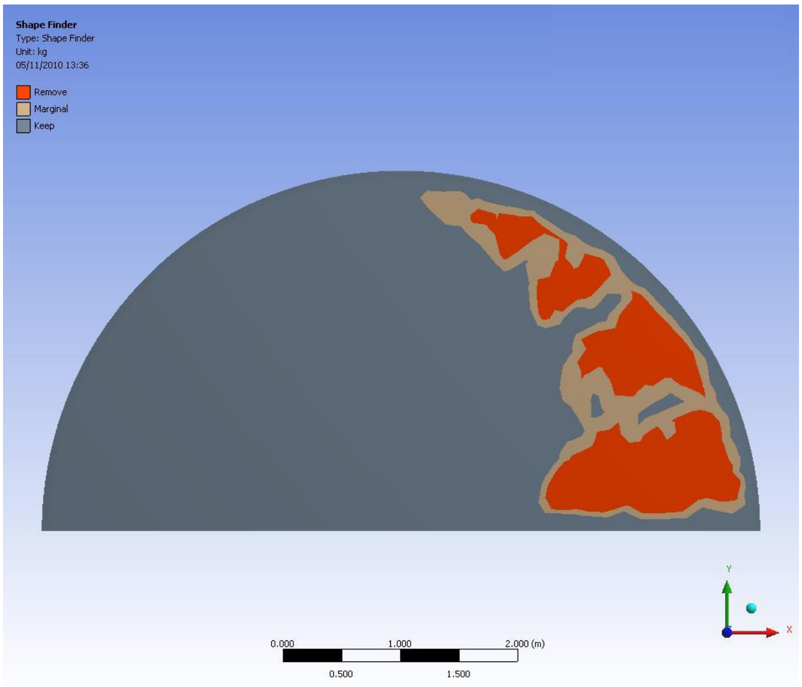

Figure 93 - Shape Finder output

Once the outlined part was removed (Figure 94) the new geometry was introduced as a pattern in the design tool in order to create a complete rotor with disc with the desired shape (Figure 95).

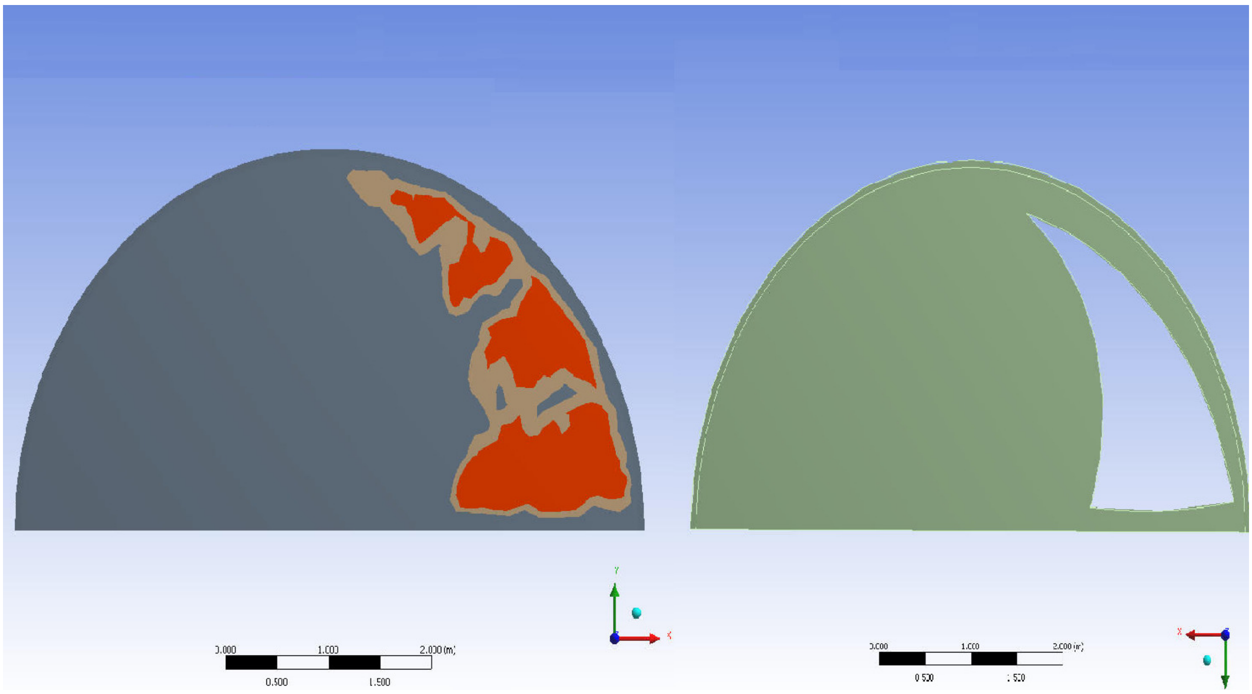

Figure 94 - On the left the shape finder's output. On the right the designed geometry

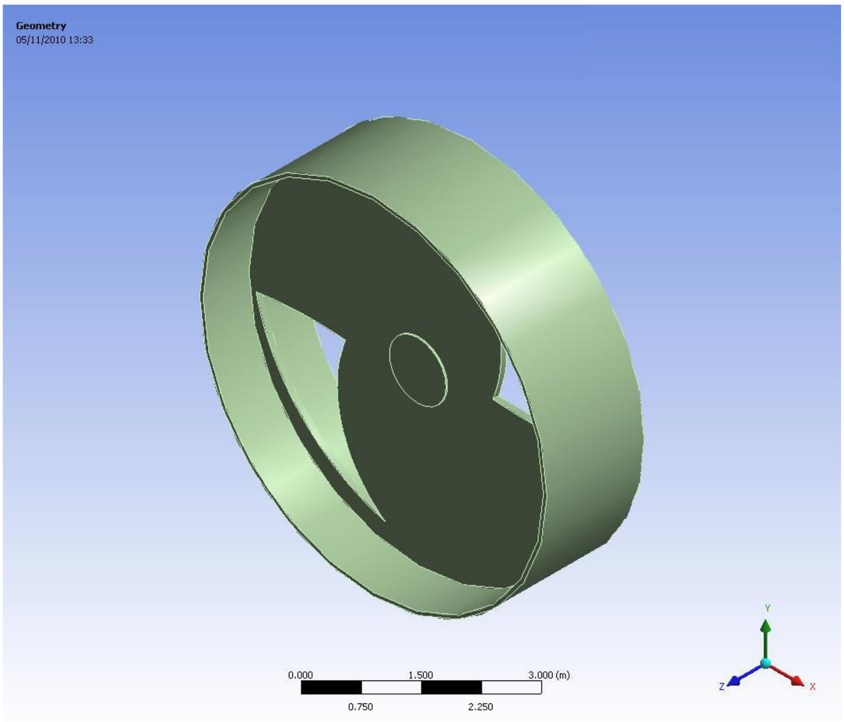

Figure 95 - Full rotor with 2 pattern repetitions

The total mass of the disc rotor was reduced compared to the original disc rotor design from 37900kg to 34300kg (9.5% mass reduction). This rotor design was tested for its stiffness against the two major deflections. The radial deflection was $u_A = 3.06\times10^{-4}$ m ($u_{A\_max} = 3\times10^{-4}$ m) and the circumferential deflection due to rotation was $z_A = 6.04\times10^{-4}$ m ($z_{A\_max} = 6\times10^{-4}$ m) (Figure 96).

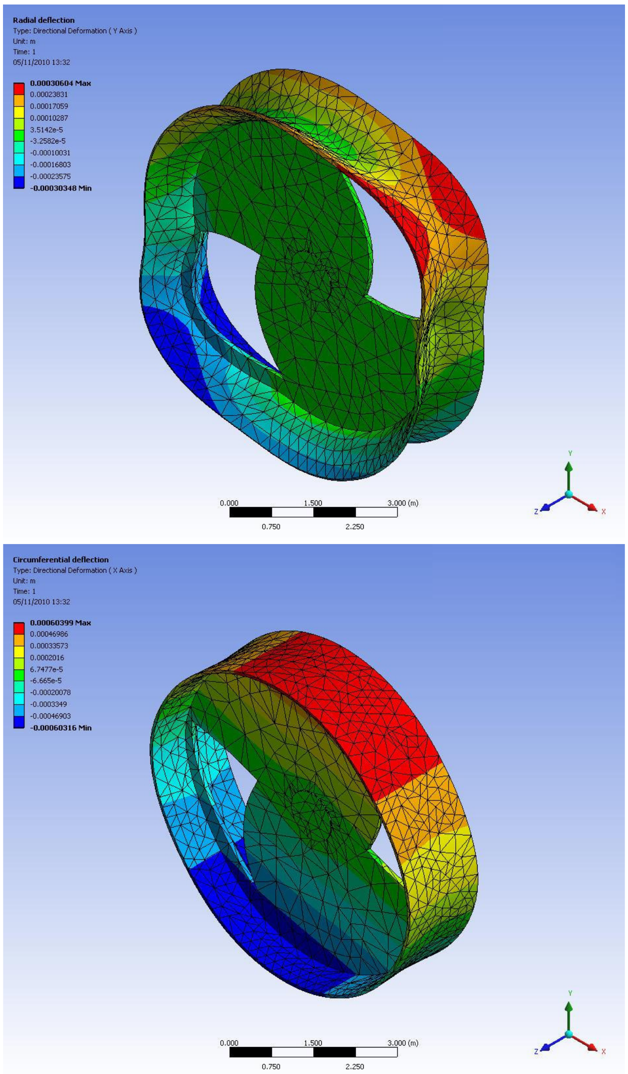

Figure 96 – Radial and Circumferential deflection for 2 pattern repetitions

The radial deflection increased by 0.29×10^{-4} m compared to the full disc structure. The circumferential deflection increased by 0.46×10^{-4} m.

3.3.8 Conclusions

After conducting a large number of experiments the best results occurred for structures with large number of pattern repetitions (Figure 97).

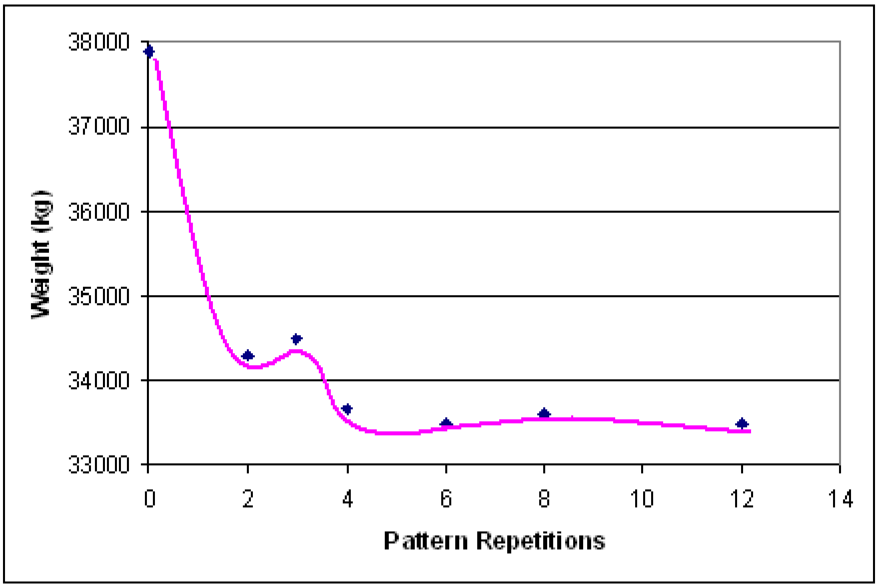

Figure 97 – Weight comparison of optimised structures

The following general conclusions can be outlined:

- Structures with large numbers of pattern repetitions on their disc are lighter and more robust compared to structures with fewer pattern repetitions.
- The most lightweight structures were those with 6 (33535kg) and 12 (33480kg) pattern repetitions with the second one being slightly lighter.
- For a small number of pattern repetitions the radial and circumferential stress was greater compared to structural designs with more pattern repetitions.
- The maximum mass reduction that was achieved was 11.7%. Any further mass reduction than that resulted in a radial or circumferential stress greater that the allowed one.

In order to check whether an even more increased number of pattern repetitions would lead to a further mass reduction, a structural model with 18 repetitions was created, based on the mass optimisation of a shape with an arc of 20° (Figure 98).

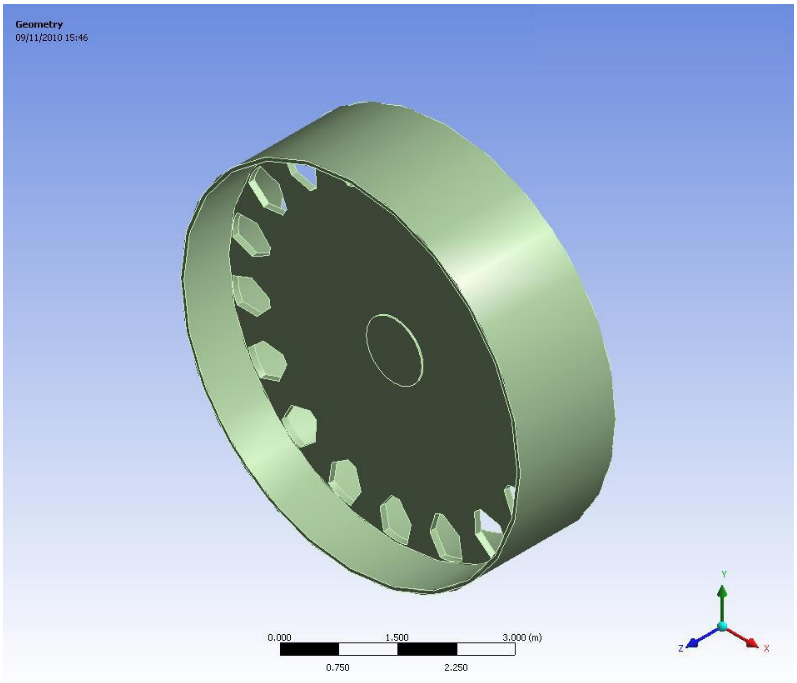

Figure 98 - Full rotor with 18 pattern repetitions

The structure was once again robust enough to withstand both structural stresses that were applied on it. The total weight of the structure was 33420kg, merely 60kg less than the 12 pattern structure. It seems that any further attempt to increase the removable parts would not lead to any noticeable mass reduction.

A topology with many small parts missing near the outer circumference of the disc of the rotor also agrees with the output of the shape optimisation tool when a complete rotor with disc is under investigation. Figure 99 suggests that a part near the end of the disc could be removed without the structure losing its stiffness. Of course such a topology is not easy to model or construct for commercial use since there is no distinguishable pattern on the disc.

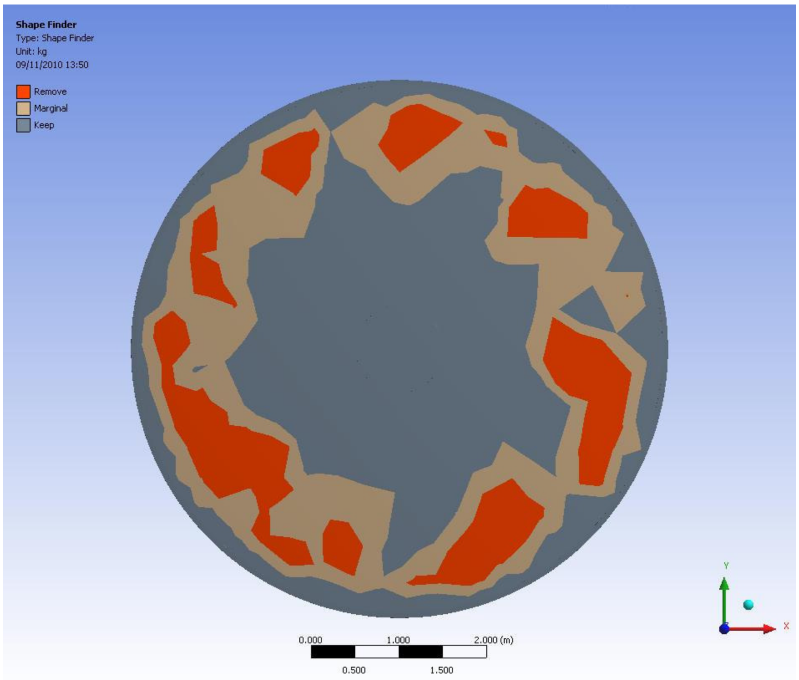

Figure 99 – 35% target reduction for full rotor with disc

The results of this research could be of great use in the designing of a novel lightweight rotor topology. The only downside is that some of the resulting pattern shapes are rather controversial and would be difficult to carve on a rotor that could be produced in large numbers. For this matter, the same research could be made using a more conventional pattern in order to see whether the same good results could be achieved.

The same optimization procedure was applied to stator structures with discs, giving similar results.

4. Overall Conclusions

As it has been pointed out from this research, the structure of a large direct drive generator with permanent magnets can be decreased effectively by following the outlined conclusions of this research. The two different optimisation methods – analytical and structural – can optimise a predefined structure first by changing its structural parameters to make it lighter and then further decreased the structural weight by removing pieces that do not contribute to the structure's stiffness.

The optimisation method presented here can provide guidelines for decreasing the weight of many different machines, given a structural description and an electromagnetic model, making it a very useful tool for wind generator designers.

5. Further Work

This work has already been extended to a structural-electromagnetic optimisation for transverse-flux machines with UPWIND partners from TU Delft [9]. Beyond UPWIND, the work presented here can be applied to other direct drive generator topologies such as axial-flux machines or switched reluctance generators. Different materials other than structural steel and different electromagnetic models can be tested. Continuing work at the University of Edinburgh will also look at the dynamic performance of the optimised generator structures here and in [1] and [2].

6. References

[1] M. A. Mueller and A. S. McDonald, "Development of analytical tools for estimating inactive mass", UPWIND Report

[2] M. A. Mueller and A. S. McDonald, "Structural optimisation of a radial-flux permanent magnet generator (for a direct-drive wind turbine) using a Genetic Algorithm", UPWIND Report

[3] A.S. McDonald, "Structural analysis of low speed, high torque electrical generators for direct drive renewable energy converters", PhD thesis, School of Engineering, University of Edinburgh, 2008, available at: http://www.see.ed.ac.uk/~s0459405/public_html/PhD Thesis A.S.McDonald 2008.pdf

[4] Evolutionary Computation Research Team, University of Sheffield, http://www.shef.ac.uk/acse/research/ecrg/gat.html

[5] A. J. Chipperfield and P. J. Fleming, "The MATLAB Genetic Algorithm Toolbox", IEE Colloquium on Applied Control Techniques Using MATLAB, Digest No. 1995/014, 26 Jan, 1995

[6] D. Bang, "Design of Transverse Flux Permanent Magnet Machines for Large Direct-Drive Wind Turbines", Ph.D. dissertation, Delft University of Technology, Delft, The Netherlands,, 2010.

[7] A. Zavvos, A.S. McDonald, M. Mueller 'Electromagnetic and Mechanical Optimisation of Direct-Drive Generators for Large Wind Turbines', University of Edinburgh, Scotland, PEMD conference, Brighton 2010

[8] ANSYS Workbench, www.ansys.com

[9] A. Zavvos, D. Bang, A. McDonald, M. Mueller, H. Polinder 'Structural Analysis & Optimisation of Transverse Flux Permanent Magnet Machines for Direct Drive Wind Turbines', submitted for publication in Wind Energy, July 2010